CHEMICAL REVIEWS

pubs.acs.org/CR

Review

Artificial Metaphotonics Born Naturally in Two Dimensions

Zhigao Dai, Guangwei Hu, Qingdong Ou, Lei Zhang, Fengnian Xia, Francisco J. Garcia-Vidal, Cheng-Wei Qiu,* and Qiaoliang Bao*

Cite This: *Chem. Rev.* 2020, 120, 6197−6246

Read Online

ACCESS | Metrics & More | Article Recommendations

ABSTRACT: Recently, two rich and exciting research fields, layered two-dimensional (2D) materials and metamaterials, have started overlapping. Metamaterials are artificial, engineered materials with broad metaphotonic prospects such as negative refraction, perfect lensing, subwavelength imaging, and cloaking. The possibility of achieving metaphotonic properties using metamaterials based on layered 2D materials has been extensively exploited. Because they are highly tunable and adjustable with the ease of micro- and nanofabrication, 2D materials exhibit diverse optical properties such as natural negative refraction, natural anisotropic behavior, and even hyperbolic dispersion. A combination of 2D materials with conventional metamaterials promises a variety of prospective applications. In this review, we illustrate how the concept of metamaterials and their associated metaphotonic capabilities are naturally born in 2D materials. The multifunctionality of 2D materials may enable the manufacture of novel optical devices that work in a broad frequency range, from visible to terahertz, with particularly low loss, high speed, gated tunability, and miniaturized sizes. This new area of research links the fields of photonics, optoelectronics, and plasmonics with that of metamaterials and may provide insights to future innovations for 2D-material-inspired metaphotonic devices.

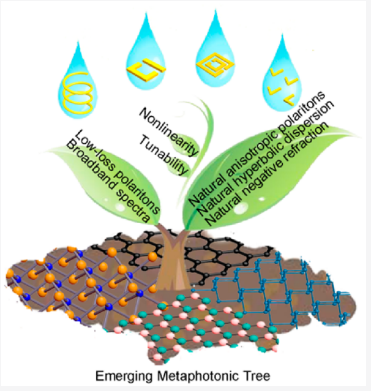

CONTENTS

Received: September 20, 2019
Published: June 4, 2020

https://dx.doi.org/10.1021/acs.chemrev.9b00592
Chem. Rev. 2020, 120, 6197−6246

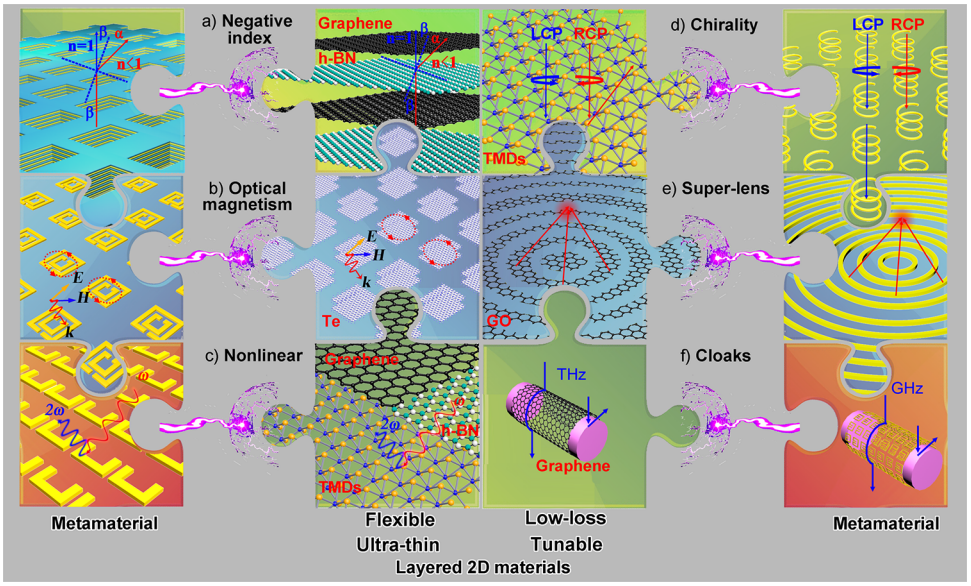

Figure 1. Overlapping of metaphotonics and layered 2D materials. (a) The left panel: the metal−dielectric−metal fishnet structure that is an array of periodic nanoholes milled on a multilayer metal−dielectric stack and operates at optical frequencies. The right panel: a vertical stack of multilayer graphene or multilayer graphene−hBN for unlimited bandwidth and all-angle negative refractions. (b) The left panel: an array of nonmagnetic double SRRs that consist of two concentric annuli of conducting material (each with a gap situated oppositely) and achieve THz magnetic response. The right panel: layered Te cubic metamaterials with electric and magnetic responses in the mid-IR. (c) The left panel: an array of nanoscale SRR Au metamaterials for the SHG. The right panel: odd layers of TMDs, hBN, or graphene with strong nonlinear optical response for SHG. (d) The right panel: an array of 3D Au helices that blocks the circular polarization with the same handedness as that of the helices but transmits the orthogonal polarization. The left panel: the monolayer TMDs with broken inversion symmetry supporting that the left (right)-handed circularly polarized light only couples to the band-edge transition at K (K') points. (e) The right panel: an Al film-based superoscillatory lens with resolution better than $\lambda/6$. The left panel: the GO ultrathin lenses with a 3D focusing volume of $\lambda^3/5$. (f) The left panel: an atomically thin graphene for surface cloak at THz frequencies. The right panel: a cylindrical metamaterial of an array of copper SRR suppresses the scattering from the hidden object at microwave frequencies.

1. INTRODUCTION

The goal of attaining unconventional physical properties that are not observed in nature has been pursued intensively in recent years. This goal requires a comprehensive understanding of fundamental material physics, mature fabrication techniques, and easily obtainable ingredients. New materials with feasible fabrication and improved properties are sought for optical, electric, and mechanical applications. Conventional approaches such as chemical synthesis, epitaxial growth, and chemical vapor deposition (CVD), focus on controlling growth or synthesis conditions such as temperature, pressure, and components to produce new materials by directly arranging atoms. Alternatively, a novel type of artificial material has been proposed and extensively explored via shaping composite materials into desired architectures or geometries to achieve various unusual and exciting physical phenomena such as negative refraction, diffraction unlimited optical imaging, and cloaking.[1−6] These functional materials with a macroscopically homogenized response are termed metamaterials, which is a new research frontier in fundamental science and engineering that has emerged during the last two decades. A major reason for the widespread enthusiasm in metamaterials is their unconventional properties and phenomena, which are not supported in typical materials observed in nature. The word "meta" means "beyond" in Greek.[7] To differentiate from conventional photonics and optics, we use the words metaphotonics and/or metaoptics when referring to electromagnetic (EM) phenomena associated with metamaterials.

Victor Veselago proposed the concept of negative refractive index in 1967 and predicted the anomalous propagation of EM waves in materials with negative refractive index.[8] The material presenting a negative refractive index requires a negative value of both its permittivity and permeability, where the electric field, magnetic field, and wavevectors follow a left-handed rule, and the group velocity direction is opposite to the phase velocity. Light will be refracted at the side of incident plane defined by the incident wavevector and the normal direction of the interface between a material with a negative refractive index and a conventional material. However, this topic remained a purely theoretical curiosity for several decades because such extraordinary materials do not exist in nature.

https://dx.doi.org/10.1021/acs.chemrev.9b00592
Chem. Rev. 2020, 120, 6197−6246

However, by the end of the twentieth century, researchers realized that both negative permittivities and negative permeabilities can be sustained in the same frequency range after a careful design of the resonance behaviors of the composite unit cells that form the metamaterial.[1−6] As a result, negative refraction was subsequently achieved in several frequency regimes, from the microwave range to the visible range, with exciting applications such as the *perfect* lens.[8−11] In 2006, several groups further envisioned that EM invisibility cloaks can also be achieved with metamaterials devised within the theoretical framework provided by the concept of transformation optics.[12,13] In subsequent years, metamaterials flourished and were extended to other disciplines such as acoustics, thermodynamics, and mechanics.[14]

Metamaterials manifest themselves via novel effects that are rarely observed in naturally occurring materials, such as negative refraction (Figure 1a), optical magnetism (Figure 1b), imaging based on enhanced nonlinear effects (Figure 1c), chirality (Figure 1d), diffraction-unlimited resolution (Figure 1e), and invisibility cloaks (Figure 1f).[14−16] Currently, metamaterials provide a flexible platform to engineer EM phenomena in an artificial way. The essence of the metamaterial concept is the functionality of the unit cells, termed meta-atoms or meta-molecules, which are the building blocks of the metamaterial. To obtain a desired EM response, each unit cell should be carefully designed. These unit cells need to be considerably smaller than the operating wavelength to justify the homogenization model but are also expected to display strong light−matter interactions. Metamaterials are usually designed in a way to work near the resonant EM mode of the unit cell, which inevitably introduces the problem of a finite operation bandwidth and considerable losses from both the composite materials and the associated resonance damping. Therefore, the composite materials that are utilized to build up the metamaterial to reduce losses should be carefully chosen. To boost light−matter interactions in deep subwavelength unit cells, most feasible demonstrations have relied on the use of plasmonic materials or high-index dielectrics. The addition of judicious mechanisms is usually required to dynamically tune their properties, to increase their bandwidth, to enable a nonlinear regime, and if possible, to reduce their size for miniaturized multifunctional metadevices. The exploitation of new advanced materials as the building meta-atoms is critical to fulfill these demanding requirements and fully achieve the promising applications of metamaterials.

The discovery of graphene in 2004 opened a new platform to explore strong light−matter interactions due to its reduced dimensionality (2D). Researchers have predicted that more than 600 potential 2D materials can exist in a stable manner.[17] In general, layered 2D materials can be classified into two groups: 2D allotropes of various fundamental elements such as graphene, black phosphorene,[18−20] and silicene[21,22] and compounds such as transition metal dichalcogenides (TMDs, with general formula of MX_2),[23−25] hexagonal boron nitride (hBN),[26,27] and MXenes (layered transition metal carbides and carbonitrides with the general formula $M_{n+1}X_nT_n$).[28] Graphene and other 2D materials have attracted the attention of science and engineering research communities since 2004 due to their unique optical, electronic, mechanical, and thermal properties.[29−31] One of the most important features of 2D materials is their atomic thickness. As a result, EM energy can be highly confined to an even smaller volume than that associated with conventional surface plasmons (SPs) supported by noble metals, and as a consequence, the quantum limit can be more easily attained.[30,32,33]

Layered 2D materials that support strong light−matter interactions can also be employed as building blocks for designing metamaterials. In conventional metamaterials, a negative refractive index is displayed in 3D cascaded double-fishnet structures that consist of alternating layers of metal and dielectric films with a thickness of $\lambda/40$ at optical frequencies (Figure 1a, left).[4] In these structures, the negative permittivity is provided by the diluted metal part, while the negative permeability is introduced by the strong coupling between EM waves and magnetic resonances (usually termed magnetic polaritons).[34] Similar effects can be realized by stacking alternate layers of graphene and hBN (Figure 1a, right).[35,36] These multilayered graphene/hBN structures are versatile for supporting various effects, such as perfect absorption[37] and polarization selection devices[38] in atom-thick structures, which were not identified in previous approaches using metal−dielectric multilayers.

The magnetic response of materials at terahertz (THz) and optical frequencies is especially important for the implementation of several devices such as compact cavities, adaptive lenses, tunable mirrors, isolators, and converters.[2,39] Standard approaches utilize planar structures that are composed of nonmagnetic conductive resonant elements (such as double split ring resonators, SRRs), of which the geometry should be redesigned to match with the operating frequency range (Figure 1b, left).[2] In particular, these magnetic resonances can be tuned over the entire EM frequency range by scaling the size of the meta-atoms and the period of the array. How this magnetic response can be realized by naturally high-refractive-index layered Te-based 2D materials in the entire mid-infrared (mid-IR) range without requiring any new design has been recently demonstrated (Figure 1b, right).[40,41] The advantages of this 2D material, compared with conventional metal−dielectric metamaterials, are its intrinsic electrical and magnetic responses in the mid-IR range and low ohmic losses as well as the angle-invariant and feasible integration into three-dimensional (3D) volumes. Due to these properties, metamaterial-based devices such as wide-angle lenses and cloaks can be more easily implemented by stacking these naturally occurring 2D materials than the use of standard metal/dielectric multilayers.

Nonlinear optical effects possess an essential position in modern photonic/optoelectronic devices such as lasers, optical switches, and single photon sources. In most materials, nonlinear effects are usually very weak and several orders of magnitude lower than linear effects.[42] Efforts to boost the nonlinearity of metamaterials have been made by constructing high-quality-factor micro/nanocavities that can substantially enhance nonlinear light−matter interactions; however, these effects work in a very narrow band (Figure 1c, left).[43,44] Alternative solutions can be 2D materials that display naturally high nonlinearities, such as graphene.[45] For instance, third-order nonlinear signals in graphene are very strong: tunable third-harmonic generation (THG) and four-wave mixing (FWM) have been recently demonstrated.[46−48] Even more interesting is the phenomenon of second-harmonic generation (SHG), which in principle should be absent in pristine graphene due to its centro-symmetric crystal structure. However, SHG has been observed in trimmed graphene by hybridizing graphene with other materials[49] by electrical/chemical doping[50] or patterning.[51] These intrinsic strong nonlinearities are essential for the use of graphene as a perfect

https://dx.doi.org/10.1021/acs.chemrev.9b00592
Chem. Rev. 2020, 120, 6197−6246

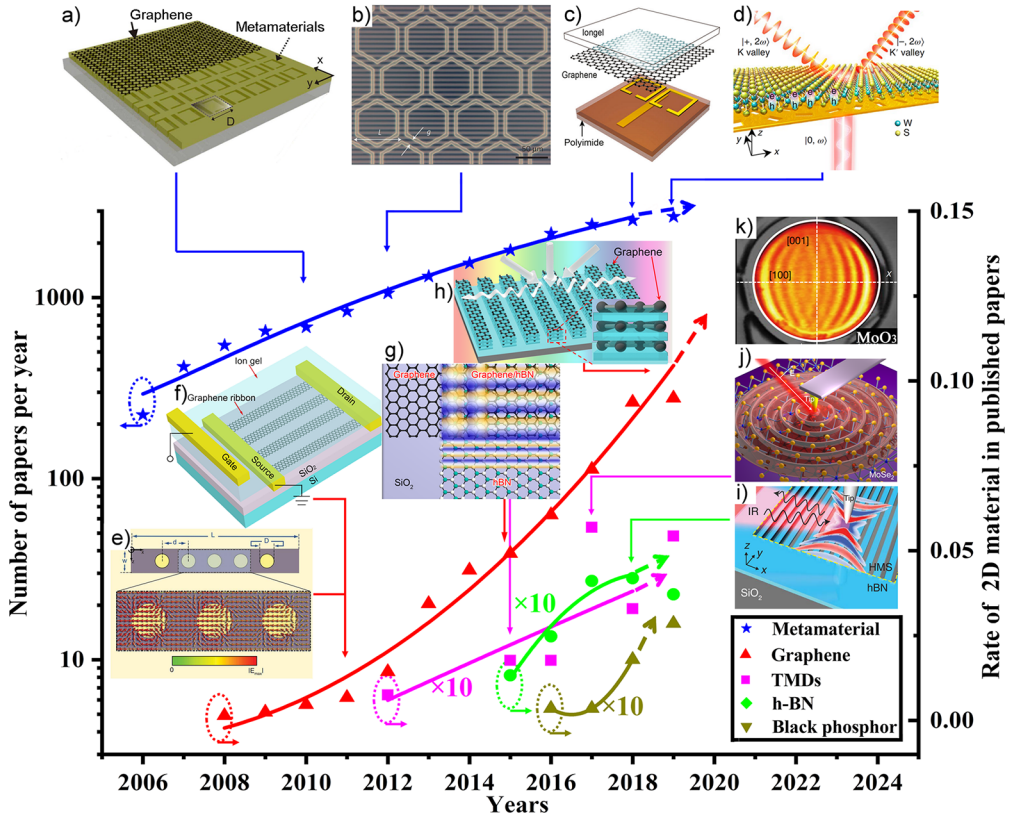

Figure 2. Number of publications per year in the field of metaphotonics (blue line) and the rate of publications relevant to graphene (red line), TMDs (magenta line), hBN (green dots), and BP (dark yellow dots) between January 2006 and December 2019 (data from ISI Web of Knowledge, February 2020). Solid lines represent the exponential growth experienced in these areas. Dashed arrows depict the deliberate speculations of future trends. The insets show the representative studies in the evolution of each research field. Inset images: (a) Monolayer graphene integrated with metamaterials.[80] The addition of graphene greatly enhanced the optical transmission at the resonance frequency linked to the Fano-type plasmonic mode of the SRRs. Reprinted with permission from ref 80, Copyright 2010 Optical Society of America. (b) Graphene integrated with a layer of hexagonal metallic meta-atoms,[81] showing substantial gate induced persistent switching and linear modulation of THz waves. Reprinted with permission from ref 81. Copyright 2012 Nature Publishing Group. (c) Graphene−SRR pair with a cut wire.[82] An active control over the group delay of THz light and the dissipative loss of SRRs could be achieved by the tunable conductivity of graphene via electric gating. Reprinted with permission from ref 82. Copyright 2012 American Chemical Society. (d) TMDs that combine with the Au photonic spin-Hall metasurface,[83] exhibiting simultaneous enhancement and manipulation of nonlinear valley-locked chiral emission in monolayer WS_2 at RT. Reprinted with permission from ref 83. Copyright 2019 Nature Publishing Group. (e, f, and h) Theoretical and experimental results and applications of metamaterials made of layered 2D materials.[79,84,85] The theoretical study (e) demonstrated the transformation optical devices by spatial modulation of the graphene conductivity. Tunable plasmon excitations in engineered graphene microribbon arrays were experimentally realized via electrostatic doping (f). A 90 nm-thick graphene−dielectric metamaterial absorber with ∼85% absorptivity of unpolarized light ranging from 300 to 2500 nm could enable the heating to 160 °C in natural sunlight, ideal for practical application of solar energy harvesting (h). Reprinted with permission from ref 79. Copyright 2011 AAAS. (g) Tunable layered hyperbolic metamaterials,[86] where the graphene−hBN heterostructure supports hyperbolic plasmon−phonon polaritons with low loss and active controllability. (i) IR hyperbolic metasurface based on nanostructured hBN,[13] supporting phonon polaritons with in-plane hyperbolic dispersion. Reprinted with permission from ref 13. Copyright 2018 AAAS. (j) Exciton−polariton transport in $MoSe_2$ flakes,[87] showing thickness-dependent waveguide exciton polariton (down to the wavelength of 300 nm) and excitation-energy-dependent propagation length (up to 12 μm). (k) Natural in-plane hyperbolic layered 2D materials.[88] The semiconducting α-MoO_3 could allow the deeply subwavelength phonon polaritons with ultralong polariton lifetimes. Reprinted with permission from ref 88. Copyright 2018 Nature Publishing Group.

building block for designing nonlinear and tunable metamaterials when combined with either other 2D materials or subwavelength metastructures (Figure 1c, right).[52−61]

In a different scenario, chirality exists in macrostructures and microstructures associated with optical polarization rotation and circular dichroism. This effect can be used not only to detect and analyze secondary structural information and conformation of molecules but also for applications in engineering and modulation of optical fields.[62] However, the optical chirality of naturally occurring 3D materials is very weak, and therefore, most current approaches depend on metamaterials for devising chirality-based applications in optics and nanophotonics (Figure 1d, right).[63−65] Constructing atomically smooth chiral materials for developing novel nanodevices remains challenging due to the limited fabrication accuracy. These limitations and shortcomings can be overcome using 2D materials. For example, by stacking graphene layers with a slight difference in the orientation of the lattices, the coupling between the incident magnetic field and a magnetic dipole moment in the twisted graphene layers would depend on the helicity of the incident light, which causes the emergence of circular dichroism.[66−68] Similarly, chiral atomically thin films can be achieved with other 2D materials.[69] In addition to the optical responses that are controlled by the

https://dx.doi.org/10.1021/acs.chemrev.9b00592
Chem. Rev. 2020, 120, 6197−6246

helicity of incident photons, engineering the electron behavior in 2D materials also produces two novel areas of research: spintronics and valleytronics. Spintronics are associated with the spin of electrons,[70,71] whereas valleytronics take advantage of the electronic valley degree of freedom (DoF) (Figure 1d, left)[72−74] to store and carry information, which can also be synthesized with optical metamaterials.

By further employing advanced nanofabrication technologies, 2D materials can also be patterned to display other interesting and promising EM responses. For example, ultrathin ($\lambda/5$) lenses that are constructed of graphene oxide (GO) can focus a 3D subwavelength spot ($\lambda^3/5$) in the far field (Figure 1e, left).[75] Making an object electromagnetically invisible is one of the most exciting achievements using metamaterials.[76−78] By designing the unit cells with SRRs of different sizes to simultaneously support both electric resonances and magnetic resonances,[9] an impinging EM wave is restored by the cloaking layer after the hidden target (Figure 1f, right). However, large intrinsic material loss deteriorates the cloaking effect.[76] Conversely, due to the low loss and strong field localization, graphene can be used as an excellent building material for designs based on transformation optics.[79] The ability of a single layer graphene in either a planar or cylindrical form to hide an object in a narrow band THz frequency has been recently demonstrated (Figure 1f, left). By electrically or chemically tuning the Fermi level, the cloaking effect can be readily shifted from THz frequencies to the far-IR spectral range.

Research on the potential of 2D materials remains a prominent area in both fundamental science and practical engineering. The number of scientific papers that are published per year to study the photonic properties of 2D materials is exponentially increasing (Figure 2), in addition to exploration in other fields such as electronics, mechanics, and chemistry. With the development in fabricating 2D materials and tuning their properties, 2D materials should have exciting applications in multiple disciplines.

In this review, we introduce the metaoptics/metaphotonics properties of 2D materials and their fabrication and feasible applications by comparing them with conventional metamaterials. We illustrate the potential of naturally occurring 2D materials as perfect candidates to build new metamaterials in a synthetic way. Metamaterials and 2D materials can benefit each other and enable compound multifunctional devices to surpass their individual composites.

2. OPTICAL PROPERTIES OF LAYERED 2D MATERIALS TO INSPIRE METAMATERIALS

2.1. Natural Metamaterials

2.1.1. Natural Hyperbolic Dispersion in 2D Materials.

Hyperbolic materials have attracted substantial attention in recent years due to their ability to control the propagation of EM waves and their interactions with matter, which cause extreme anisotropy in their electrical responses.[89−91] In nonmagnetic and uniaxial hyperbolic materials,[92] the magnetic permeability tensor reduces to a unit tensor, while the permittivity tensor can be expressed after diagonalization as follows:

$$\hat{\varepsilon} = \begin{bmatrix} \varepsilon_\perp & 0 & 0 \\ 0 & \varepsilon_\perp & 0 \\ 0 & 0 & \varepsilon_\parallel \end{bmatrix} \tag{1}$$

where the subscripts ∥ and ⊥ indicate components parallel and perpendicular, respectively, to the optical axis (chosen as the z-axis). Therefore, the dispersion relation for the EM waves that propagate in the bulk of a nonmagnetic hyperbolic material can be written as follows:[91,92]

$$\frac{k_x^2 + k_y^2}{\varepsilon_\parallel} + \frac{k_z^2}{\varepsilon_\perp} = \left(\frac{\omega}{c}\right)^2 \tag{2}$$

where k_x, k_y and k_z are the wavevectors along the x direction, y direction and z direction, respectively; ω is the angular frequency; and c is the speed of light in a vacuum. For a metal or any other material with a negative permittivity ($\varepsilon_\perp$, $\varepsilon_\parallel < 0$), the medium does not support propagating EM waves in the bulk, and as a consequence, no real wavevector can be obtained from eq 2.[89] For isotropic materials with positive permittivity, i.e., $\varepsilon_\perp = \varepsilon_\parallel > 0$, EM waves can propagate inside the material but with a finite wavevector (Figure 3a), which

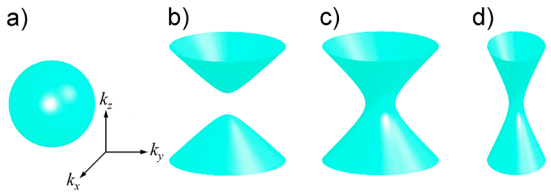

Figure 3. Isofrequency dispersion given by $\omega(k)$ = constant in a 3D k-space for an (a) isotropic medium ($\varepsilon_\perp = \varepsilon_\parallel = \varepsilon_x = \varepsilon_y > 0$) and a hyperbolic medium with (b) type I ($\varepsilon_\perp > 0$, $\varepsilon_\parallel < 0$) and (c) type II ($\varepsilon_\perp < 0$, $\varepsilon_\parallel > 0$) responses. (d) Elliptical medium ($\varepsilon_x = \varepsilon_\parallel \neq \varepsilon_y > 0$, $\varepsilon_\perp < 0$).

explains the diffraction-limited imaging in the far-field. The photonic density of states (PDOS) is also finite due to the finite volume between two isofrequency surfaces in isotropic dielectrics.[89−91] In anisotropic materials, the propagation of EM waves critically depends on the propagation direction. In the case in which $\varepsilon_\perp$ and $\varepsilon_\parallel$ have opposite signs, the dispersion relation follows a hyperbolic behavior, from which the name "hyperbolic material" is coined. According to the signs of these two permittivities, the hyperbolic dispersion can be categorized into two types: type I with $\varepsilon_\perp > 0$ and $\varepsilon_\parallel < 0$, and type II with $\varepsilon_\perp < 0$ and $\varepsilon_\parallel > 0$. In principle, for both types of hyperbolic materials, wavevectors can be extremely large inside the bulk with an upper limit at the edge of Brillouin zone, which is determined by the size of the hyperbolic unit cell (Figure 3b, c). This implies that deep subwavelength geometrical information can be recovered in the far-field of hyperbolic metamaterials in principle, which enables the hyperlens.[93−95] Recently, we reported a third type of hyperbolic medium, in which $\varepsilon_x = \varepsilon_\parallel \neq \varepsilon_y > 0$, $\varepsilon_\perp < 0$ (Figure 3d); it is referred to as an elliptical hyperbolic medium due to this peculiar relation among the components of the electrical permittivity tensor.[88] In all hyperbolic media, the extremely infinitely large wavevectors that are supported within the bulk also generate a strong light−matter interaction that is associated with these highly confined EM fields.[13,89] However, this divergent behavior cannot occur in reality because large wavevectors will be eventually cut off when the wavelength of the

https://dx.doi.org/10.1021/acs.chemrev.9b00592
Chem. Rev. 2020, 120, 6197−6246

corresponding propagating EM mode is comparable to the size of the hyperbolic unit cell a. Therefore, the resultant maximum wavevector that is attainable in hyperbolic materials is of the order $1/a$. In addition, the propagation of EM waves follows an angle that is defined as $\theta = \text{atan}((-\varepsilon_{\perp}/\varepsilon_{\parallel})^{1/2})$, which is very different from the isotropic propagation in normal media.[31] From an applied point of view, the peculiar properties of dispersion relation associated with hyperbolic media have been exploited for novel applications such as negative refraction,[96,97] light emission,[98,99] thermal radiation,[100−103] and sensing.[104,105]

Due to the extreme anisotropy needed for both dielectric components and metal components to achieve a hyperbolic dispersion, hyperbolic media are rare in nature. Thus, a substantial amount of attention has been focused to structured materials (metamaterials) using layered metal−dielectric structures or metal wire arrays embedded in a dielectric host. In these cases, the total response can be described using an effective medium theory, which is valid only when the long wavelength approximation is satisfied.[106] However, the finest feature achieved using state-of-the-art fabrication technologies is typically 10 nm, which limits the maximum value for the attainable wavevectors that can propagate inside the media (refer to previous discussion).

The recent discovery of layered 2D materials has been revealed with the hyperbolic response of superior performances, such as low loss and broadband operations, compared with those displayed by hyperbolic metamaterials.[107,108] For example, a hyperbolic equifrequency dispersion is observed in crystalline graphite in the ultraviolet (UV) range using ellipsometry.[109] When the electric field is polarized along the graphene plane, the hybrid resonance of π- and σ-electrons generates a negative permittivity. However, when the electric field is perpendicularly polarized to the graphene plane, the forbidden π bands produce a positive permittivity. Graphite-like materials such as magnesium diboride (MgB_2) also support hyperbolic dispersion in the blue and UV range of the EM spectrum.[110] Other compounds such as superconductor-type cuprates[108] and perovskite-like ruthenates[111,112] can also display hyperbolic dispersion according to the ratio of the constituent elements, with operation frequencies that range from UV to THz. In general, the origin of hyperbolic dispersion in these 2D materials can be categorized into three groups depending on the combination between the metal components and the dielectric components (Figure 4). For either metals or dielectrics, the sign of the permittivity is opposite at the two sides of the plasmon frequency.

Recently, 2D van der Waals (vdW) materials have emerged as feasible candidates for hyperbolic EM responses with unit cells reduced to the atomic level. EM fields strongly interact with 2D materials, and the resulting hybrid entities are usually referred to as *polaritons*. Depending on the type of quasiparticle that is coupled to the EM field, polaritons may be plasmon polaritons, phonon polaritons (PhPs), or exciton polaritons.[30,88,113] These polaritons can form at the frequency range of interest, which generally occur in most 2D materials. Surface plasmon polaritons (SPPs) exhibit low-loss and broadband performance from THz to IR frequencies, and feasible tunabilities in 2D materials, for example, graphene.[30] PhPs have been demonstrated in a few layers of hBN, which exhibit hyperbolic features.[114] Excitons, the electron−hole combinations, are observed in all 2D materials that support an electronic band gap, which has prompted an increasing interest

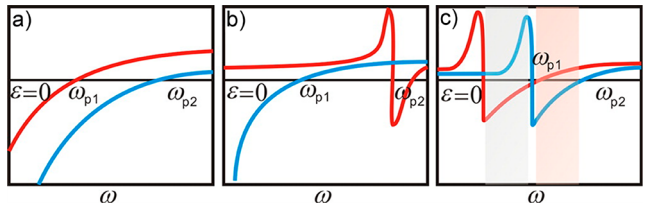

Figure 4. Basic mechanisms of the intrinsic hyperbolic medium. (a) Drude type, conductance along all orientations of the crystal in the incident plane is metallic but with different conductive ability; (b) Drude−Lorentz type, the conductances along different orientations are very different from each other; and (c) Lorentz type, conductance properties along all orientations are dielectric.[108] Here, ω_{p1} and ω_{p2} in each dielectric spectrum refer to the two different plasma frequencies; the permittivity tensor in the frequency range between ω_{p1} and ω_{p2} is indefinite, leading to the negative refraction of the incident light waves. Reprinted with permission from ref 108. Copyright 2014 American Chemical Society.

in different research communities.[115] A detailed discussion of the capabilities of both SPPs and PhPs to enable high-performance metamaterials and metasurfaces (M&Ms) is provided in Sections 2.2 and 2.3, and interested readers can explore recent reviews for an in-depth understanding of the exciting possibilities of excitons in 2D materials.[115,116]

Hexagonal boron nitride, which is a potential optoelectronic material for light emission and detection in the deep UV frequency range,[26,117,118] can support hyperbolic PhPs at mid-IR frequencies with low loss. This 2D material presents metallic (negative permittivity) and dielectric (positive permittivity) EM responses along orthogonal principal axes (Figure 5a).[13,113,114,119−121] Not only the volume-confined bulk hyperbolic polaritons[114] but also sidewall-confined hyperbolic surface polaritons[120,122] are detected in hBN. The optical phonon modes of this material present two widely separated stopbands that are induced by its light atomic masses, strong out-of-plane anisotropy and the polar band between B and N. The out-of-plane crystal vibrations (transverse optical phonon, TO) produce type I hyperbolic responses, whereas the in-plane vibrations (longitudinal optical phonon, LO) produce type II hyperbolic behaviors. Due to its inherent layered structure, the hyperbolic PhPs modes can even be supported by hBN flakes with thicknesses of approximately 1 nm, which implies an unprecedented potential in breaking the fundamental limit of photon confinement in hyperbolic EM modes.[31,114]

Recently, a family of natural electrodes such as Ca_2N were theoretically demonstrated to support high-performance hyperbolicity with low loss and a broad operation band that ranges from the near IR regime to the mid-IR frequency regime. Their hyperbolicity can be tuned by strain and can even be switched between an elliptic response and a hyperbolic response for a particular frequency range.[125] Layered TMDs can support a large variation of controllable hyperbolicity that ranges from near IR to UV by stacking different types of 2D TMDs.[126]

Note that the hyperbolic response in hBN arises from anisotropic phonon modes, which are produced by the hybridization of longitudinal phonons with transverse phonons by quasi-static Coulomb interaction mediated by large momentum photons. In the next section, we introduce the propagation characteristics of in-plane anisotropic PhPs in 2D layered materials.

https://dx.doi.org/10.1021/acs.chemrev.9b00592
Chem. Rev. 2020, 120, 6197−6246

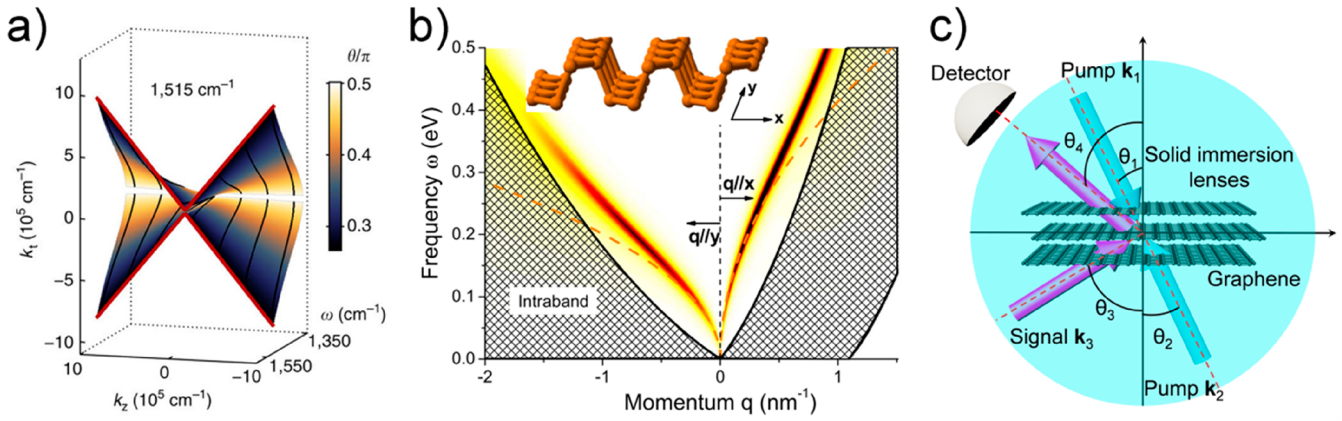

Figure 5. Optical properties of inspired metamaterials composed by layered 2D materials. (a) Hyperbolic dispersion of hBN polaritons.[123] The axes refer to the tangential momentum k_t, the axial momentum k_z, and the frequency ω. The momentum−frequency dispersion surface for the hyperbolic polaritons of the upper band (ranging from 1370 to 1515 cm^{-1}) resembles a "butterfly" composed of individual hyperbolas. Reprinted with permission from ref 123. Copyright 2015 Nature Publishing Group. (b) Energy loss and plasmon dispersion of BP.[124] The loss function was calculated for monolayer BP with an electron doping of 10^{13} cm^{-2} and T = 300 K. $q_{\|x}$ and $q_{\|y}$ refer to q along the two crystal axes x (right) and y (left), respectively. Shaded regions are the Landau damping regions. The plasmon disperses differently due to their mass anisotropy, where the smaller mass along x leads to higher resonance frequency. Reprinted with permission from ref 124. Copyright 2014 American Physical Society. (c) Illustration and experimental verification of optical negative refraction in graphite thin films.[35] Two pump beams k_1 and k_2 are focused on atomic graphene layers (honeycomb lattice) at angles θ_1 and θ_2, respectively. The incident beam k_3 is refracted in the negative direction and detected by a photodetector. The refracted beam exhibits a resonance at $\theta_3 = \theta_4$; that is, the incident signal beam is refracted in the negative direction.

2.1.2. Natural Anisotropic Polaritons in 2D Materials. Propagation of anisotropic polaritons along the surface of layered 2D materials is caused by an in-plane anisotropic structure and electronic and/or optical phonons characteristics. In these materials, in-plane elliptical and hyperbolic polaritons can be supported, which causes an increased PDOS and ray-like propagation along the surface. Recently, we reported the experimental observation of anisotropic PhPs that propagate in α-MoO_3, which is a natural layered 2D material (Figure 1k).[88] PhPs in α-MoO_3 are highly confined with a wavelength of $\lambda_0/120$ (λ_0, free-space wavelength of photons); its hyperbolic EM response can be tuned by altering the thickness of the 2D flakes. Furthermore, real-space imaging with scattering-type scanning near-field optical microscopy (s-SNOM) has confirmed the long lifetime of hyperbolic PhPs (8 ps), which is ten times longer than the counterpart of graphene SPPs at room temperature (RT) and four times longer than the best values obtained for PhPs in isotopically engineered hBN.[127] In-plane anisotropic α-MoO_3 PhPs add a new member to the ever-increasing list of polaritons in 2D layered materials.[88]

SPPs, which are quasi-particles formed by photon and collective oscillations of electrons, have been observed in graphene via direct IR nanoimaging, which enables the exploration of plasmonics in 2D vdW materials.[128,129] Recent theories predict in-plane anisotropic and even hyperbolic SPPs in naturally layered black phosphorus (BP) without the need for nanostructuring due to its inherent in-plane anisotropy in their electronic and structural properties (Figure 5b). Although BP has a relatively isotropic static screening, its band nonparabolicity produces highly anisotropic SPPs with resonance scaling via doping concentration. The calculated dispersion in Figure 5b for monolayer BP presents two distinct in-plane loss functions, where the SPP that propagates along the y direction is damped at mid-IR frequencies, while the SPP that runs along x persists to the near-IR frequency range. The SPP modes that propagate along one of the crystallographic directions of BP are long-lived because they are Landau-damped only for near-IR frequencies. The anisotropic plasmonic effects are also expected in Weyl semimetals.[130] Layered transition metal chalcogenides such as $MoTe_2$ and WTe_2 also show anisotropic vibrational and electronic characteristics, which indicates the potential to be natural anisotropic plasmonic materials.[131]

2.1.3. Natural Negative Refraction in 2D Materials. In principle, negative refraction can be supported by any anisotropic material but is usually unobservable due to the currently small anisotropy.[108,132] In contrast to negative refraction in metamaterials, where both electric and magnetic resonances are involved in generating negative permittivities and permeabilities, nonresonant hyperbolic materials can support negative refraction, which presents lower loss and broader operation bandwidth, as previously discussed. Negative refraction, for example, can be achieved at the interface between a vacuum and a type II hyperbolic material because the tangential component of the averaged Poynting vector for the transmitted wave can be expressed as follows:

$$S_x^t = \frac{\omega \varepsilon_{\|}}{2\pi k_x} |H_y|^2 < 0 \tag{3}$$

Therefore, the incident light will be refracted with a negative angle if $\varepsilon_{\|}$ is negative.[105]

The widespread approaches to achieve negative refraction, such as the use of plasmonic materials and nonlinear components, usually suffer from strong dispersion with the incident angle, high loss and limited bandwidth. Interestingly, 2D materials such as graphene exhibit large optical nonlinearities with extremely low absorption; for example, the third-order nonlinear susceptibility of graphene is two orders of magnitude larger than that of gold (Au). Combined with their low surface scattering due to their atomic smoothness, layered 2D materials can act as inherent negative refraction materials at optical frequencies. Graphite thin films have shown a controllable negative refraction as demonstrated using degenerate FWM (Figure 5c).[35] The graphite surface enables

https://dx.doi.org/10.1021/acs.chemrev.9b00592
Chem. Rev. 2020, 120, 6197−6246

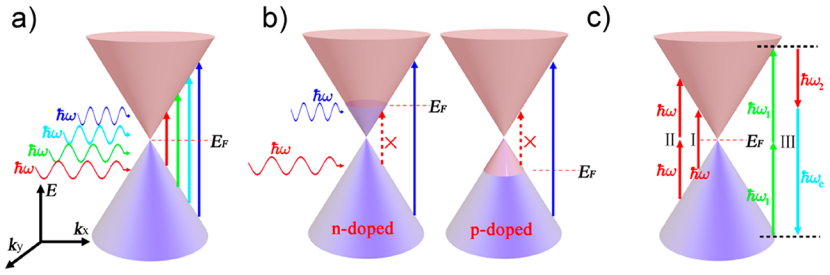

Figure 6. Interaction of light with graphene. (a) Interband transitions occur at visible to IR. (b) In n-doped and p-doped graphene, an optical photon with energy less than $2E_F$ cannot be absorbed due to Pauling blocking and lack of electrons available for the interband transition, respectively. (c) One-photon (I) and two-photon (II) absorption process and FWM process (III). E_F and $\hbar\omega$ refer to Fermi level and optical photon energy, respectively.

highly efficient phase conjugation, which can reverse the phase of the EM fields by acting as an analogue of a negative index boundary. The negligible thickness of the layers causes very low optical loss in this structure, and the linear band structure of graphene further enables broadband operation, in principle from radio frequencies to gamma ray frequencies. Moreover, hBN with hyperbolic properties can support negative refraction in the upper band. However, its high reflective index causes transmission.[123] By alternatively stacking graphene and hBN, a negative refraction with improved efficiency can be achieved.[36]

2.2. Optical Transitions in Layered 2D Materials for Advance Metamaterials

As mentioned in this review, conventional M&M constructed of plasmonic metals (such as Au, silver (Ag), copper, and aluminum (Al)) and/or dielectric materials (silicon and titanium dioxide) usually work in a very narrow band, especially in the visible and near IR range; their geometries and EM performances cannot be easily tuned once fabrication is complete.[133−137] The nonlinear properties of M&M depend on the intrinsic microscopic nonlinear polarizabilities of the constituent materials, which are usually weak compared with layered 2D materials and their low damage threshold with strong pumping intensity. These problems hinder various applications that require the broadband and tunable nonlinear M&M.[138−140] Inspired by the remarkable EM properties in 2D materials such as pristine graphene, hBN, BP, and TMDs, which usually display tunable intraband and interband transitions and large nonlinearities, we envision that these 2D materials can be very important for circumventing the previously mentioned disadvantages of the metal/dielectric framework for constructing M&Ms.

In this section, we illustrate the opportunities that facilitate the promise of 2D materials as perfect candidates for advanced M&M applications. We review the fundamentals of the broad spectrum of light−matter interaction in 2D materials, which range from the UV range to the IR frequency range and from the linear regime to the nonlinear regime, in which feasible approaches can be easily applied to tune light−matter interactions via electrical gating, chemical doping, strain, background dielectric environment, and stacking orders.

2.2.1. Broadband Spectra of Light−Matter Interactions. The past two decades have witnessed the tremendous efforts of searching M&M from the microwave, IR, and visible range to the UV frequency range. To establish the promise of 2D materials as the meta-atoms of M&M, a broadband light−matter interaction should be required; this interaction is possible by carefully selecting appropriate 2D materials from its burgeoning family, such as graphene, TMDs, BP, perovskites, Mxene, layered metal oxides, and metal carbides, according to their electronic band structures that determine the associated optical properties.

For example, graphene, which is the most investigated and the first experimentally demonstrated 2D material, has a zero band gap and linearly supports dispersed massless Dirac Fermions near the Dirac point, where the conduction and valence bands meet (Figure 6a). This consequence is attributed to the sp^2 hybridization between 2s electron orbitals and two 2p electron orbitals of carbon in the 2D hexagonal lattice. For a large range of photon energies, the absorption ($\pi\alpha \cong 2.3\%$, $\alpha = 1/137$ is the fine structure constant) and transmission ($1 - \pi\alpha$) will remain nearly constant, which are solely determined by $\alpha = e^2/\hbar c$ (c is the speed of light in free space, and $\hbar$ is the Planck's constant).[141−143] In this case, the absorption of a weakly coupled few-layer graphite (N layers) can be simply estimated by the scaling law: $N\pi\alpha$. The constant absorption of light in graphene can also be explained by the dynamic excitation process (Figure 6a). Electrons in the valence band can be excited into the conduction band; those hot electrons will thermalize and cool until a hot electron−hole equilibrium distribution with the electronic temperature T_e is attained after the short excitation process (approximately 150 fs).[144] The new distribution of electron−hole pairs blocks further absorption of light, whose energy is $k_B T_e$ within 1 ps. Subsequently, the intraband scattering through phonons will cool the thermalized quasiparticles, and the interband electron−hole recombination process will dominate. With large excitation intensities, saturated absorption will occur, which produces a transparency window for light at energies immediately above the band-edge and cause constant absorption of graphene.[145] These schemes of light−matter interaction can occur in an amazingly broad band from the microwave band to the THz band and IR frequency regimes and even to the optical range due to the zero bandgap near Dirac points. This broadband constant absorption in pristine monolayer graphene can be extremely useful in the design of ultrabroadband M&Ms, where light modulators, sensors, or photodetectors can be realized (refer to Section 4.6).

Different from semimetal graphene, some other 2D materials support a moderate electronic band gap, which behaves as a monolayer semiconductor for IR and optical frequencies. For instance, BP has a layer-dependent direct band gap that monotonically increases from 0.3 eV in its bulk form for larger than 8 layers to 2 eV for a monolayer.[146,147] This fascinating feature originates from the self-energy correlation in its vdW bonding, which can enable strong interactions with EM waves and can be used for photodetection or imaging applications

https://dx.doi.org/10.1021/acs.chemrev.9b00592
Chem. Rev. 2020, 120, 6197−6246

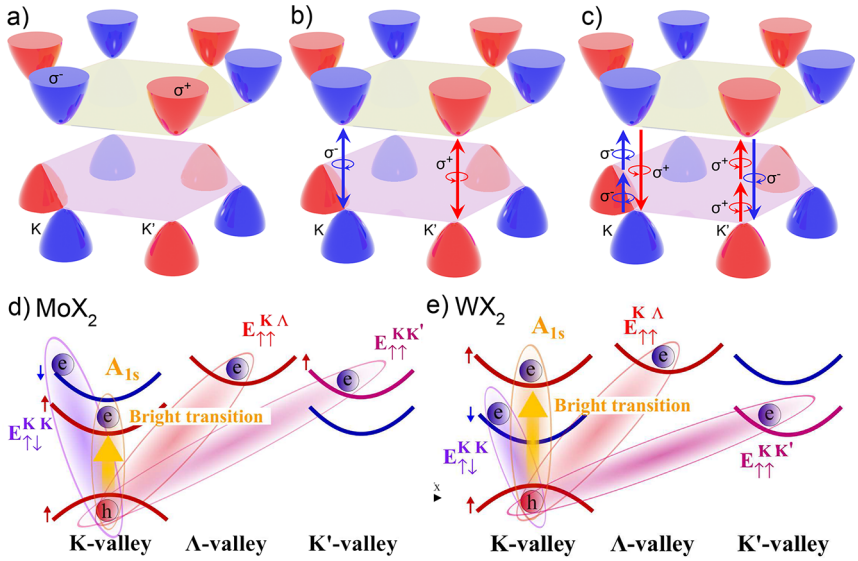

Figure 7. Light interactions with TMDs at its valleys. (a) Valence band of MoS_2, conduction band of MoS_2, and the degree of circular polarization (σ^- and σ^+) of the interband transitions.[74] (b) Spin-related absorption and photon generation of valley excitonic photoluminescent emission.[73] The left (right)-handed circularly polarized light σ^+ (σ^-) only couples to the band-edge transition at K (K') points due to the angular moment conservation and time reversal symmetry. (c) SHG selection rule with the spin valley-exciton-locking phenomenon.[157] Two left circular σ^- (right-circular σ^+) photons at the fundamental frequency (ω) generate a single right-circular σ^+ (left circular σ^-) photon at the second-harmonic frequency (2ω) with near-unity polarization. (d, e) Schematic energy-band structures around the K and Λ valley for (d) MoX_2 and (e) WX_2 (X = S and Se). The highest valence and the lowest conduction band have the opposite spin. The red and blue curves represent the spin-up and spin-down bands, respectively. The spin-down valence band is not presented because it is ∼100 meV away from the energy of B excitons that are not shown here. The lowest optically induced transition between the bands of the same spin is described as the yellow arrow at the K point. The correlated electron−hole pairs are enclosed by a yellow (bright A_{1s} exciton), red and orange (momentum-forbidden dark $K-\Lambda$ and $K-K'$ exciton, respectively) and purple ovals (spin-forbidden dark $K-K$ exciton).[158] Reprinted with permission from ref 158. Copyright 2018 American Physical Society.

from the mid-IR range to the visible range.[18,148,149] Another interesting property of BP is its in-plane anisotropy that is derived from the atomic bonding in two inequivalent directions, which renders BP as transparent for light polarized along the zigzag direction and highly absorbing for light polarized along the armchair direction.[146,147,150,151] Anisotropic M&Ms have been searched, and the intrinsic strong anisotropy of BP presents a natural solution with a high sensitivity to the linear polarization angle and the momentum vector,[124,146,152] which can produce more sophisticated applications if its structure is properly designed. As discussed in Section 2.1, the intrinsic electric permittivity of unstructured BP displays different signs along the two directions. This property is very appealing because it supports hyperbolic surface waves, which act as a natural hyperbolic metasurface[152] and can reduce the demanding fabrication requirements of conventional hyperbolic metasurfaces constructed of Ag[153] or graphene nanoribbons.[154]

TMDs usually exhibit a direct electronic band gap in the visible range (1.0−2.5 eV), and therefore, are excellent candidates for next-generation optoelectronic applications such as light-emitting devices (LEDs) and photodetectors. They usually share the chemical formula AB_2, where A represents Mo, W, or Ta and B denotes S, Se, or Te. Similar to BP, TMDs also have in-plane anisotropy due their inequivalent in-plane atomic bonding, and their band gaps depend on the layer number due to their weak vdW force and interlayer hybridizations among different layers.[24,155] The most interesting property of TMDs perhaps is its valley DoF.[72−74,156] The broken time-reversal symmetry in monolayer TMDs cause two energetically degenerate band gaps at the extrema of the conduction and valence bands in the hexagonal Brillouin zone: the valleys (Figure 7a, b). These two valleys, however, have opposite Berry curvatures, and consequently, different valley pseudospins. As a result, each valley can only interact with one of the specific spin angular momenta of light and manifests in a spin-valley-locked light−matter interaction that operates for both absorption of photons and emission of photons.

Owing to the complex electronic band structure consisting of multiple spin-split valleys, dark excitonic states that are inaccessible by light (refer to Figure 7d, e) can be formed.[158] Dark exciton states play a formerly unpredicted but significant role in determining the degree of polarization of the photoluminescence (PL) emission from TMDs. Intervalley scattering, which is dominated by the electron−hole exchange interaction, is active only for bright excitonic states. A dark exciton ground state offers a vigorous reservoir for valley polarization, which helps to maintain a Boltzmann distribution of the bright exciton states in the same valley via intravalley scattering between bright and dark excitons. Because the spin−orbit coupling can be positive or negative in the TMDs material, there are potentially two different orderings of spin states: (1) while in MoX_2 TMDs (X = S, Se), electrons in the lowest conduction band have the same spin as those in the highest valence band; (2) an opposite spin ordering have the same spin in WX_2 TMDs, as shown in Figure 7d, e.[158] In WX_2 TMDs, in which the dark exciton is the ground state, 20−40% polarization can be achieved, even without resonant excitation. By contrast, the MoX_2 TMDs with bright exciton ground states require almost resonant excitation to achieve the same polarization degree.[159] Furthermore, the dependence of the degree of polarization on the detuning energy of the excitation

https://dx.doi.org/10.1021/acs.chemrev.9b00592
Chem. Rev. 2020, 120, 6197−6246

in $MoSe_2$ suggests that the electron−hole exchange interaction dominates over the mechanism of two longitudinal acoustic phonon emission for inter valley scattering in TMDs.[159] Past efforts to search M&Ms with spin-dependent applications have focused on stacking nanostructures or building 3D meta-molecules,[68,160] while natural TMDs with the valley DoF enables applications such as circular dichroism[74] by taking advantage of the spin-valley-locking phenomenon.

Interestingly, an indirect quasi-particle gap with the conduction band minimum located at the *Q*-point (instead of *K*) was observed in single layer WSe_2 as resolved by a comprehensive scanning tunneling spectroscopy approach, albeit the two states are nearly degenerated.[161] The optical properties of TMDs are widely dominated by excitons, Coulomb-bound electron−hole pairs. These quasi-particles show huge oscillator strength and give rise to narrow-band, well-pronounced optical transitions.[162] Studies of strong light−matter coupling in layered TMDs demonstrate outstanding progress. This strong coupling regime emerges in different cavity systems such as planar microcavities and structures contain metallic components.[163]

In addition to BP and TMDs, 2D metal halide perovskites also own layer-dependent electronic band gaps that encompass the entire visible EM range, which are highly promising for LEDs and solar cells. An interested reader can explore additional details about the optoelectronic properties of 2D metal halide perovskites in other in-depth reviews.[164] The electronic band gap of these 2D materials can be very large, which render these materials perfect insulators for deep UV light sources. hBN can also support band gaps as large as 6 eV.[26,165] Although its bulk form was first recognized as an excellent smooth substrate for encapsulating graphene,[33,166] that the use of its 2D form as a gate dielectric and the use of their defects, while acting as color centers, as quantum single-photons sources, were rediscovered.[33]

2.2.2. Tunable Properties of 2D Materials. Efforts in establishing tunable and reconfigurable M&Ms for dynamic functionalities are ongoing. EM properties of meta-atoms constructed of noble metals, semiconductors (such as indium tin oxide, ITO), or dielectrics can be modified by doping, for example.[167] However, the doping level cannot be easily tuned once fabrication is complete. In a few successful examples, tunable M&Ms resort to modification via heat, in the case of phase changing materials,[168] chemical reactions such as hydrogenation or dehydrogenation of Mg,[169,170] or electrostatic doping of ITO[171] and other materials.[172−174] Despite these efforts, the feasibility of tuning material properties to determine the EM response of M&Ms remains weak, especially when it requires both a broadband frequency range and an active modification. Therefore, 2D materials are excellent candidates for building tunable M&Ms because their properties can be easily modified via many external means such as chemical doping, electrical control, thickness or number of layers, background environment, strain, and temperature.

As an exemplary case, optoelectronic properties of graphene can be tuned by chemical doping or electrical bias. The density of carriers (n) and its Fermi level ($E_F = \hbar v_F \sqrt{n\pi}$) can thus be modified at will (Figure 6b). Here, v_F (approximately 10^6 m/s) denotes the Fermi velocity of the electron. With excitation energies less than $2E_F$, no photon can be absorbed in the interband transition because all electron states in the conduction band are occupied (for n-doped graphene) or because no electrons are available in the valence band (for p-doped graphene). For slightly doped graphene, this finding implies that only intraband transitions will contribute in the THz range ($2E_F > \hbar\omega$, ω is the angular frequency), where the interband transition is forbidden. At higher frequencies such as the visible and IR range, the intraband and interband channels compete with each other and the interband transition usually dominates the EM response of graphene. From a physical point of view, the contributions of interband and intraband electronic transitions in graphene can be included in a Kubo-like formula, as derived with the random-phase approximation as follows:

$$\sigma = \sigma_0 \frac{8E_F}{h} \frac{i}{\omega + i\gamma} + \sigma_0 \left[\Theta(\hbar\omega - 2E_F) + \frac{i}{\pi} \ln \left| \frac{\hbar\omega - 2E_F}{\hbar\omega + 2E_F} \right| \right] \tag{4}$$

where the first term applies to the contribution of the intraband transitions within a Drude model and the second term corresponds to the interband transition.[175,176] Here, γ is the finite relaxation rate of the intraband transition process and $\sigma_0 = e^2/4\hbar$, where e is the electron charge. With photon energies approaching $2E_F$, the loss associated with interband transitions becomes dominant in the visible and IR frequency regimes, which causes constant absorption in this EM range, as previously discussed. By tuning the Fermi level, a person can dynamically modulate the properties of graphene, and a transition from a metal to an insulator character can be induced. Ways to change the Fermi level includes gate biasing[177,178] or chemical doping such as boron and nitrogen.[179−182] Tunable M&Ms based on graphene that presents a dynamical control of the Fermi level can be designed in the THz frequency range, where intraband transitions dominate.[183] Furthermore, a waveguide platform can be introduced to graphene by turning on/off the interband transition to design an optical modulator in the near-IR frequency range.[184] This electrical control or chemical doping can also be applied to bandgap materials such as BP[185] or TMDs.[186,187] The basic physics of this procedure is to modify the electron/hole carrier density and the Fermi level in the system. In this way, polaritonic modes such as SPs or exciton polaritons[187] can be tuned.

Layer dependence is another feasible approach to tune the EM properties of 2D materials. Vertically stacked atomically thin materials are bonded by vdW forces. Therefore, the bandgap, absorption and dispersion of the EM modes supported by 2D materials can be changed by altering the number of layers. As previously discussed, the bandgap and exciton binding energies of the BP[124,146,152] and TMDs[155,188] also vary as a function of the number of layers. Absorption of light is proportional to the number of layers of graphene. More interestingly, stacking can also change the symmetry of 2D materials. For example, an odd number of layers of graphene and TMDs produce centrosymmetric structures, while an even number of layers breaks the inversion symmetry of the system. This property significantly affects their nonlinear properties because only noncentrosymmetric materials can support SHG, which will be further discussed in the next section. Researchers are increasingly interested in stacking monolayers that are constructed of different 2D materials to construct vertical heterostructures[189] that support hybrid polaritons-like graphene−hBN layers.[86,190] In addition, recent studies suggest a rich physics in Moiré structures, in which superconductivity in bilayer graphene can emerge at magic angles, depending on the

https://dx.doi.org/10.1021/acs.chemrev.9b00592
Chem. Rev. 2020, 120, 6197−6246

rotation angle between different monolayers,[191,192] and suggest that Moiré excitons with unconventional properties are supported.[189,193−196]

The properties of materials that surround 2D materials are also responsible for the EM performances of the resulting structures. Among these properties, we highlight the inherent smoothness,[166,197] the dielectric screening,[198,199] and the possibility of polariton dispersion engineering.[200,201] Graphene deposited on a SiO_2 substrate suffers from a reduced quality because the substrate impurities and the large surface roughness introduce the unwanted doping of graphene. This problem, however, has been solved by transferring graphene on high-quality hBN, which is insulating and shares a compatible hexagonal atomic lattice.[166] Thus, the carrier mobility can be substantially faster, and the damping of graphene plasmons can be significantly reduced. The same philosophy of reducing losses also applies to the suspension of 2D materials,[45] which will be discussed in Section 2.3. Furthermore, the dispersion of these highly confined polaritons in 2D materials also critically depends on the dielectric permittivity of the substrate.[200,201] The substrate can be designed to tune the EM properties of the 2D material that is placed on top.

Other ways to tune the properties of 2D materials exist, such as through temperature and strain. The temperature is a critical factor in determining the carrier mobility and scattering of electrons with phonons. An ultimate fundamental limit for the propagation loss of the polaritons when light interacts with 2D materials is usually established.[202,203] Strain can also be exploited for band gap engineering in highly flexible 2D materials.[204,205] Monolayer graphene, which is identified as one of the strongest 2D materials,[206] can support a band gap when the strain is sufficiently large. In a similar way, hBN bilayers with a specific pattern can exhibit the transition from the insulator to the semiconductor.[207] This strain induced insulator-semiconductor transition or band gap engineering can also occur in most TMDs, as shown in both the *ab initio* calculations and experimental demonstrations.[208,209] For example, unstrained monolayer WSe_2 is actually an indirect gap material, as manifested in the observed PL intensity−energy correlation. By imaging the direct exciton populations in monolayer WSe_2−MoS_2 and $MoSe_2$−WSe_2 lateral heterojunctions, it was found that the strain was generated from inherent strain inhomogeneity.[210] These various methods for tuning 2D material properties have rendered them as an advanced and perfect candidate for tunable and reconfigurable M&Ms.

2.2.3. Extraordinary and Tunable Optical Nonlinearities. Controlling nonlinear light−matter interactions has fundamental significance in optics and photonics. In the framework of M&Ms, nonlinearities can be derived from the meta-atoms, the substrate, the superstrate, or the constituent materials shaped with specific geometries. One of the main challenges that hinder the full exploration of nonlinear M&Ms is the low intrinsic nonlinear susceptibilities of conventional metals or dielectrics. As a solution, EM-resonant meta-atoms are usually involved to boost nonlinear light−matter interactions. However, the strong dispersion associated with these resonant structures considerably limits the bandwidth operation of enhanced nonlinearities in M&Ms. The flexibility to dynamically tune the EM nonlinear response of meta-atoms remains a critical issue. In this section, we attempt to establish the potential of 2D materials as building blocks of nonlinear M&Ms, because 2D materials support large nonlinearities in a broadband range and are easily tunable, as previously discussed. We also review recent efforts to combine 2D materials and plasmonic or dielectric M&Ms to build versatile nonlinear platforms in photonics.

The microscopic origin of nonlinearity is the breakdown of the linear dependence of electrons' restoring force on their displacement from the equilibrium positions when a strong EM field interacts with atoms. With the electric dipole approximation, the net polarization field can be written as $\boldsymbol{P} = \varepsilon_0(\chi^{(1)}\boldsymbol{E} + \chi^{(2)}\boldsymbol{E}^2 + \chi^{(3)}\boldsymbol{E}^3 + ...)$. When the electric field is strong, high-order terms such as quadratic and cubic terms become significant. While the linear susceptibility ($\chi^{(1)}$) determines the refractive index and loss/gain of a material,[211] other terms such as the second harmonic ($\chi^{(2)}$) and third harmonic ($\chi^{(3)}$) control nonlinear processes in light−matter interaction, such as three-wave mixing (for example, SHG) and FWM (such as THG). Those nonlinear susceptibilities are highly dependent on the symmetry of the atomic lattices of a material. For example, SHG can only occur in noncentrosymmetric materials, while THG can exist in all materials. This finding implies that monolayer graphene or monolayer BP, which are characterized by an inversion-symmetric honeycomb lattice, do not show SHG due to cancellation of the second-order polarization with the inversion symmetry,[212] while 2D TMDs and hBN, in which inversion symmetry is broken, can display SHG.[61] Using the same argument, SHG can be detected in layered graphene or BP with an even layer number and layered TMDs or hBN with an odd layer number. This interesting layer dependence guarantees the approach to tune SHG by the number of layers, or vice versa, by probing the symmetry and crystal orientation of a layered 2D material by SHG studies.[61,213]

Specifically, we discuss the second-harmonic and third-harmonic properties of graphene. Note that the discussion of centrosymmetric-forbidden SHG is only derived with the electric dipole approximation, and the electric quadrupole and magnetic dipole (although very weak) can be employed to induce SHG in graphene.[214] Other approaches can take advantage of strain engineering,[215,216] asymmetric interfaces with a substrate,[50,217] and chemical functionalization[218] to break the inversion symmetry of monolayer graphene to induce SHG. Dielectric-graphene layered metamaterials with double resonant features have been exploited to excite the second-harmonic field.[219] SHG can be tuned by an in-plane electrical current due to a quantum-enhanced two-photon process in bilayer graphene.[220] The third-harmonic susceptibility in monolayer graphene that is associated with many nonlinear processes, such as the FWM,[221,222] THG,[223,224] and Kerr effect,[225,226] are expected, on which most nonlinear applications of graphene are based. Although atomically thin, graphene has an impressively large third-harmonic susceptibility (approximately 10^{-7} esu),[227] several orders of magnitude larger than traditional nonlinear materials,[29] which enables the potential to optically tune the nonlinear refractive index of metamaterials with very low power.[228−231] The third-harmonic susceptibility of graphene is dispersionless in the visible and near-IR frequency range,[227] which renders graphene a perfect candidate for building broadband nonlinear metamaterials.[232] Associated third-harmonic phenomena can be easily tuned by applying a gate voltage[47] or varying the input field intensity to change the refractive index of graphene, which creates possibilities for tunable metadevices. For example, nonlinear graphene−dielectric layered metamaterials can be exploited to

https://dx.doi.org/10.1021/acs.chemrev.9b00592
Chem. Rev. 2020, 120, 6197−6246

reshape the light pulse[233] and achieve ultralow-power all-optical active manipulation of metamaterial induced transparency regardless of the polarization,[229,234] to demonstrate all-optical switching of optical bistability or multistability[235] and other effects.[236,237] The behaviors of Dirac points in monolayer graphene can be mimicked with nonlinear negative-zero-positive index metamaterials to obtain tunable bandgaps via self-focusing and self-defocusing of nonlinear surface waves[238,239] and large bistable Goos−Hanchen shifts.[240]

In 2D TMDs such as MoS_2,[241,242] $MoSe_2$,[243] WSe_2,[157,244] and WS_2,[245] inversion symmetry is broken and can support SHG. Their second-harmonic susceptibilities can be as large as approximately nm/V, which is substantially larger than those of traditional nonlinear photonic crystals (PCs). This large $\chi^{(2)}$ can account for the resonant enhancement due to the interband transitions and joint PDOS, as revealed by density functional theory calculations.[245] Moreover, the excitonic effect can also contribute to SHG enhancement when an exciton is involved in the nonlinear process.[157,246] This exciton can be tuned by an electric field and generated via spin electron injection,[187] which enables potential mechanisms to dynamically modify SHG in 2D TMDs for tunable M&M applications. Interestingly, the second-harmonic intensity of monolayer 2D TMDs exhibits a sixfold rotation symmetry due to their unique threefold rotation-symmetric atomic lattice.[61,157,244,245] This property supports the previously mentioned application of probing the symmetry and crystal orientation of materials using SHG. As previously commented, the most interesting property of 2D TMDs is their valley DoF.[246] In the scenario, of the interaction among nonlinear light-TMDs, a spin-valley-exciton locked nonlinear selection rule is associated. In this process, a complex interplay of various angular momenta occurs: lattice angular momentum, photon spin angular momentum, valley angular momentum and excitonic angular momentum.[246] Only left-handed circularly polarized fundamental-frequency light can be absorbed at the *K* valley, while the generated second-harmonic photons have opposite spins (Figure 7c).[157,246] These spin-valley-exciton-related nonlinear processes may provide an exotic new ingredient to design nonlinear M&Ms.

In general, the SHG spectrum resembles a pump pulse. However, Lin et al. recently reported a unique quantum interference phenomenon observed in the SHG spectra of single-layer WSe_2.[247] A strong splitting that resembles the phenomenon of electromagnetically induced transparency, is observed in the SHG spectrum. This experimental finding has been theoretically elucidated using a three-level model system, which is a standard approach to treat an atomic gas system for slow light. With an increase in the Rabi cycles included in the driven interference process, a single-dip SHG spectrum can intriguingly evolve into a double-dip spectrum. A non-perturbative character was further manifested by a Fano-like dependence of the SHG power-law dependence on the excitation and emission wavelengths, which strongly deviate from the typical value of 2. This type of destructive interference seems to share the same physical origin as that proposed for the phenomenon of graphene plasmon induced transparency (PIT) in metamaterials.[39] Different from the states built by the plasmonic EM modes in metamaterials,[39] this three-level model system seems to be intrinsic of monolayer TMDs, which can create opportunities in solid-state quantum nonlinear optics for various applications in M&M research.

Although they present a giant nonlinearity, 2D materials with a subnanometer thickness have a weak nonlinear light−matter interaction strength. Therefore, novel approaches should be devised to enhance nonlinear processes. One solution is to take advantage of plasmonic resonances, in which deeply confined plasmonic mode can be used to excite 2D materials. In this scenario, the plasmonic M&M that supports a high-quality resonance can be an excellent platform to enhance nonlinearities of 2D materials.[44,248] An impressive approximately 7000-fold SHG enhancement in WSe_2 has been achieved in Au trenches due to the extreme plasmonic near-field localization in the regions among Au trenches.[244] More interestingly, the plasmonic metasurface, when simultaneously synthesized with 2D materials to boost plasmon-enhanced SHG of monolayer TMDs and address the interesting valley DoF via the manipulation of the spin angular momentum of light (Figure 2d).[83] An alternative solution is to use all-dielectric resonant M&Ms,[249] where the near-field enhancement can boost the nonlinear light−matter interaction. For example, silicon gratings that support hybrid waveguide modes with a large overlap between the fundamental propagating mode and the nonlinear mode show a nearly approximately 280-fold enhancement of SHG from monolayer $MoSe_2$.[250] A promising opportunity can be the integration of 2D materials with all-dielectric M&Ms that support Mie resonance and collective Mie resonances as flexible platforms to enhance the nonlinearity of 2D materials and design multifunctional synthesized meta-devices.

2.3. Low-Loss Polaritons in 2D Materials

For several decades, addressing losses in noble metals such as Au, Ag, Cu, and Al has been a continuous goal in the plasmonic and metamaterial communities.[167,251,252] Although Au and Ag, which have relatively high DC conductivity and low ohmic loss, have been employed as suitable plasmonic materials for building M&Ms, their interband electron−hole transitions introduce significant losses in the visible frequency regime. In the IR and THz frequency range, where the interband transition is absent, intraband transitions that originated from electron−electron scattering events dominate the material properties, which causes a high loss of metals. Other mechanisms of losses in metals also hinder various applications of plasmonic M&Ms, such as the surface roughness and inevitable existence of grain boundaries in bulky metals in the nanofabrication process[253,254] and their lack of tunability and poor compatibility with silicon-based electronic devices.[167,254] In the current stage, to circumvent the losses in plasmonic metals, several methods have been proposed, which range from engineering the electronic band structure of metals[255] and heavy doping of semiconductors for phase changes[256−260] to reducing the carrier density in metals,[261] which either are not practical[255] or display poor performances.[167]

In this section, we focus on reviewing the recent progress in exploring the potential of low-loss M&M enabled by 2D materials such as graphene and hBN. As previously discussed, graphene exhibits the feature of dominant intraband transitions and forbidden interbands transition for excitation energies less than the Fermi energy, which provides a small loss for graphene plasmons and highly confined EM volume and renders graphene a promising alternative candidate for low-loss plasmonic M&M.[29,84,262−264] As a representative example of a polar dielectric, hBN shows a negative permittivity in the

https://dx.doi.org/10.1021/acs.chemrev.9b00592
Chem. Rev. 2020, 120, 6197−6246

Reststrahlen band that presents a long optical phonon lifetime, which supports low-loss deep-subwavelength PhP modes,[113,114,123,265] and may be an alternative choice in the design of lossless M&M. Furthermore, it is shown that plasmon−phonon interaction helps to further reduce the damping of these polaritonic modes by hybridizing a monolayer graphene with BN to form graphene−BN heterostructures.[86,197] Thus, we review lossless SPPs in 2D materials, study low-loss PhPs, and explore plasmon−phonon coupling for creating ultralow-loss 2D materials.

2.3.1. Low-Loss Surface Plasmon Polaritons in 2D Materials. A plasmon polariton is the quantized quasi-particle of collectively oscillated electrons and photons in materials with free electron gases. For example, light-metal interaction excites the charge density fluctuation on the surface of metal, which comprise SPPs. Due to the strong subwavelength confinement that exceeds the diffraction limit and the strong field enhancement for increased light−matter interaction, plasmonic EM fields have been extensively employed for several phenomena and techniques such as super-resolution imaging,[266] surface-enhanced Raman scattering,[267−269] plasmonic sensors,[270] and building blocks of M&M.[136,251] In particular, plasmonic M&Ms have enabled applications such as lensing,[271] cloaking,[272] negative refraction,[251,273] and optical magnetism.[274] As previously commented, the main shortcoming in the use of plasmonic structures in practical applications is their inherent loss. Although plasmonic loss may be preferable only in a few scenarios due to the heat due to ohmic loss, loss is detrimental for most metamaterial-based applications. A continuous endeavor to reduce losses in single crystal fabrication is underway by doping the semiconductor and/or reducing the carrier density in metals.[275] Materials with a 2D nature-like graphene are potential candidates for low-loss plasmonics with an even stronger field confinement and more flexibility for tuning, which can be synthesized for atomically thin tunable and lossless M&M. In this section, we review graphene and analyze other 2D materials, such as TMDs, for low-loss plasmonics.

As shown in eq 1, when the carrier density in doped graphene is sufficiently large to satisfy $2E_F > \hbar\omega$, intraband transitions dominate, and interband transitions are forbidden. With a surface conductivity of $\sigma \approx \sigma_{intra} = \sigma_0 \frac{8E_F}{h} \frac{i}{\omega + i\gamma}$, graphene becomes inductive (metal-like) with $\mathrm{Im}(\sigma) > 0$ at the IR and THz frequency range. For highly doped graphene at low temperatures, plasmonic modes are supported not only for transverse magnetic (TM) polarization ($0 < \hbar\omega/E_F < 1.667$) but also for transverse electric (TE) modes ($1.667 < \hbar\omega/E_F < 2$) due to its linear dispersion,[276] the latter of which cannot exist in conventional metals with parabolic dispersion. We focus on the TM mode on which graphene-based M&Ms rely. The dispersion of the TM mode can be obtained via the following:

$$\frac{\varepsilon_1}{\sqrt{k_{SP}^2 - \varepsilon_1 k_0^2}} + \frac{\varepsilon_2}{\sqrt{k_{SP}^2 - \varepsilon_2 k_0^2}} + \frac{i\sigma}{\omega\varepsilon_0} = 0 \tag{5}$$

where graphene is sandwiched between two nonmagnetic dielectric layers with the relative permittivities ε_1 and ε_2.[277] In eq 5, k_0 and k_{SP} denote the free-space wavevector and the graphene plasmon wavevector, respectively. Within a non-retarded approximation, SPP of highly doped graphene with $E_F > \omega$ can be simplified as follows:

$$k_{SP} = \frac{\pi\hbar^2}{e^2 E_F} \varepsilon_0(\varepsilon_1 + \varepsilon_2)\omega(\omega + i\gamma) \tag{6}$$

$$\frac{\lambda_{SP}}{\lambda_0} = \frac{\alpha}{\varepsilon_1 + \varepsilon_2} \frac{4E_F}{\hbar\omega} \tag{7}$$

where α is the fine structure constant and $\lambda_{SP} = 2\pi/\mathrm{Re}(k_{SP})$ is the graphene plasmon wavelength. Note that the graphene plasmon is very sensitive to the environment dielectric condition because the wavenumber is proportional to $\varepsilon_1 + \varepsilon_2$, while the wavenumber in a standard metal is proportional to $\sqrt{\frac{\varepsilon_1\varepsilon_{metal}}{\varepsilon_1 + \varepsilon_{metal}}}$. This finding indicates that carefully designed graphene plasmonic devices can act as very good sensors with a high figure of merit. From another perspective, eqs 6 and 7 highlight the capability of graphene plasmons to be easily tuned by a dielectric environment. In addition to this way of modifying their properties, graphene plasmons can also be easily tuned by changing the Fermi level.[86] These features are key approaches toward tunable graphene M&M.[278,279]

To obtain a quantitative analysis of the plasmonic performance in graphene, its performance must be compared with that of monolayer Au. Assume that monolayer graphene is suspended in air ($\varepsilon_1 = \varepsilon_2 = 1$). For graphene, the thickness is 0.33 nm and $\sigma \approx \frac{e^2 E_F}{\hbar^2\pi} \frac{i}{\omega + i\gamma}$, where $\gamma = 2 \times 10^{12}$ s^{-1}; for monolayer Au, the thickness is $L = 0.24$ nm and the conductivity is $\sigma = \frac{\omega^2 L}{4\pi} \frac{i}{\omega + i\gamma}$, where $\gamma = 10^{14}$ s^{-1}. At the normal doping level with $E_F \approx \hbar\omega = 0.5$ eV, $\lambda_{SP} = 36$ nm for graphene, with the decay length defined as $1/\mathrm{Im}(k_{SP}) = \left(\frac{\omega}{2\pi\gamma}\right)\lambda_{SP}$, which is approximately 60 λ_{SP}. In Au, however, $\lambda_{SP,Au} = 240$ nm, and the decay length is only $1.2\lambda_{SP,Au}$. Thus, although graphene plasmons are substantially more confined with a smaller SPP wavelength, they can propagate even longer than those on a Au surface, which exhibits low-loss features due to the forbidden interband transition loss channel. This reason explains why graphene M&Ms usually work more efficiently than conventional plasmonic metamaterials in the mid-IR and THz frequency range. With a larger doping level, graphene plasmon can operate at near IR and visible frequency regions.[280] In this range, tunable and efficient SPs were theoretically studied in atomically thin Au nanodisks,[281] in which the working frequencies can be effectively modulated by doping charge density. While the 2D metals support SPs with large cross sections, it is technically challenging to fabricate these metal nanostructures with high crystallinity and large lateral area. Alternatively, one can implement feasible patterning techniques on large size single-crystal monolayer graphene film to achieve a variety of plasmonic structures that support relatively low-loss SPs in the visible and near IR spectral range. To further reduce graphene plasmon losses, in principle, the damping constant (γ) can also be decreased by increasing the carrier mobility in graphene with fewer charged impurities or fewer atom defects, for instance. Another way to reduce the losses of graphene plasmons is to work at lower temperatures.[202]

Not only graphene but also other naturally born 2D materials with 2D electron gas (2DEG), such as MoS_2 and BP, can also support 2D SPs. Monolayer MoS_2 has been expected to have a feature of dielectric functions that is similar

https://dx.doi.org/10.1021/acs.chemrev.9b00592
Chem. Rev. 2020, 120, 6197−6246

to graphene and 2DEG, which can support plasmon resonances.[199] Recently, Scholz et al. have shown that 2D SPs can exist in n- and p-doped monolayer MoS_2 in the far-IR and THz frequency range.[199] Graphene has the same dispersion regardless of the carrier dopant because the electron−hole symmetry and graphene plasmon energy is proportional to $n^{1/4}$ (n is the carrier density) due to the relativistic massless Dirac Fermions. However, n- and p-doped MoS_2 have different plasmon dispersions, and the plasmon energy is proportional to $n^{1/2}$ similar to 2DEGs constructed of inorganic doped semiconductors. Similar to graphene, intraband transitions instead of interband transitions contribute to the damping of plasmon in 2D MoS_2 at the large momenta. Moreover, the large absorption of monolayer MoS_2, approximately 5−10%, indicates stronger light−matter interactions than 2D graphene,[282] which demonstrates the potential for the application of 2D TMDs in low-loss plasmonic applications. However, challenges are the low carrier density (10^{12} to 10^{14} cm^{-3}) in intrinsic MoS_2 and the restriction on the operating frequency range from the far-IR regime to the THz frequency regime.[199] This problem can be solved by doping MoS_2 with Li, for example. Ultradoped MoS_2 nanoflakes with Li^+ (Li_xMoS_2) can exhibit a plasmon resonance in the visible and near UV range by increasing the doping level.[186] Via the application of an intercalation voltage, the 2H to 1T phase conversion of MoS_2 can be achieved to facilitate the modulation of plasmon frequency, and the doping level can be controlled with $0.5 < x < 0.8$ at −10 V, where the light emission is nearly perfectly quenched. To take advantage of these monolayer semiconductors (MoS_2, WS_2, and WSe_2) for practical low-loss plasmonics M&Ms, future efforts in highly efficient doping and the modulation of the carrier mobility are needed.

BP with orthorhombic crystal structures are another notable plasmonic 2D material. BP possesses a thickness-dependent direct bandgap that ranges from 2 eV (monolayer) to 0.3 eV (approximately 8 layers), which bridges the bandgap between gapless graphene and 2D TMDs (1.5 to 2.5 eV).[151] In addition, a large carrier mobility of 50 000 $cm^2V^{-1}s^{-1}$ has been observed in bulk BP at 30 K.[30,151] The bandgap of BP can also be tuned with chemical doping and/or strain.[283] Unlike TMDs, the bandgap in BP is always direct from monolayer film to thicker thin film (approximately 20 nm), which may be preferable for electronic applications. As discussed, a large in-plane anisotropy of BP exists due to the different effective carrier mass along the zigzag and armchair directions.[18,284,285] By examining its dynamic dielectric function,[124,150] BP is predicted to support SPPs with the plasmon frequency $\omega_p \propto n^{\beta}$ ($\beta = 0.5$ for a monolayer and $\beta < 0.5$ for thicker samples).[124,146] The surface plasmon in monolayer BP is also intrinsically anisotropic, i.e., plasmon polariton that propagates along the y direction is damping at the mid-IR frequencies, while a polariton that runs along the x direction is damping at near-IR frequencies. This phenomenon can be further tuned to achieve various hyperbolic plasmonic applications.[286] The major loss channel in this frequency range is Landau damping of the intraband transition[124] rather than the interband transition due to its large bandgap (approximately 2 eV), which underpins the potential for low-loss plasmonics devices and M&Ms.[287−291]

2.3.2. Low-Loss Phonon Polaritons in 2D Materials. For SPPs in metals, doped semiconductors, graphene, TMDs or BP, a common problem is the fast scattering rate of free/unbounded carriers (electrons or holes) in these materials (approximately 10 fs), which always exists regardless of whether the interband transition or the intraband transition provides a negative permittivity, or equivalently, a positive value of the imaginary part of the surface conductivity in the frequency of interest. This situation will establish the fundamental bounds of the minimum value of the plasmonic damping and the lowest threshold of loss. However, to identify alternative materials to achieve plasmonic functions, such as subdiffractive field confinement with the same, preferably better, figure of merit, the negative permittivity (at least one tensor component in anisotropic materials), is always required. This process stimulates the search for low-loss PhPs, which are coherent oscillations of the EM field and optical phonons (vibration of the bounded electron on the atomic lattice), because the lifetime of PhPs (approximately 1 ps) is several orders of magnitude longer than a plasmon, which suggests a low-loss feature.

In the Reststrahlen band, which is defined between the TO frequency and the LO phonon frequency, polar dielectric materials, which span silicon carbide (SiC), silicon dioxide (SiO_2) to 2D or bulk vdW materials (for example, hBN), display a negative (in-plane) permittivity that can be approximated by a Lorentz function as follows:

$$\varepsilon(\omega) = \varepsilon_\infty\left(1 + \frac{\omega_{LO}^2 - \omega_{TO}^2}{\omega_{TO}^2 - \omega^2 - i\omega\gamma}\right) \tag{8}$$

where ω_{LO} and ω_{TO} are the LO frequency and TO frequency, respectively; ε_∞ is the high-frequency permittivity; and γ is the damping rate of the PhPs. Thus, the evanescent wave in the form of PhPs can be supported in these materials, which overcomes the diffraction limit. The Reststrahlen band usually locates in the mid-IR range (hBN and SiC) and THz (CaF_2) frequency range, and the fundamental loss channel is the intrinsic phonon scattering in the material with a lifetime longer than that of SPPs, which renders polar dielectrics as perfect candidates for lossless mid-IR and THz nanophotonics. However, the large momentum mismatch between the free-space photon and PhPs poses a challenge regarding the excitation of these surface EM waves. To this regard, special techniques and nanoarchitecture designs should be delicately considered. In particular, SiC nanopillar antenna arrays are used for excitation and subdiffractional confinement (>5000×) of lossless PhPs with an exceptional quality factor of 40−135. The cavity quantum electrodynamics of such nanostructure can be manipulated so as to provide a high local density of photonic states for enhanced emission, and such enhancement phenomenon is named as the Purcell effect.[292−294] The above-mentioned SiC nanopillar arrays support a small mode volume that enables a Purcell effect factor (the ratio of the enhanced spontaneous emission rate over the free-space one, proportionally to the mode's quality factor divided by the mode volume[294]) as large as approximately 10^7, which exceeds the previous plasmonic demonstrations.[295] Another special technique is the use of s-SNOM, where an AFM tip integrated with SNOM simultaneously enables both the excitation and real-space imaging of PhPs.[296,297]

hBN is a natural anisotropic vdW material[203] that supports low-loss highly confined hyperbolic PhPs,[86,114] whose dielectric responses perpendicular to and along the crystallographic direction differ within the Reststrahlen band. With s-SNOM, these PhPs can be launched, detected, and imaged in real

https://dx.doi.org/10.1021/acs.chemrev.9b00592
Chem. Rev. 2020, 120, 6197−6246

space.[113,298] These hyperbolic PhPs can exist in atomically thin layers and can be tuned by changing the thickness of the hBN layer, which has been demonstrated in three and four atomic layers.[86] The structure of bulk hBN can be engineered to form, for example, nanocones[114,298] and one-dimensional nanotubes[299] to achieve the subdiffraction confinement/focusing,[123,265] anomalous internal reflection and high effective refractive index ($n_{eff} > 70$) of hyperbolic volume PhPs. More recently, research has demonstrated that hyperbolic surface PhPs can also emerge at the edge of bulk hBN[122,300] and an hyperbolic metasurface that operates at THz frequencies can be achieved in nanostructured hBN (Figure 2i).[13] We envision that hyperbolic PhPs can inspire interest in the study of M&M based on hBN or similar polar materials for both nanophotonic applications and thermal applications in the IR and THz frequency range.[301]

To further reduce the loss in PhPs, understanding the loss mechanism in these materials is important. The fundamental limit that restricts the fundamental phonon lifetime is the phonon−phonon scattering that is derived from the anharmonic oscillations of the lattice. An important source to minimize this scattering is the isotope enrichment. For example, natural BN contains 20% ^{10}B and 80% ^{11}B. The small difference in the ratio of B isotopes causes a large variance of the mass of hBN, and therefore, changes the homogeneity of the underlying crystal lattice where the bound electrons coherently oscillate, i.e., optical phonon. The lifetime of PhPs in materials that present a higher purity of the isotopes may be longer, which represents a feasible approach to reducing the losses of PhPs. As verified in an experiment, a threeold improvement of phonon lifetime with ultralow-loss characteristics in isotropically enriched hBN has been observed.[127] Consequently, the increased propagation length of the PhPs and pronounced higher-order oscillation modes can be observed. The other significant loss channel of PhPs occurs via imperfections during the nanofabrication process, including atomic defects, surface roughness, and impurities, which critically depends on the fabrication conditions. For instance, ion implantation of Be^{3+} into SiC can introduce significant damping when focused ion beam implantation is utilized.[302] This process tends to broaden the PhP resonance and even diminish the quality factor of the resonance. Moreover, recent findings of high-quality α-MoO_3 have shown the potential of low-loss PhP with a reported lifetime of 22 ps due to the ultranarrow line widths of the Raman peaks. Less loss can be expected if the isotopic purity of the sample is increased.[88]

2.3.3. Low-Loss Plasmon−Phonon Polaritons. The high quality of 2D materials is very important to improve the performance of 2D nanodevices and minimize the plasmon loss. For example, the first experimental technique used to create graphene monolayers was CVD, in which graphene is placed on top of a SiO_2 substrate. However, the large roughness of the substrate ruins the flat carbon atomic plane of graphene, and the large amount of charged impurities of the SiO_2 can induce electron−electron/holes scattering at SiO_2/graphene interface.[303] Driven by the idea of constructing flatter substrates, subsequent findings have confirmed that this problem can be solved by transferring the graphene to a high-quality hBN, because the surface roughness of hBN can be reduced to the atomic scale[166,304] and the atomic distance between the B and N atoms in hBN is similar to the C=C bond length in graphene. To encapsulate graphene by an hBN layer is the best way to achieve an exceptional mobility rate, a higher electron density, a longer lifetime and less damping for graphene plasmon polaritons.[305] In layered systems such as hBN−graphene−hBN, the surface PhPs sustained in the substrate or superstrate can couple to graphene plasmons and form a hybrid quasi-particle, i.e., a plasmon−phonon polariton, which shows considerably less damping and a longer propagation length.[86,197] In this part, we review the recent progress in the study of plasmon−phonon polaritons and their promising characteristics.

The 2D surface plasmon and optical phonon frequency of polar dielectrics usually locate at the IR and THz frequencies, which can facilitate the plasmon−phonon coupling in structures that combine graphene with SiC,[306,307] SiO_2,[200] hBN,[197,303,308−310] and other materials.[311−314] Theoretical results indicate that plasmon−phonon coupling is strong in monolayer graphene with a weak dependence on electron density, which can be very appealing in practical applications.[315] The system that has received the most attention is the hBN−graphene heterostructure. As a polar dielectric with two Reststrahlen bands in the mid-IR frequency range, hBN can support two branches of hyperbolic PhPs (type I and type II), where doped graphene can have the plasmon mode. The dispersion relation of the EM modes supported by a graphene monolayer with a Fermi level of 0.37 eV placed on top of a 58 nm-thick hBN substrate has been reported.[86] In the type I band ($\varepsilon_\perp > 0$, $\varepsilon_\parallel < 0$), the hybridized EM mode becomes phonon-like due to the predominance of the A_{2u} phonon mode, where the interplay between the graphene plasmon mode and the hBN PhP mode pushes the latter toward higher frequencies due to mode repulsion. Conversely, in the type II band ($\varepsilon_\perp < 0$, $\varepsilon_\parallel > 0$), significant coupling of the zeroth-order PhP mode occurs in hBN with the graphene−plasmon modes, and the hybrid plasmon−polariton mode can cross the longitudinal optical phonon frequency. However, the higher-order phonon modes cannot couple to the graphene plasmon due to field symmetry mismatching.[309] The different hyperbolic character of hBN affects the flow of energy along the z-direction (sign of Poynting vector component S_z) and the wavevector along the z-direction, which causes a significant distinct dispersion and coupling behaviors in two Reststrahlen bands of hBN. Regarding roughness, as revealed by scanning tunneling microscopy, graphene shows a roughness that displays a Gaussian distribution with a standard derivation of 224.5 ± 0.9 pm on top of SiO_2 and a standard derivation of 30.2 ± 0.2 pm on top of hBN. In addition, the Moiré lattice pattern of graphene−hBN can be more clearly resolved than that on top of SiO_2.[304] This flatter surface of hBN, in addition to fewer charged impurities by polymer-free assembly fabrication,[305] can provide a substantially cleaner environment, which enables the graphene plasmon to propagate due to an exceptional large mobility and minimizes defect scattering. Moreover, the loss channel associated with surface plasmon−phonon polaritons depends on two mechanisms: the first mechanism is scattering with acoustic phonons in graphene and optical phonons in hBN, and the second mechanism is dominant due to the larger damping of graphene acoustic phonons.[303,305,316]

This hybridized plasmon−phonon polariton has many important applications in metaphotonics due to its extreme field confinement and strong light−matter interaction. The PDOS near the graphene layer encapsulated with hBN can be increased, which can further enhance the Purcell factor and spontaneous emission rate of a quantum emitter place in close

https://dx.doi.org/10.1021/acs.chemrev.9b00592
Chem. Rev. 2020, 120, 6197−6246

Table 1. Comparison of Polaritons in Traditional Plasmonic Metals and Layered 2D Materials

	polaritons	excitation wavelength (μm)	confinement ratio	quality factor	lifetime (fs)	references
definition		λ_0	λ_0/λ_p	q'_p/q''_p $q = q' + iq'' = k_0$	$\tau = 2q'_p/q''_p\omega$ or $\tau_x = L_x/v_g$,	
Ag[a] (T = 10 K)	plasmon	visible	~1	36	14	202
Au[a]	plasmon	0.486	~1	9.6	5	321
Cu[a]	plasmon	0.365	~1	11.5	4.5	321
graphene (exp., RT)	plasmon	9.7	~40	~90	934	128
graphene (exp., RT)	plasmon	11.2	51	~7.4	88	129
graphene (experimental, T = 60 K)	plasmon	11.286	66	130	1600	202
graphene (intrinsic, T = 60 K)	plasmon	11.286	66	970	12 000	202
graphene in hBN	plasmon	10.688	150	25	500	197
graphene on hBN	plasmon-phonon	6.6889	37	16.7	260	86
hBN[b]	out-plane hyperbolic phonon	6.410	25	18	120	113
hBN 99%	out-plane hyperbolic phonon	6.410	thickness dependent	~100	~8500	127
α-MoO_3[c]	in-plane hyperbolic phonon	11.198	~9		~1900	88
α-MoO_3[d]	in-plane elliptical phonon	9.98	~10		~22 000	88

[a]Evaluated where real (ε) = −2 and the ambient environment is air. [b]Thickness <10 nm [c]Thickness is 250 nm. [d]Thickness is 45 nm.

proximity.[309] The interaction of the plasmon and phonon modes can attain the strong coupling regime due to the small mode volume that is associated with the highly confined EM field and large quality factor of the resonances provided by their low-loss features.[306,315,317] Analogous to the phenomenon of EM induced transparency in metamaterials,[39] the strong coupling of phonon and plasmon modes also exhibit a transparency dip in the characteristic spectrum by the detuning of two mode frequencies, which are usually referred to as the phonon induced transparency.[308,311,318] This effect can be employed for sensing applications.[311] This hybrid plasmon−phonon mode can be utilized in tunable metamaterial designs,[190,311,319,320] which have led to an experimental demonstration of all-angle negative refraction.[190]

As a brief summary of this section, Table 1 summarizes the polaritons kinds, excitation wavelength (μm), confinement ratio, quality factor, and lifetime (fs) for traditional plasmonic metals and layered 2D materials. The SPPs and PhPs in 2D materials are much more confined, while the propagation length is longer, compared with the conventional evanescent waves in metals. The lower temperature can lead to longer polaritonic lifetime. The lifetime of PhPs are usually higher than the SPPs in 2D materials, while the further isotopic enrichment of the polar dielectrics can produce better low-loss features.

3. REALIZATION OF METAPHOTONICS INSPIRED BY LAYERED 2D MATERIALS

In the previous section, we explored the promising optical properties of 2D materials and their interaction with light. To improve and expand the application of 2D materials in metaphotonics, strategies such as micro- and nanofabrication of layered 2D materials, by stacking with 2D materials or metamaterials, are usually adopted. By combining traditional metamaterials with 2D materials such as graphene, TMDs, hBN, and BP, optically and electrically tunable metasurfaces can be realized.

3.1. Micro- and Nanostructured 2D Materials for Metaphotonics

Rapid advancements in micro- and nanofabrication technologies have enabled researchers to miniaturize layered 2D materials to resemble real-world metaphotonic applications. Nanofabrication is commonly employed to produce systems with reduced dimensionality, including ribbons, disks, and cones of layered 2D materials. Conventional periodic metal strips and holes are considered metamaterials,[322,323] and therefore, similar strategies for layered 2D materials, including grating, ribbon resonators, polaritonic crystals and SRRs, are discussed in this section.

3.1.1. Grating or Ribbon Resonators. One of the key actors of optical metamaterials research is SPs, which are collective oscillations of electrons. As described in Section 2, SPs that originate from massless electrons in graphene can enable new tunable plasmon metamaterials and may have optoelectronic applications in the THz and/or mid-IR frequency range. To construct graphene metamaterials, researchers have analyzed the experience of previous traditional metamaterials to construct graphene metasurfaces such as ribbons, rings, SRRs, and discs.

As shown in Figure 8a, graphene ribbon arrays can be prepared from graphene sheets using standard photolithography and oxygen plasma etching.[84,316] In this way, plasmon resonances in graphene can be controlled in graphene microstrip arrays with different sizes, which represent the simplest graphene metamaterials. The spectral location of the graphene plasmon resonance can be adjusted over an extensive range of THz frequencies by varying the width of the graphene microstrip or the doping level in graphene. As the plasmon line width decreases, the peak absorption at resonance can become stronger, which is currently limited by the scattering rate associated with its Drude conductivity (refer to discussion in Section 2). The bandwidth of the plasmon frequency of the graphene ribbon and the carrier doping dependence not only prove the power law behavior of the 2D massless Dirac electrons but also have a very large oscillation strength, which demonstrates a prominent room-temperature optical absorp-

https://dx.doi.org/10.1021/acs.chemrev.9b00592
Chem. Rev. 2020, 120, 6197−6246

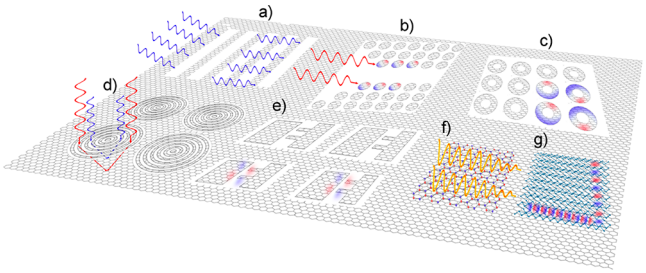

Figure 8. Micro- and nanostructured of 2D materials for metamaterials. (a) Grating/nanoribbon, topological insulator grating, graphene–hBN grating. (b) Photonic crystal based on nanodisks. (c) Nanorings. (d) Lens. (e) SRRs. (f) A combination of hBN and graphene. (g) A combination of BP and graphene or hBN.

tion peak. These results demonstrated the photoplasmon coupling in graphene and highlighted potential graphene-based THz metamaterials. By combining state-of-the-art s-SNOM techniques with rigorous simulations, nano-IR imaging studies of the localized surface plasmon modes in graphene nanoribbons were performed.[324−326] Furthermore, the combination of enhanced sensitivity of graphene ribbons and tunable spectral selectivity creates exciting prospects for mid-IR biosensing.[327] Alternative Dirac plasmon excitation was also observed in patterned topological insulator (TI, Bi_2Se_3) ribbons, and the plasmons are associated with Dirac quasiparticles of the conducting 2D edge state.[328]

Another outstanding 2D natural metamaterial is hBN, which is a layered polar vdW crystal with a uniaxial dielectric constant that demonstrates exotic properties such as hyperbolic dispersions. Rainer et al. developed hBN sheets with a thickness of a few hundred nanometers, which were prepared by mechanical exfoliation to construct nanogratings using electron beam lithography and reactive ion etching.[13] In-plane anisotropic hBN mid-IR hyperbolic metasurfaces were obtained in this way. The hBN metasurface supports PhPs with a deep subwavelength scale, which have in-plane hyperbolic dispersion. Visualizing the concave (anomalous) wavefront of a diverging polariton beam by the s-SNOM technique (Figure 2i), which represents a milestone feature of hyperbolic polaritons, demonstrates that highly variable and compact hyperbolic IR metasurfaces devices can be constructed based on nanostructured vdW materials.[13,104]

The desired multilayer structures can be fabricated by stacking graphene and/or hBN with multiple transfer processes, in which graphene and hBN are prepared by the CVD method or mechanical exfoliation. Subsequently, nanoribbons or microdisks in heterostructures can be patterned using electron beam lithography and reactive ion etching or oxygen plasma etch.[308,329,330] In graphene and hBN heterostructures, not only the classical EM strong coupling of the highly confined near-field but also the phonon hybridization with the atomic thin hBN layer enables the production of two new surfaces–phonons–plasmon–polariton modes. Moreover, the plasmon–phonon hybridization and the total plasmon oscillation intensity in the graphene–hBN multilayer heterostructure can be simultaneously controlled,[308,329] and the phonon induced transparency in the heterostructure device affords strong spectral selectivity that can be used for optical filtering.[331]

Fabrication of micro- or nanoscale patterns in 2D materials by advanced lithography and etching techniques has matured. Thus, we can envision more abundant hyperbolic metasurfaces based on other 2D layered materials (TMDs and TI), multilayer graphene, and polar-layered oxide. The combination of different materials can produce hyperbolic metasurfaces to encompass the entire spectral range from the mid-IR frequency to the THz frequency. The combination of strong polariton-field confinement, anisotropic polariton propagation, geometry and electric gated adjustability, and the potential of developing vdW heterostructures can create exciting new possibilities for planar IR, thermal and optoelectronic applications such as IR chemical sensing, flat and hyperlens, and near-field heat transfer manipulation.

3.1.2. Polaritonic Crystals Made of Layered 2D Materials. Polariton resonances of layered 2D materials feature technologically significant advantages such as subwavelength confinement and adjustability. Therefore, the first observations of plasmon resonances in graphene,[128,129] the resonance of PhPs in hBN with far-IR excitation,[113] and the exciton polariton in TMDs fueled efforts to engineer polariton resonances in layered 2D materials.[87] These efforts have focused on localized polariton resonances in gratings or ribbons of layered 2D materials, as previously mentioned. Other geometries, such as discs, rings, or holes, have been fabricated to tune the polariton frequency of the layered 2D material due to their distinct boundary conditions.

Ashkan et al. theoretically predicted that graphene disks, if properly designed, can be employed as 2D versions of metamaterials that are formed by collecting subwavelength metal nanoparticles, which may exhibit backward wave propagation in certain conditions.[79] When the cross-section of each graphene disk is comparable to the area of the lattice unit, a closely packed graphene disk array that is located above the metal plane can be used to achieve complete optical absorption.[332]

Theoretical predictions have been experimentally confirmed despite some challenges and limitations in terms of sample preparation and measurement. Xia et al. experimentally investigated the coupling of graphene disks on the same plane (refer to Figure 8b), the vertical coupling of graphene disks, the plasmon hybridization in graphene rings (refer to Figure 8c), and the plasmon coupling of surface-polarized phonons.[333] Due to the density-dependent plasmon quality factor, the vertical coupling of graphene disks produces nonintuitive consequences compared with a single layer disk. In the case of coupling to surface polar phonons, the intensity is very high due to the thickness of one atomic layer of graphene.[333] With a tightly arranged array of graphene nanodisks, optical absorption can be increased to more than 30% at the resonant frequency of IR light, which is considerably stronger than the 2.3% absorption exhibited by a single undoped graphene monolayer. The optical absorption of a graphene nanodisk array can be determined by its size and the Fermi level caused by electrostatic doping.[334] The hybridization of SPs in graphene nanodisks was further investigated. By varying the nanoring size, its EM response to light wavelengths as short as 3.7 μm is achieved. By electrically doping a patterned graphene array with an applied gate voltage, a fundamental change in plasmon energy and intensity is observed, which further demonstrates an unexpected increase in plasmon lifetime as energy increases.[335] Similarly, a series of graphene/hBN vertically stacked micron sized discs were prepared by photolithography and transfer techniques. As the layer thickness of the $(G/hBN)_n$ disk

https://dx.doi.org/10.1021/acs.chemrev.9b00592
Chem. Rev. 2020, 120, 6197−6246

increases, the plasmon resonance can be tuned to higher frequencies.[336] By constructing rings and disks in a layered 2D material and utilizing the coupling in each part of the structure, not only can Fresnel zone plate lenses (Figure 8d) be superimposed but also polaritonic crystals can be realized.[337]

While patterning a layered 2D sheet of material into a periodic array, the array serves only as a structural repeat and enhances the total polarization exciter absorption by superimposing each individual local effect. Notice that electrostatic coupling between adjacent nanodisks provides an additional mechanism for controlling the local plasmon resonance frequency in each disk.[333] Despite the polariton localization, this result proposes a global method for designing the dynamics of a polariton resonance array using its periodicity. Engineering polariton wave dynamics by medium periodicity is a hallmark paradigm for creating polariton-based devices. In contrast to ref 333, this principle can be applied to the delocalized plasmons in continuous graphene media with periodic structural perturbations. Thus, the design of the valence band of the polariton metamaterials is performed in a manner that is similar to a PC.[338]

Graphene plasmonic crystals have been created by introducing a hexagonal hole array in monolayer graphene. The periodic interaction between a local graphene plasmon and the medium (air) forms a plasmonic optical band. This formation introduces a new way for creating a large number of subwavelength components via band engineering, such as bandgap filters, modulators, switches and metamaterials. As the mobility of large-area CVD graphene continues to increase, the area of high-mobility stripped graphene also increases, and the emergence of higher-quality factor devices are expected in the near future. The theory predicts the band topology of 2D SPs in periodically patterned graphene with time-reversed symmetry breaking, which is caused by static magnetic fields. This effect can promote the creation of a 2D topologically protected plasmonic crystal.[339,340]

The periodic structure of doped semiconductors and graphene-supporting plasmon polaritons and polar dielectrics-supporting PhPs (such as SiO_2 or Al_2O_3) can be considered "polaritonic crystals". However, the inherent loss of these materials is relatively high (quality factor <30). In addition to SiC, in which PhPs have a long lifetime, large practical difficulties are encountered in its manufacture. Many layered 2D materials that support polaritons with diversiform properties for IR polaritonic crystals, such as larger confinement, adjustability, and negative phase velocity, contain promising alternative materials. In particular, hBN crystals exhibit anisotropic phonons in the mid-IR frequency range, as previously described. In the structured layered 2D material hBN, deep subwavelength polaritonic crystal based on hyperbolic PhPs was realized.[341] In the simplest case of square symmetry, the hBN-based polaritonic crystal supports a high-confined Bloch mode with a flat band, which also produces a geometrically tunable resonance that is independent of angle and polarization. hBN polaritonic crystals can be used not only for subwavelength omnidirectional IR absorbers, couplers and reflectors but also for suppressing spontaneous emission, which can be achieved by adjusting the parameters of the polaritonic crystal, such as symmetry, to activate the fully polaritonic band gap.

The layered structure of 2D materials facilitates the simple manufacture of a high-quality thin layer by exfoliation. Polaritonic crystals based on graphene and hBN or other layered 2D materials can be employed as polaritonic hypercrystals with high PDOS. In addition, the combination of hBN polaritonic crystals/hypercrystals with other low-dimensional materials (e.g., BP-encapsulated hBN; refer to the next section) can promote the use of hybrid metamaterials with unique optoelectronic properties at the nanoscale. These studies enabled the application of layered 2D materials in sensing, IR light detection, light modulation, and IR-THz metamaterials.

3.1.3. Split-Ring Resonators Predicted in Layered 2D Materials. In many metamaterials/metasurface studies, SRRs have become core elements.[133,342,343] They exhibit an artificial negative permeability that can be adjusted from the microwave range to the visible frequency range by varying the size of the SRR. Moreover, with the negative dielectric constant, they display a negative phase velocity for light even at optical frequencies.[133] In addition, they are capable of supporting strong induced currents, which produce a resonant magnetic response to the near IR.[343] SRRs can be driven by plasmon excitation that propagates along the circumference of the ring, especially when the length of the size SRR is half the plasmon wavelength. This situation causes the formation of standing waves that are similar to those by dipole antennas.

The performance of metamaterials is hindered by optical losses and the lack of a rapid means of regulating the spectral response. Layered 2D materials have significant advantages. Considering graphene as an example, as previously discussed, graphene is considered a promising plasmonic material due to two important properties that are beneficial to metamaterial design: (a) high-confinement surface plasmon, and (b) graphene plasmon frequencies can be tuned by injecting charge. Therefore, a graphene split-ring that is based on a 2D layered material is expected to exhibit a small-sized resonance compared with a conventional noble metal split-ring. In addition, metamaterials formed by graphene SRRs inherit the adjustability of their atomic-scale thin fabrics.

An extensive variety of graphene split-rings are predicted with rich performance (Figure 8e), such as tunable metamaterials beyond Au,[344−347] optical extinction and absorption enhancement,[348−351] strong magnetic dipole responses,[344,352] atomic electromagnetically and plasmon induced transparency,[353,354] tunable plasmonic filters,[355] coherent perfect absorption,[356] and ultrasensitive THz sensors,[357,358] which are not easily attainable with conventional noble metals and can be beneficial for the fabrication of compact, versatile metamaterials to the THz regime. These results offer a way of developing tunable metamaterials that enable applications in the THz range of the EM spectrum and IR detection and modulation for layered 2D materials photonics and optoelectronics.

3.2. Stack of 2D Materials

Research on the properties of heterostructures based on layered 2D materials is rapidly developing.[60] Heterostructures and devices are constructed by stacking different 2D materials. The strong covalent bonds provide the in-plane stability of the 2D materials, while the relatively weak force that is similar to the vdW forces are sufficient for keeping the stack intact.[60] New heterostructure devices such as tunnel transistors, resonant tunnel diodes and light-emitting diodes begin to emerge.[359] Layered 2D material heterostructures also provide potential approaches for the implementation of metaphotonic devices.[360]

https://dx.doi.org/10.1021/acs.chemrev.9b00592
Chem. Rev. 2020, 120, 6197−6246

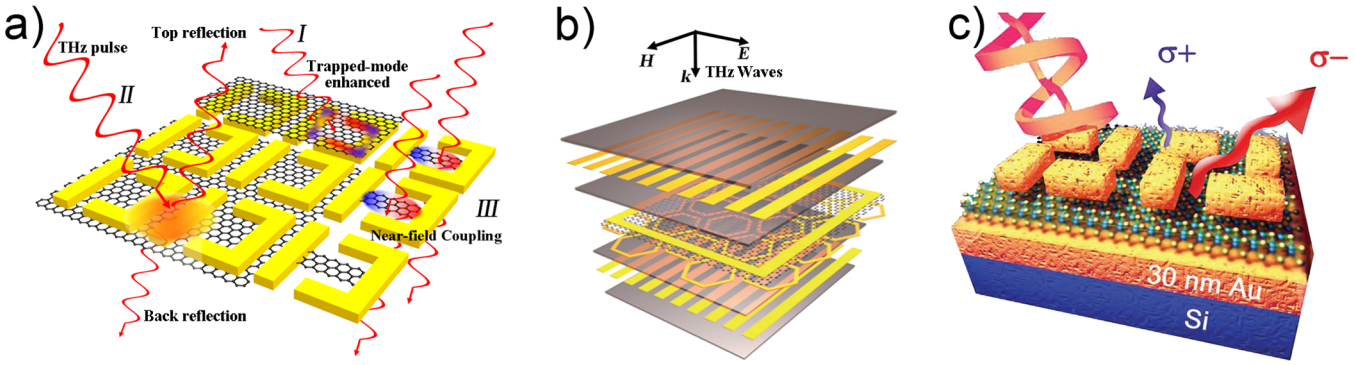

Figure 9. Layered 2D materials and metal M&M heterostructures. (a) *I* graphene on split-rings; *II* split-rings on graphene; *III* graphene in split-rings. (b) A single-layer graphene deposited on a layer of hexagonal metallic meta-atoms.[81] Reprinted with permission from ref 81. Copyright 2012 Nature Publishing Group. (c) Schematic of MoS_2-metasurface structure, where valley-polarized PL of MoS_2 is tailored with near-field interactions and excitation of specific circularly polarized light.[365] Reprinted with permission from ref 365. Copyright 2018 John Wiley and Sons.

The epitaxial layered 2D materials are restacked to prepare vertical heterostructures, in which the EM coupling between layers produces new optical properties beyond the individual components. Subdiffractional metaphotonics can be achieved using either SPPs or PhPs. SPPs that originate from layered 2D materials (graphene and BP) can provide gate-adjustable, wide-bandwidth responses with relatively high optical loss, while PhPs in hBN and MoO_3 have relatively low-loss, crystal-related optical responses in a narrow spectral range with limited tunability.

As discussed in Section 2.3.3, when hybridized with PhPs of polar layered 2D materials, mid-IR SPs in graphene overcome the limitations of each individual polariton.[361] Theoretical and IR transmission experiments reveal the mid-IR optical properties of graphene−hBN heterostructures, which originate from their coupled plasmon−phonon modes (refer to Figure 8f).[190,308,309] Graphene plasmons couple differently with the PhPs of the two Reststrahlen bands because they have different hyperbolic properties. The near-field, highly confined graphene plasmons hybridizes with the PhPs of the atomic-scale thin hBN layer to produce two distinctly divided new surface-plasma phonon-polariton modes.[309] The hyperbolic polaritons that are observed in the graphene−hBN heterostructures succeed the electrostatic tunability from graphene and the long propagation length from PhPs in hBN.[86,336] The surface plasmon that propagates in high-quality graphene wrapped between two hBN films was further imaged using s-SNOM.[197] The hBN−graphene−hBN sandwich structure has unprecedented low plasmon damping, strong field confinement, and high uniformity. The observation and understanding of this low plasmon damping is the key to the development of graphene nano-optoelectronic and metaphotonics devices.[197]

Furthermore, hBN/BP heterostructures were demonstrated by placing an in-plane anisotropic PhP mode associated with hBN in layered 2D stacks that were constructed with BP (similar to Figure 8g).[362] Due to the high confinement of the PhPs in hBN, the optical anisotropy in the hBN/BP heterostructure exceeds that of pure BP. The heterostructure that consists of BP/hBN/BP can produce a higher in-plane optical anisotropy due to the high confinement of the PhPs in hBN. This strategy can be extended to other heterostructures by utilizing electrostatic gating to tune in-plane optically anisotropic substrates such as BP and 2D TMDs,[363] which produces tunable PhPs in polar dielectric materials or anisotropic plasmon polaritons in graphene.

Stacking can also change the symmetry of layered 2D materials to achieve attractive new features. As discussed in Section 2, odd layers of graphene and TMDs are center-symmetrical, while even stacking breaks the inversion symmetry, which significantly affects their nonlinear characteristics. The interest in stacking vertical heterostructures with different rotation angles has increased. Variations in the electronic structure generated from interlayer interactions can further produce altered polaritonic responses. In rotationally aligned graphene−hBN stacks, the formation of long-period Moiré superlattice changes the dispersion and lifetime of composite plasmon polaritons.[364] By positioning 2D materials layer by layer, the interlayer rotation (θ) and polarity can be rationally controlled to produce the final stackable adjustable chirality. For example, left- and right-handed bilayer graphene, which is a two-atom thick chiral film, can be prepared. These chiral properties are derived from large in-plane magnetic moments associated with optical transitions between layers. Recently, stacked magical-angle bilayer graphene exhibited surprising superconductivity.[191,192] Moiré excitons were detected in layered 2D TMDs heterostructures such as $MoSe_2/MoS_2$,[189] $MoSe_2/WSe_2$,[193,194] WSe_2/WS_2,[195] and $MoSe_2/WS_2$.[196] The Moiré exciton bands provide an attractive platform from which to explore and control excited states of matter in TMDs. These results suggest the feasibility of engineering artificial excitonic crystals using layered 2D heterostructures for nanophotonics and quantum information applications.

3.3. Stack with Metamaterals and Metasurfaces

3.3.1. Stack 2D Materials with Metallic Metamaterals and Metasurfaces. Due to the atomic thicknesses, layered 2D materials typically can only modulate light in terms of frequency, phase, and amplitude by a very narrow tuning range. One way to overcome this limitation is to structure or pattern layered 2D materials, as described in Section 3.1. Another effective solution is to combine layered 2D materials with metal M&M, which affords enhanced light-mater interaction from the visible frequency to the THz frequency. The hybrid structures that consists of layered 2D material/metal M&M show more fascinating features that are not possible in individual layered 2D material or metal M&M.

Since the original SRR proposed by Pendry in 1999,[9] researchers have conducted extensive research on SRRs with different geometries.[9,366,367] Due to the double negative material properties of SRR, it is considered an indispensable

https://dx.doi.org/10.1021/acs.chemrev.9b00592
Chem. Rev. 2020, 120, 6197−6246

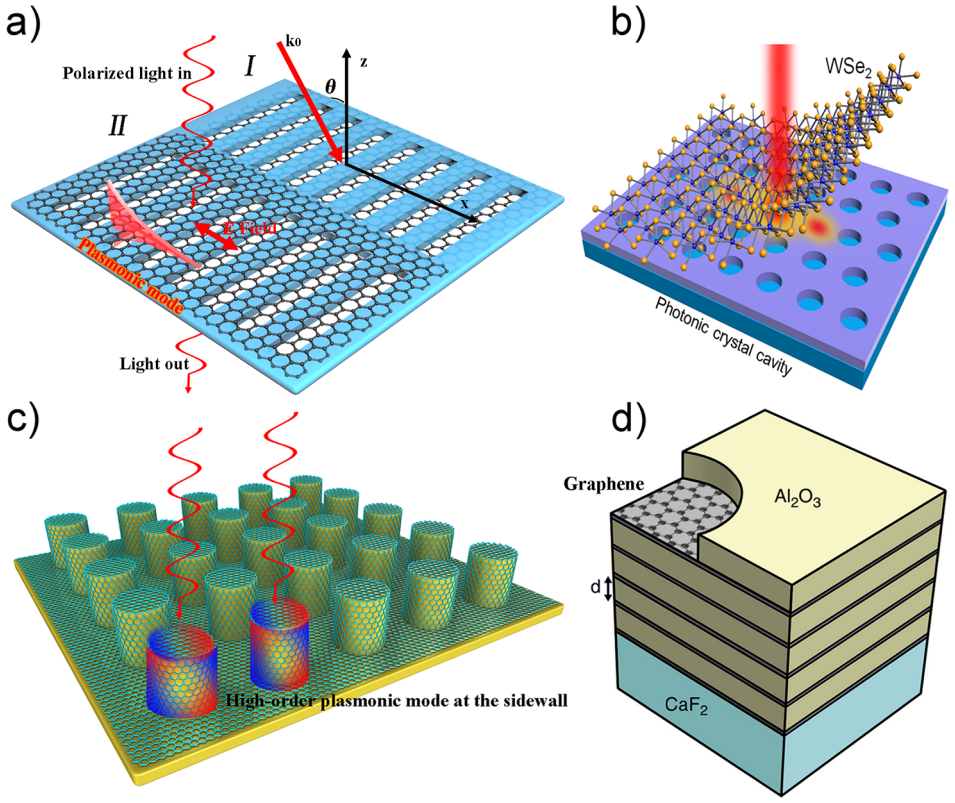

Figure 10. Layered 2D materials and dielectric M&M heterostructures. (a) Graphene below (*I*) or on (*II*) the grating. (b) Hybrid monolayer WSe_2–PC and electric-field intensity profile.[401] (c) Flat graphene into complex 3D pillars. (d) Graphene–dielectric multilayer structure.[402] Reprinted with permission from ref 402. Copyright 2016 Nature Publishing Group.

component and is extensively applied in the design of leaky wave antennas,[368,369] compact phase shifters,[370] and microwave band narrow bandwidth band filters.[9,371,372]

By varying the dimensions of SRRs, the resonant frequency can be adjusted over an extensive range. The amplitude e/phase of the SRRs can be modulated by applying a bias voltage to the n-doped GaAs substrates.[373,374] Compared with traditional semiconductor materials, graphene is an ideal candidate for designing new M&M devices because the light–matter interactions in graphene have strong confinement and can be rapidly modulated and broadly tuned. Note that the hybrid M&M structure that consists of a graphene layer that interacts with upper SRRs enables compact, fast, tunable optical modulations at RT (Figure 9a I).[375−377] Furthermore, flexible tunability can be achieved by using more efficient top-gated architecture voltage modulation and integration with different frequency independent resonant arrays.[378] Graphene/SRRs composite structures also exhibit cascaded Fano resonances, which are associated with the strong coupling of subradiative graphene plasmons with SRRs metasurface modes and significant enhancement of light absorption and nonlinear effects.[379] Inversely, when 2D materials are overlaid on SRRs (Figure 9a II), optical coupling and reformation between polariton resonances and plasmon resonances of SRR array-based metamaterials are expected. Consequently, the figure of merits of hybrid SRRs, such as transmission,[80,380,381] Raman enhancement,[267,268,382,383] and modulation,[384] have been significantly improved. Patterned graphene resonators, which are strongly coupled with conventional metal SRRs (graphene ribbons hybridized with SRRs, refer to Figure 9a III), are electrostatically tunable hybrid metamaterials that exhibit strong EM responses with high tunability.[385] Therefore, these hybrid metamaterials manifest as a fascinating platform for discovering cavity-enhanced processes, in particular, light–matter interactions in hybrid 2D materials metamaterial structures.[385,386] The interaction of structured graphene plasmons with SRRs is also applied in the design of PIT metamaterials. These PIT metamaterials exhibit sharp PIT peaks that are caused by the destructive interference between the direct-excited plasmon resonance in the graphene patch and the coupling excited inductive–capacitive resonance in the SRR with an adjustable PIT window by tuning the Fermi level in graphene.[387,388]

In addition to SRRs with electrical resonances, metallic resonators can also exhibit strongly enhanced local fields for modulation by controlling the Fermi level of an adjacent graphene layer, for example, Au-graphene gratings with plasmon resonance,[389] a sandwich structure that supports a magnetic resonance,[390] and an asymmetric structure with Fano resonances.[379,380,391] Layered 2D materials can also be hybridized with other metal M&M. As shown in Figure 9b, an array of hexagonal metallic meta-atoms, an atomic-thin graphene layer, and a row of metal wire gate electrodes are configured to form an ultracompact, thin, flexible, and gate-controlled active THz graphene metamaterial.[81] The gate-controllable light–matter interaction in the graphene layer can be substantially enhanced by the strong resonance associated with the metamaterials. Because the thickness of graphene is more than six orders of magnitude smaller than the wavelength of THz waves, the combination of graphene and metamaterial can modulate both the amplitude of the incident THz wave by 47% and its phase by 32.2° at RT. The gate-controlled active

https://dx.doi.org/10.1021/acs.chemrev.9b00592
Chem. Rev. 2020, 120, 6197−6246

graphene metamaterial exhibits hysteresis behaviors in the transmission of THz waves, which indicates a sustained photon memory effect.[81] By varying the Fermi level, the surface conductivity and resonant frequency of graphene exhibit a substantially tunable range.

For layered 2D semiconductor materials, several studies have realized the enhanced effects of TMDs with different metal M&M, such as fluorescence emission and nonlinear effects. The SPP focusing field of the metal spiral-ring metamaterial is used to amplify the exciton emission of the MoS_2 single layer. By changing the incident optical spin states, the laser power and the spiral geometries can actively control the MoS_2 PL enhancement (Figure 9c). The planar LEDs that are based on the spin−orbit coupling effect were further realized and flexibly controlled by changing the polarization of incident light.[392] By coupling the resonant EM field of the chiral metasurfaces with the valley-polarized excitons of single layer MoS_2, the valley-polarized PL of the MoS_2-metasurface can be customized in the regime of the near-field interaction with circularly polarized light.[365] A new type of nonlinear hybrid metasurfaces for nonlinear transformation optics consists of Au-nanohole-based metasurfaces and single-layer 2D material in the visible region. A large SHG susceptibility is achieved, which is 2−3 orders of magnitude larger than that of traditional M&M.[393] This new nonlinear optical interface is employed for the efficient manipulation of nonlinear energy valley-photons in single-layer WS_2 through the Au-nanohole-based metasurfaces with gradient phase information. When the left (right) circularly polarized light passes through the hybrid metasurfaces, a right (left) circularly biased fundamental light with phase information is generated. The SHG photon locked by the valley can carry phase information and control various functions (Figure 2d).[83]

3.3.2. Stack 2D Materials with Dielectric Metamaterals and Metasurfaces. In these subsections, we outline the hybrids of layered 2D materials/metal M&Ms. However, at the near-IR and optical frequency, nonradiative losses in metal cause low quality-factor resonances and further limit the strength of light-mater interaction. The atomic thickness of layered 2D materials enables them to be naturally integrated into planar PCs and achieve efficient coupling to the evanescent fields in these structures.

The interaction of light with graphene can be greatly enhanced by coupling to a 1D and 2D PC, as shown in refs 211 and 394. In the case of 1D PC (optical grating), the dielectric diffractive grating effectively excited highly confined surface plasmon polaritons that propagate at the surface of the single-layer graphene (as shown in Figure 10a).[232,395−399] When incident light is coupled with graphene and form surface plasmon, the guided-wave resonance of the combined structure produces a strong absorption.[232,395−397] A new hybrid architecture for monolithically integrated photodetector devices was built by integrating silicon gratings, plasmonic gratings, and layered 2D materials.[400] In the case of 2D PCs, ultralow-power resonant optical bistability, self induced regenerative oscillations, and coherent FWM were observed in graphene−silicon hybrid optoelectronic devices, which recirculate energies in few-femtojoule cavities.[221] Graphene transferred on a local optical cavity at the wavelength scale not only enhances thermal nonlinearities but also induces ultrafast effective Kerr nonlinearity, which provides a new parameter for chip-level optical physics and ultrafast optics in optical information processing.[221] A monolayer WSe_2 was directly transferred to a planar PC nanocavity to form a laser with an ultralow threshold that consists of 2D TMD and a PC cavity (Figure 10b).[401] Two effects occur in the layered 2D TMDs material-PC coupling system: photonic band gap effect and Purcell effect.[162] Because the exciton resonance energy of the layered 2D TMDs material resides inside the photonic band gap of the PC nanocavity, emission to the 2D plane of the PC is strongly suppressed, and therefore, the PL is redirected in the out-of-plane direction, which generates stronger PL emission. The photon density of the PC nanocavity is considerably higher than that of the free space, and the Purcell effect enhances the spontaneous emissivity of the layered 2D TMDs.[401,403,404]

In addition to 1D and 2D PCs, 2D materials can also be integrated with 3D silicon pillars, where strong high-order plasmon modes were observed (Figure 10c).[405] The excitation efficiency of higher order modes is highly dependent on graphene wrapping on the sidewalls of silicon pillars, which can be tuned by changing the geometry of the silicon pillar array and material parameters (e.g., thickness). The 3D graphene structure not only retains the advantages of 2D materials but also introduces a new dimension for controlling light−matter interactions. Moreover, the manufacturing techniques in this work can be readily applied to other 2D materials that have various optical responses.[405] The proposed 3D form of 2D materials will contribute to the design of additional sophisticated plasmonic devices and metamaterials that are based on 2D materials and enable new ways of controlling THz, far IR, and visible radiation.

Layered 2D materials can also be integrated with asymmetric dielectric M&Ms. Asymmetric dielectric M&Ms originate from early developed plasmonic M&M for PIT and protein monolayer sensing.[406,407] Each unit cell consists of straight and curved Si nanorods, in which the curved Si nanorod is responsible for breaking the two mirror inversion symmetries of the unit cell and coupling the bright (electric dipole) and dark (electric quadrupole/magnetic dipole) resonances, where the surface charge density at the air/Si interface is plotted for the eigenmodes with and without symmetry breaking curvature. Asymmetric Si-based II and π-shaped resonators had high quality-factor Fano resonances and strongly localized field enhancement in the gaps. After covering a monolayer graphene, the strength of the light−matter interaction is promoted by changing the Fermi level.[406,408] Similarly, the asymmetric periodic dielectric encompassed by graphene also shows behaviors that are identical to the behaviors of the asymmetric structure.[409,410]

Layered 2D plasmonic materials can be alternately stacked with the dielectric layer to achieve metaphotonics. Negative refraction and hyperbolic dispersion were demonstrated using a structure that consists of metal and dielectric layers. Numerous hyperbolic metamaterials that consist of different metal/dielectric pairs have been demonstrated, such as Ag/Al_2O_3,[411] Ag/TiO_2,[412] and Ag/Ti_3O_5.[413] Similar to traditional metal−dielectric multilayers, as shown in Figure 10d, alternating graphene and Al_2O_3 metamaterials for mid-IR operation are designed. Metamaterials undergo an optical topological transition from elliptical dispersion to hyperbolic dispersion with a wavelength of 4.5 μm.[402] Graphene is inserted into the quarter-wave stack of the 1D PCs, and the synergy of Bragg scattering and graphene conductance opens the photon gap at the center of the reduced Brillouin zone. This gap is not present in conventional quarter-wave stacks.

https://dx.doi.org/10.1021/acs.chemrev.9b00592
Chem. Rev. 2020, 120, 6197−6246

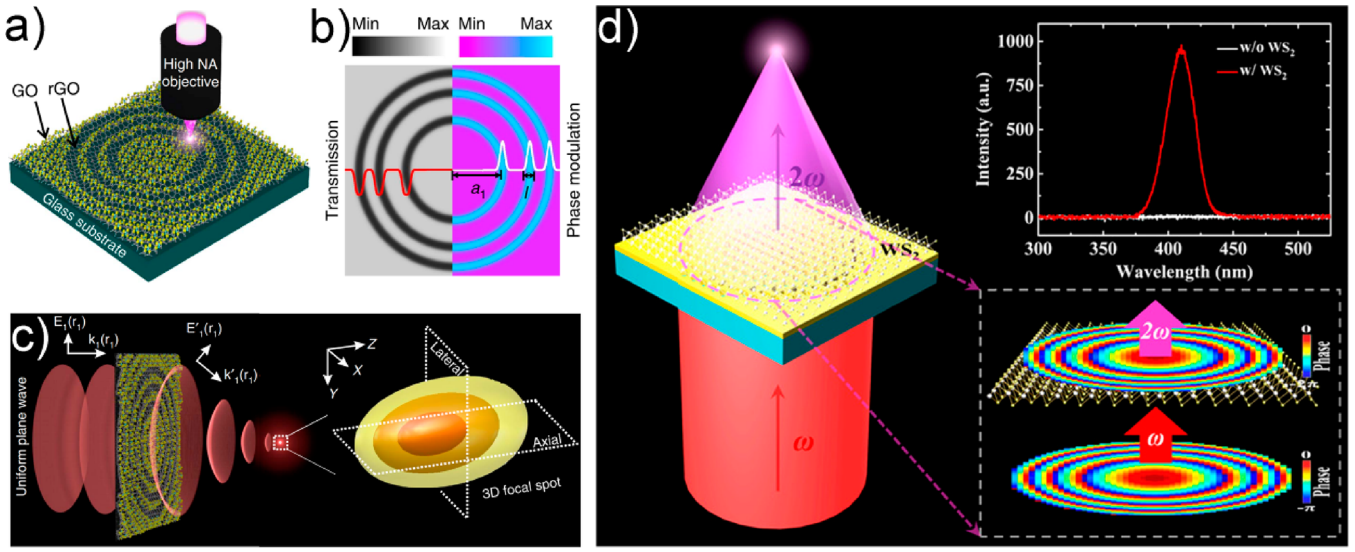

Figure 11. Lensing application enabled by layered 2D materials. (a) Conceptual design and laser fabrication of the ultrathin GO lens. (b) Amplitude and phase modulations provided by the difference in the transmission and refractive index between the GO zone and rGO zone, respectively. (c) Schematic of the focusing effect of the GO lens; lower right, intensity distributions of the 3D focal spot predicted by the analytical model for a GO lens.[75] (a–c) Reprinted with permission from ref 75. Copyright 2015 Nature Publishing Group. (d) WS_2–Gold nanohole hybrid metasurfaces for nonlinear metalenses in the visible region.[393] Reprinted with permission from ref 393. Copyright 2018 American Chemical Society.

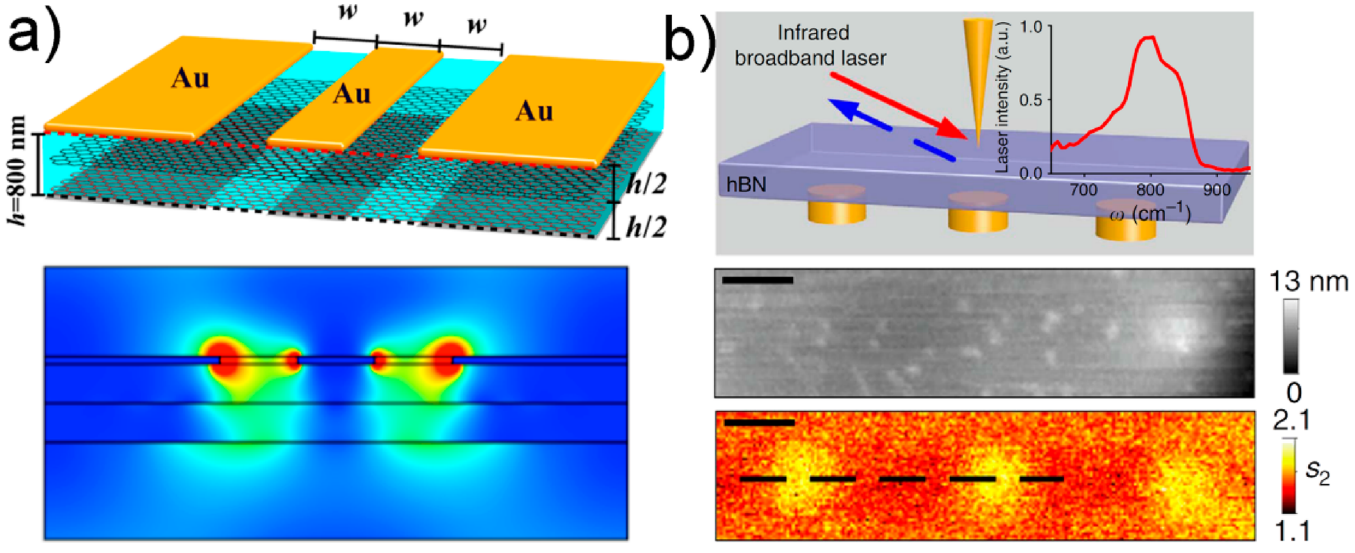

Figure 12. Near-field confinement and far-field imaging. (a) Top, sketch of a two-layered graphene lens under the Au double slit. Bottom, imaging performance of the two-layered graphene lens.[417] Reprinted with permission from ref 417. Copyright 2012 American Chemical Society. (b) Top, schematic of the experiment of super-resolution imaging with tunable hyperbolic polaritons. The Au nanodisk is within 0.3 mm diameter and 1.3 mm center-to-center separation. Middle, AFM topography taken at the top surface of the 0.15 mm-thick hBN flake. Bottom, the 2D IR optical amplitude image.[419] Reprinted with permission from ref 419, Copyright 2015 Nature Publishing Group.

This photonic gap exhibits a large, loss-independent optical state density at a fixed lower gap edge for an even multiple of the characteristic frequency of the quarter-wave stack.[414] Furthermore, the multilayer BP-metamaterial/dielectric sandwich structure and the optical, thick, and Au mirror formed a Fabry–Perot resonator that is employed for the absorber that operates in the mid-IR region.[288]

4. PENDING APPLICATIONS

4.1. Planar Lenses

One of the main advantages of metasurfaces is their planar features, which release demanding requirements on fabrication techniques for 3D counterparts while maintaining the extraordinary flexibility in efficiently controlling EM waves.[415,416] Compared with metasurfaces that are composed of metal or dielectric unit cells, 2D materials gradually emerge as a type of powerful composite materials for metasurfaces. More importantly, their optical properties can be easily tuned, which enables them to be applied to construct highly integrated and flexible optical systems with ultrathin flat profiles. For example, conventional optical elements such as a Fresnel zone plate can be devised by 2D materials.[337] As shown in Figure 11a–c, an flat lens with a 3D diffraction-limited focusing capability is demonstrated by utilizing the

https://dx.doi.org/10.1021/acs.chemrev.9b00592
Chem. Rev. 2020, 120, 6197–6246

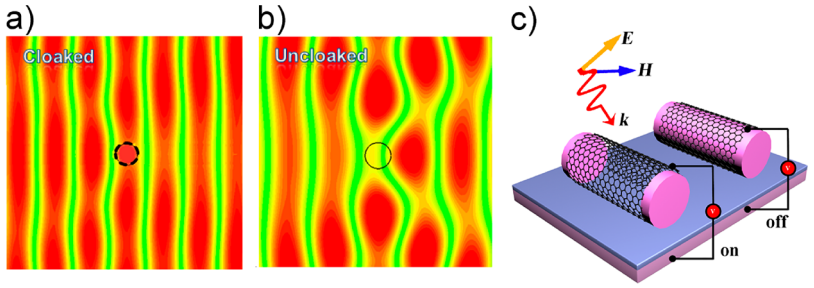

Figure 13. Cloaking with 2D materials. Snapshots of electric field distributions for (a) a cloaked dielectric cylinder and (b) an uncloaked dielectric cylinder with the patterning monolayer graphene and without the patterning monolayer graphene, respectively.[422] (a, b) Reprinted with permission from ref 422, Copyright 2013 IOPscience. (c) THz mantle cloak composed of a graphene-wrapped microtube. The surface conductivity of graphene and the total cloaking effect may be dynamically tuned and switched.

unique and giant refractive index and absorption modulation of a sprayable GO thin film.[75] With a thickness of approximately 200 nm, the flat lens can focus visible and near IR light into a 3D volume of $\lambda^3/5$ with an efficiency of 32% for a broad wavelength range from 400 to 1500 nm. Compared with EBL and FIB nanofabrication technologies, direct writing using a femtosecond laser can readily be applied to GO-based metasurface fabrication.[75] In addition, 2D materials can replace metal and dielectric unit cells as building blocks for planar optical devices. Unlike the linear metalens, a new type of nonlinear hybrid metasurface in the visible region is produced by hybridization of a monolayer WS_2 with giant intrinsic nonlinearity and a phase-controlled Au nanohole array, which can be applied for efficient nonlinear metalenses[393] and demonstrated with a focal length of 30, 50, and 100 μm and small focal spots of 1−2 μm in diameter by converting light of 810 nm wavelength into 405 nm (Figure 11d).

4.2. Subdiffraction Near-Field Confinement and Far-Field Imaging

The highly confined polaritons enable super-resolution imaging. For example, graphene plasmons are highly confined evanescent waves that enable near-field imaging considerably below the diffraction limit. As demonstrated in Figure 12a, a bilayer graphene lens can probe the subwavelength resolution of approximately $\lambda/7$.[417] Another possibility is the PhPs, especially the hyperbolic PhPs with extremely large polariton momentum. A maximum confinement factor of $\lambda_0/25$ for hyperbolic PhPs in hBN has been demonstrate, where λ_0 is the wavelength of excitation wave.[113] The confinement factor was further increased to 120 in α-MoO_3 nanoflakes with a lifetime at the picosecond level.[88,418] Furthermore, 3D confinement can be realized by patterning hBN as nanoparticles, with which the EM field can be manipulated at both Reststrahlen bands.[114]

The difference is that graphene plasmon is essentially near-field confinement, while highly confined PhPs in these nanoscale vdW materials have a propagation nature, the latter of which can be explored for far-field imaging considerably below the diffraction limit. An important example is the hyperlens.[411] While traditional efforts have been made for resonance-based multilayered metal and dielectric hyperbolic metamaterials, natural hyperbolic vdW materials provide a broadband (from mid-IR to THz) and low-loss solution.[417] Because the propagation direction of EM wave is adequately determined by the ratio of the axial permittivity and to the tangential permittivity (refer to Section 2.1.1.), the fine structure information, even below the diffraction limits, can be detected in the far field via tracing the propagation of hyperbolic PhPs. As shown in Figure 12b, the subwavelength imaging is restored using a thin layer of hBN with a thickness of 150 nm. In principle, the subwavelength geometric feature can be substantially magnified and resolved with normal optical microscopy when the thickness of the hyperbolic hBN is sufficient.[123,419] The elusive possibilities of nanoimaging via exploiting the highly confined polaritons in low-dimensional materials have future potential.

4.3. Cloaking

Another exciting application is the realization of invisibility in the broadband EM frequency range using different designs. In addition to utilizing bulk metamaterials with complex designs, the metasurface-based cloaking has been realized at optical frequencies with the potential for practical applications.[420] The nature, however, provided venues that differed from the artificial structured materials. As shown in Figure 13a, b, the thinnest mantle cloak in the far-IR and THz regimes has been theoretically proposed using a monolayer graphene that covers the subwavelength cylinder to ensure the scattering cancellation in the far field.[421] Compared with the "traditional" cloak design assisted by transformation optics, the graphene-based cloak provides the uppermost advantage due to its atomically thin nature.[421] Note that this scattering cancellation can also be tuned by the Fermi level of via the gating (Figure 13c). The more elusive but not extensively explored opportunities include artificially engineering the monolayer graphene into periodic patches or introducing other 2D materials such as BP, which may enable dynamically tunable invisibility cloaks and other switchable meta-devices based on low-dimensional materials.[421,422] Layered 2D materials have the potential to realize thin cloaks at THz frequencies, which fills the THz gap for scattering-cancellation cloaks between mantle cloaks realized with conducting metasurfaces[423] at radio frequency and plasmonic cloaks in the visible frequency.[272]

4.4. Plasmon-Induced Transparency

Electromagnetically induced transparency in atomic systems has been detected with important applications in slow light, optical switch and nonlinear optics.[425,426] An analogue has been proposed and demonstrated by mimicking the required energy levels with EM modes using plasmonic structures, which is referred to as PIT.[39] PIT can be achieved by 2D materials. To improve the tunability, graphene was incorporated to achieve a PIT effect, in which geometrical structures were designed to show the bright and dark modes.[353,427] This graphene-based PIT window and strength can be flexibly tuned by varying the Fermi level of graphene via electrical gating[353,427] or even the magnetic biases.[428] Similar to PIT

https://dx.doi.org/10.1021/acs.chemrev.9b00592
Chem. Rev. 2020, 120, 6197−6246

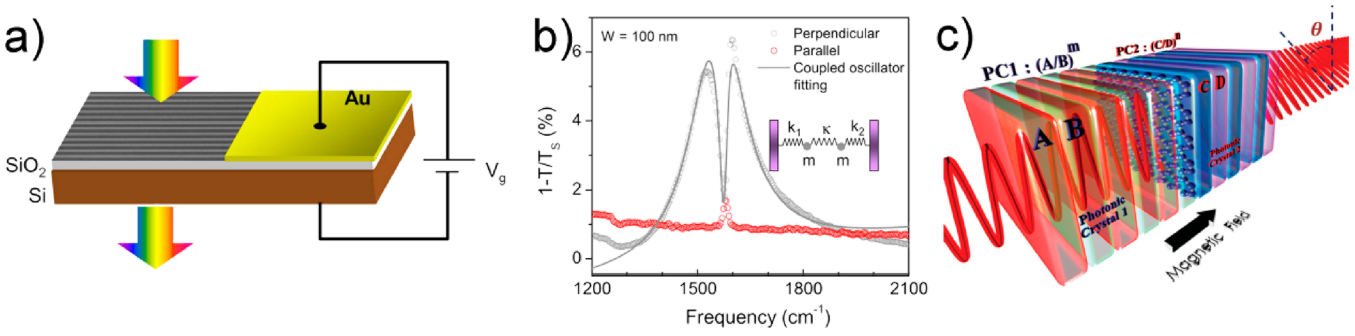

Figure 14. Plasmon induced transparency. (a) Extinction spectrum measurement scheme for a gate-tunable bilayer graphene nanoribbon array for parallel and perpendicular light polarization. (b) The spectrum for the perpendicular polarization is fitted by the coupled oscillator model, as represented by the solid curve. The inset depicts the coupled oscillator model scheme.[318] Reprinted with permission from ref 318. Copyright 2014 American Chemical Society. (c) Schematic of the proposed structure, where graphene is sandwiched by PC1 and PC2. An external magnetic field is perpendicular to the graphene sheet.[424] Reprinted with permission from ref 424. Copyright 2013 American Physical Society.

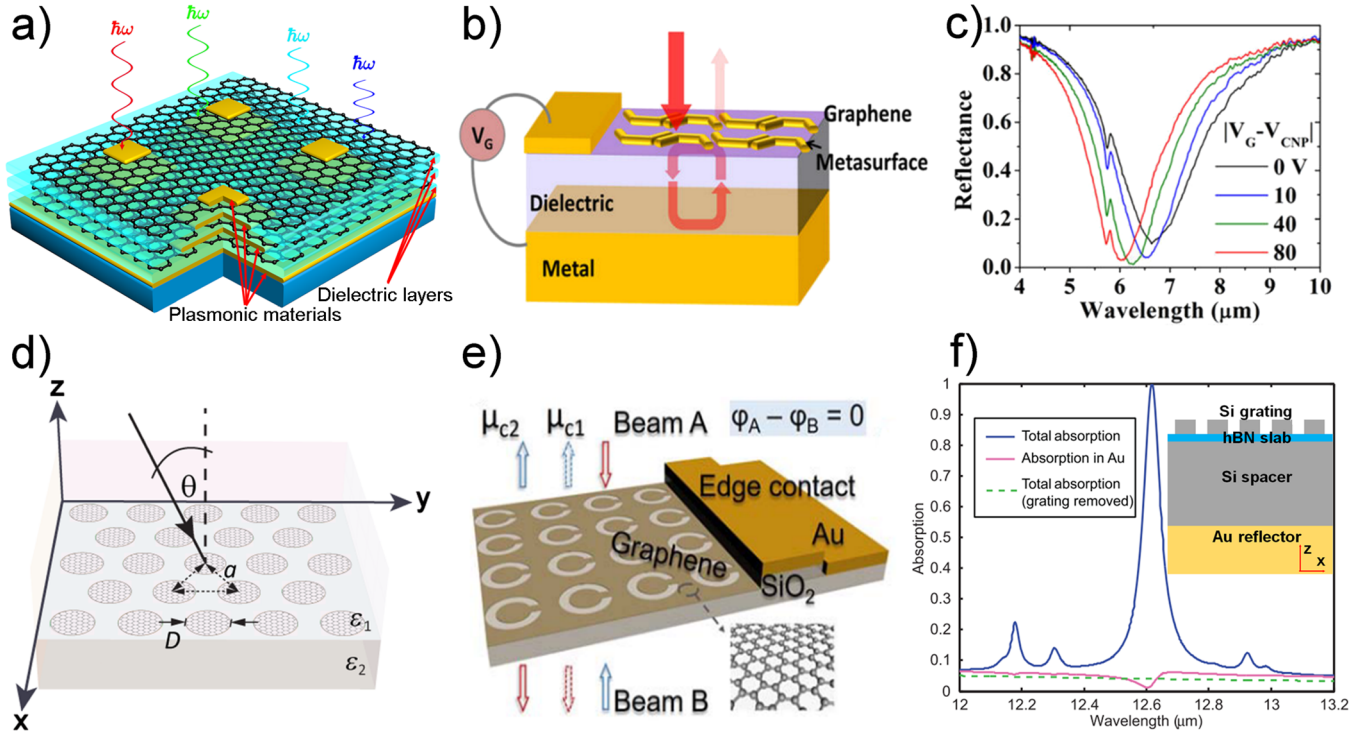

Figure 15. Perfect absorber based on layered 2D materials. (a) MPA integrated with graphene. (b) Schematic of a tunable metasurface absorber composed of an Al film, aluminum oxide layer, and a tunable metasurface on graphene. (c) Reflection spectra from a fabricated metasurface absorbers for different gate voltages.[432] (b, c) Reprinted with permission from ref 432. Copyright 2014 American Chemical Society. (d) Perfection absorption based on the patterned graphene nanodisk.[332] Reprinted with permission from ref 332. Copyright 2012 American Physical Society. (e) Gate tuning coherent perfection absorption through the graphene SRRs.[356] Reprinted with permission from ref 356, Copyright 2015 Optical Society of America. (f) Perfection absorption based on the hypercrystals, i.e., the Si grating integrated with hBN slab.[433] Reprinted with permission from ref 433. Copyright 2016 American Physical Society.

in AB stacked bilayer graphene nanoribbons, Yan et al. reported a phonon induced transparency, as shown in Figure 14a, b.[318] The physics of this effect is that the EM coupling with the IR active optical phonon suppresses light absorption due to plasma excitation in a narrow window; this behavior is similar to that of the dark plasmon mode in standard PIT.[318] Furthermore, all-optical tunable transparency was achieved using a hybrid of layered 2D materials and metamaterials using a nonlinear optical effect.[230,231,429] The threshold pump intensity can be controllably reduced with an effective tuning performance. The transmission light at the PIT window maintains the polarization state of the incident light. The simultaneous control of the polarization state at PIT can be potentially by exploiting the multilayered graphene structures[430] or coupling the optical Tamm modes in PCs and graphene.[424] Exciting applications of plasmon or phonon induced transparency in naturally occurring 2D materials are noted for broadband (from mid-IR to THz) and multifunctional switches[431] and modulators.[183,184]

Transmission light at the PIT window maintains the polarization state of incident light. To achieve polarization control, the Faraday magnetic-optical effect can be considered. By sandwiched graphene between two PCs, polarization rotation was theoretically predicted due to the coupling

https://dx.doi.org/10.1021/acs.chemrev.9b00592
Chem. Rev. 2020, 120, 6197−6246

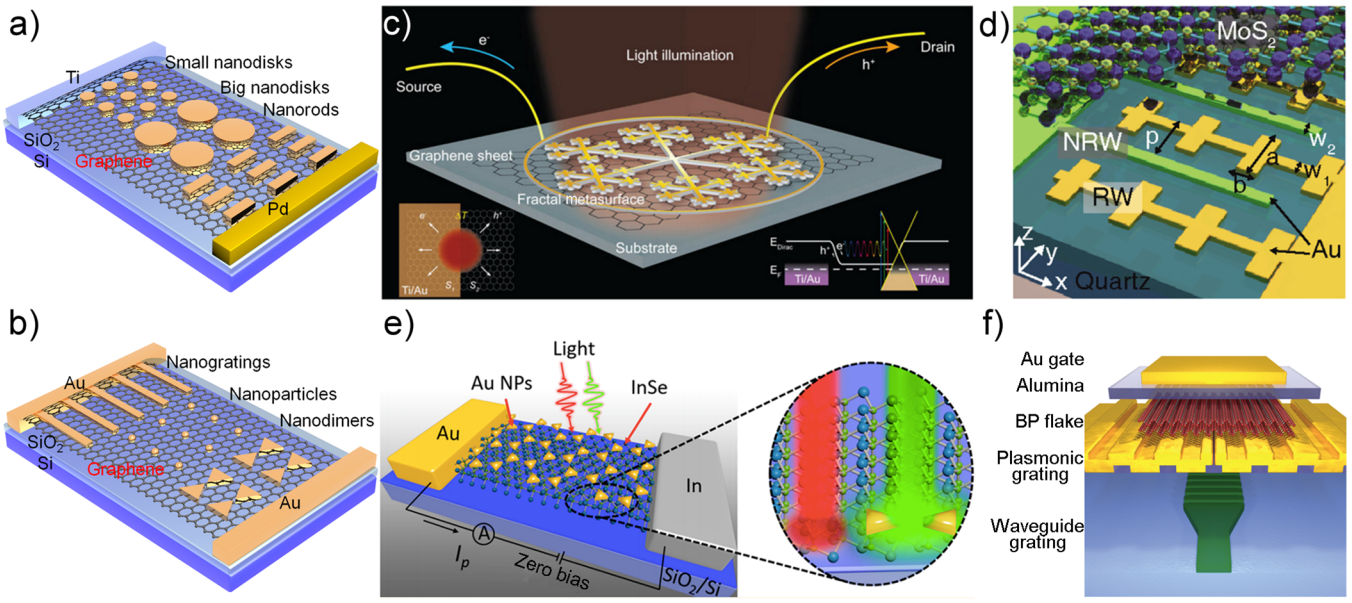

Figure 16. Photodetectors based on 2D materials enhanced by metasurface concepts. (a–c) Graphene photodetectors by using plasmonic nanostructures at metal–graphene contacts (a),[449] across the entire channel (b),[450] and by using snowflake-shape fractal metasurfaces (c).[451] (c) Reprinted with permission from ref 451. Copyright 2017 American Chemical Society. (d) Resonant plasmonic electrodes enhancing MoS_2 photodetection.[452] Reprinted with permission from ref 452. Copyright 2015 American Chemical Society. (e) Plasmonic arrays-enhanced InSe near-IR photodetectors.[453] Reprinted with permission from ref 453. Copyright 2018 American Chemical Society. (f) Plasmonic grating-enhanced waveguide-integrated BP photodetectors.[400] Reprinted with permission from ref 400. Copyright 2017 American Chemical Society.

between optical Tamm modes and graphene.[424] In particular, the performance in terms of the rotation angle and transmittance has been improved with single-layer and multilayered graphene structures.[430]

4.5. Perfect Absorbers

The challenges of 2D materials that are based optoelectronic applications are attributed to the limited light absorption in these atomically thin materials. As previously discussed, the absorption of light in weakly coupled *N*-layer graphene can be estimated by $N\pi\alpha$, which is quite low for obtaining an appreciable photoresponse. Thus, M&M that displays strong light–matter interactions can be a promising platform to promote the absorption efficiency of 2D materials. Even perfect absorbers are possible via the judicious integration of 2D materials with M&Ms.

Figure 15 a presents an illustrative case of giant light absorption (approximately 40%) in a metamaterial perfect absorber (MPA) integrated with graphene (monolayer graphene absorbs 2.3% of incident light).[434] This absorption is achieved by embedding the graphene between the MPAs, which is a device that completely suppresses the scattering of meta-atoms. The significantly enhanced light absorption in the hybrid structure is associated with a combination of multiple factors, including the impedance matching of nanostructured Au metamaterials, the surface plasmon resonance with near-field enhancement at the graphene layer and increased light recycling in the dielectric spacer layers. Moreover, the peak position of the maximum absorption can be tuned by engineering the nanostructure. The broadband or multiband boosted absorption in the near-IR is also demonstrated by vertically cascading the different metamaterial/graphene layers. Other metamaterials such as cross-shaped metallic resonators, ultrathin metasurface absorber (Figure 15 b and c),[432] multilayered MPA,[435] and nanogratings are alternative approaches to boost the light absorption in graphene.[436]

To mimic metamaterials, 2D materials can also be restructured or patterned to enable enhanced absorption or even perfect absorption. A pioneering work has reported total light absorption in a planar periodical array of monolayer graphene nanodisks with very small areas of unit cells, which occurs within a finite range of incident angles that fulfills the critical coupling conditions (Figure 15 d).[332] Graphene microribbons have been extensively investigated due to the ease of fabrication.[437] The nearly all-angle perfect absorption is demonstrated via patterned graphene nanoribbons on the dielectric layer that is positioned on top of the mirror (metal substrate), which is based on the principle of the Salisbury screen,[438] that is, total destructive interference of the reflected light. A gate-tunable coherent perfect absorber in the THz regime has also been realized by split-ring graphene (Figure 15e).[356] Nanostructured 2D materials such as graphene elliptical disk arrays[439] and graphene sidewalls[440,441] have also been reported.[442] Beyond graphene, the metasurface perfect absorption within the Reststrahlen bands of hBN has been reported by integrating Si grating with an hBN slab, hypercrystals with the Salisbury screen effect (Figure 15 f).[433] Similar to metal–dielectric layered hyperbolic metamaterials, multilayer stacking of monolayer graphene and hBN is also proposed to achieve perfect absorptions due to the anisotropy of the stacked materials.[443] Similar approaches inspired by hyperbolic metamaterials are applicable by multilayer stacking of graphene[444] and could be extended to other anisotropic layered 2D materials to achieve perfect absorptions.[445] With the demonstrated enhanced absorption, these techniques have the potential to boost the efficiency of the photodetectors, increase the light–matter interaction strength and enable other broadband EM wave harvesting applications.

4.6. Photodetectors

Traditional photodetectors based on Si and narrow bandgap III–V semiconductor materials have been widely used in many

https://dx.doi.org/10.1021/acs.chemrev.9b00592
Chem. Rev. 2020, 120, 6197–6246

areas such as communication, medical diagnostics, process control, and homeland security.[446] Nevertheless, they suffer from several issues such as low responsivity, the requirement of operation under cryogenic temperatures (for IR detection), and lack of flexibility.[447] Photodetectors based on ultrathin 2D materials are intriguing candidates to circumvent these drawbacks, owing to strong light−matter interactions and large carrier mobilities in 2D materials as well as excellent mechanical properties. In particular, high-performance room-temperature graphene-based flexible photodetectors have been constructed with a wide detection range from UV to THz frequencies due to its linear band dispersion and ultrahigh room-temperature carrier mobility.[446−448]

Generally, 2D materials are too thin (usually the scale of a few nanometers) to harvest sufficient light with normal incident to the 2D plane, which hinders the conversion efficiency from photons to electrons in 2D material optoelectronics. Various metamaterial concepts have been implemented in 2D optoelectronic devices and systems.[30,162] Photodetectors that are based on 2D materials have attracted a substantial amount of attention in the 2D community because the atomically thin 2D crystals and heterostructures are perfect candidates of photoactive media for light detection and sensing in future low-energy on-chip integrated circuits.[52,349,438−440]

One of the intriguing properties of 2D materials with zero or small bandgaps is their broadband optical responses despite their low absorption intensity. As explained in Section 2, graphene, for example, exhibits ultrabroadband photon absorption that encompasses nearly the entire EM spectrum from UV waves to radio-waves.[30] However, the ultrathin form factor (thickness of approximately 0.34 nm) and the semimetal nature (zero bandgap) limit its light absorption (e.g., approximately 2.3% from the visible range to the IR wavelength range).[143] To build 2D photodetectors with broadband response and high efficiency, integration with a metamaterial design is a promising route because metamaterial photonic structures can delicately manipulate the optical field and effectively enhance the interaction between light and 2D materials.

Plasmonic resonances-enhanced graphene photodetectors were proposed and fabricated by using arrays of Au nanostructures.[449,450] To increase the local absorption at metal−graphene contacts, Au nanostructures with strong plasmonic oscillations with incident light were introduced near the contact regions, where the major photocurrent of a graphene device is assumed to be generated (Figure 16a).[449] The considerably enhanced local electric field can directly transfer the incident EM energy to the area of the metal−graphene Schottky junction, which generates an efficiency enhancement of 20 times. In addition to using plasmonic nanostructures at the metal−graphene contacts, Liu et al. demonstrated multicolor photodetection via direct transfer of Au disc arrays to entire graphene films (Figure 16b), which was based on the spectral selective enhancements of plasmonic resonances by designing different size/period/fill factors of Au disc arrays.[450] The resulting plasmonic nanostructure-integrated graphene photodetectors exhibited a high enhancement factor of 1500% in external quantum efficiency, which is attributed to the strong coupling between the local plasmonic near-field and the atomically thin graphene. Subwavelength metallic metasurfaces have been employed in enhancing the graphene optoelectronic performance. Specifically, a Au snowflake-shape fractal metasurface was experimentally fabricated on a graphene photodetector channel, which caused a broadband photoresponse across the entire visible spectrum (Figure 16c).[451] The designed metasurface has a combination of two orthogonally oriented concentric hexagonal fractal geometries, which enable a polarization-insensitive plasmonic enhancement over all polarization angles of incident illumination.

To fully utilize metal electrodes, metamaterial-integrated Au nanostructures have been designed to induce the plasmonic enhancement of 2D photodetectors. For example, resonant Au nanostructured electrodes with optimal geometric parameters have been fabricated to boost the photodetection performance of MoS_2 (Figure 16d).[452] The injection of hot electrons from the plasmonic antenna array to MoS_2 contributed to the sub-bandgap photocurrent generation, which causes a large photogain (maximum of 10^5) in the near IR wavelength (1070 nm). Similarly, a graphene photodetector by embedding graphene into an MPA was theoretically proposed.[434] The enhanced light absorption in the graphene−MPA photodetector is caused by the near-field enhancement of a surface plasmon resonance and the light recycling within the microcavity. By utilizing the intrinsic SPs in graphene, IR plasmonic devices that use multiple graphene-insulator stacks were fabricated; they exhibit enhanced and tunable plasmon resonances with an absorption of 97.5% of EM radiation at frequencies below 1.2 THz.[330] This method can facilitate research on efficient mid- and far-IR photonic devices such as photodetectors and modulators.

In addition to the design of fractal metasurfaces and resonant electrodes, metallic nanopatterns and gratings have been introduced to 2D materials photodetectors. In this case, a high-sensitivity dual-band photodetector that is based on InSe was realized by applying Au plasmonic nanoparticle arrays on the surface of InSe (Figure 16e).[453] Compared with the pristine InSe device, the plasmonic-enhanced InSe photodetectors exhibited an additional photodetection ability across the visible to near-IR range, which is ascribed to the hybridization of quadrupole plasmonic resonances of Au arrays to InSe and the wavelength selective enhancement (e.g., maximum of 12 times enhancement in responsivity at 685 nm). Similar enhancements can be observed in MoS_2 or BP photodetectors.[454,455] For instance, to selectively enhance the anisotropic photoresponse of BP, plasmonic Au bowtie antennas were used to improve the photocurrent along the armchair direction, while bowtie apertures were employed to enhance the inherent polarization selectivity of BP; a high photocurrent ratio of 8.7 (armchair to zigzag) was yielded at 1550 nm.[454]

To demonstrate the on-chip compatibility, a plasmonic grating using Au corrugated arrays was employed in a silicon waveguide-integrated BP photodetector (Figure 16f).[400] This integration enabled a high-performance on-chip photodetecting circuit, which collects the merits of the low propagation loss of silicon waveguides and high field confinement of plasmonic nanogaps. Benefiting from the near-field enhancement, the waveguide-based BP photodetector showed an enhanced responsivity of 10 A W^{1-} and a 3 dB roll-off frequency of 150 MHz. Considering the variety of 2D semiconducting materials with different bandgaps and their heterostructures of various combinations, as discussed in Section 2.2, we can envision that metamaterial-integrated 2D material photodetectors have the potential to achieve high efficiency, broadband and highly tunable photoresponse for

https://dx.doi.org/10.1021/acs.chemrev.9b00592
Chem. Rev. 2020, 120, 6197−6246

Table 2. Performance of Representative 2D Material-Based Photodetectors with Plasmonic Enhancement

2D materials	photonic structures	detecting wavelength	photodetector responsivity (mA W^{1-})	efficiency enhancement factor	references
graphene	1D Au nanograting	514 nm	~10	~20	449
graphene	2D Au nanoparticle array	514 nm	~6.1	~15	450
graphene	Au fractal metasurface	476−647 nm		8−13	451
graphene	intrinsic nanoribbon superlattice	10.6 μm	~0.0075	~10	456
MoS_2	Au antenna array	1070 nm	5200	105	452
InSe	Au triangular nanoparticle arrays	685 nm	244	12	453
BP	Au bowtie antennas	1550 nm	14.2	1.7	454

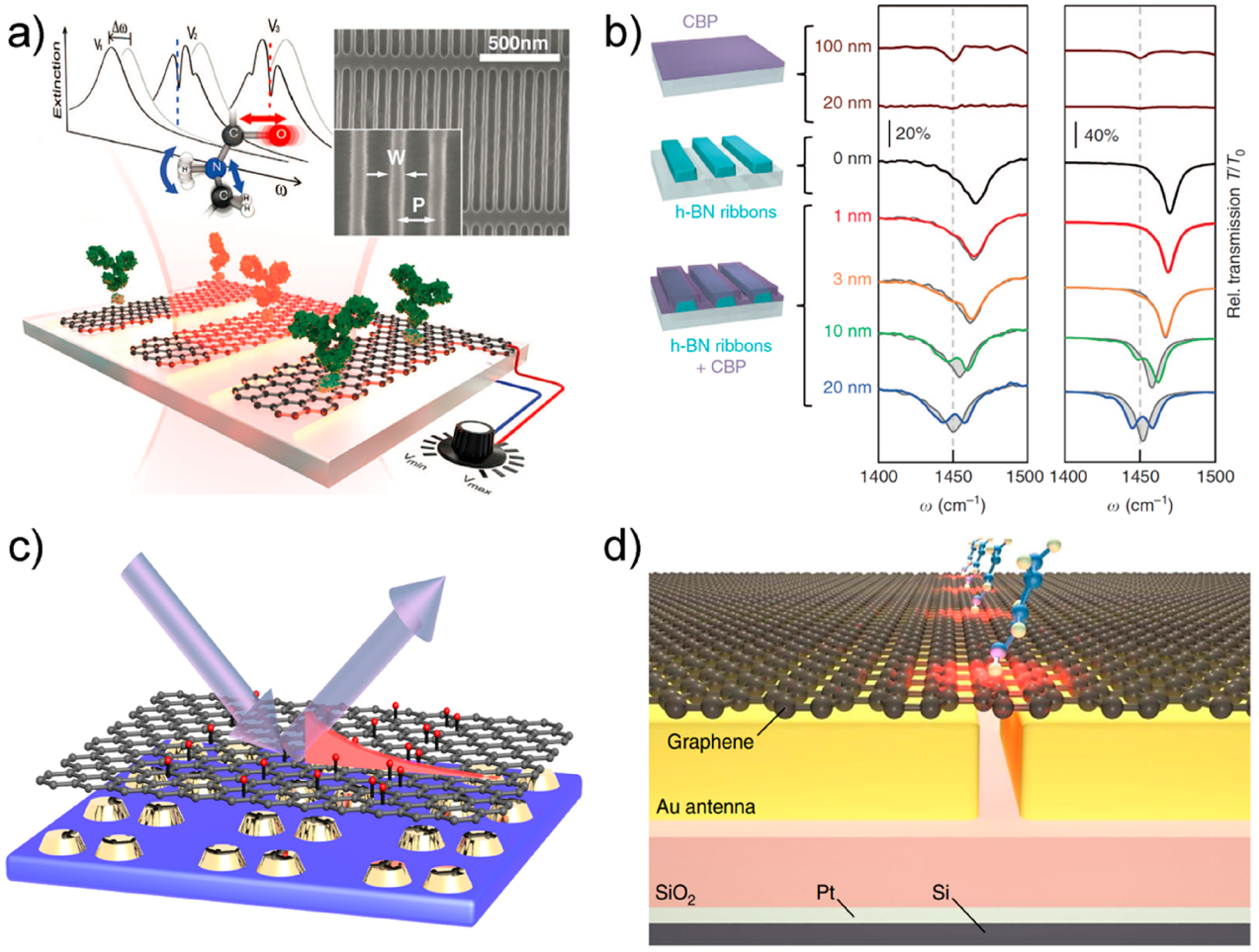

Figure 17. Optical sensors based on 2D materials. (a) Schematic of graphene biosensor. The EM field is concentrated at the ribbon edge, which enhances light interaction with the protein molecules adsorbed on graphene. Protein sensing is achieved by detecting a plasmon resonance spectral shift that is accompanied by narrow dips that correspond to the molecular vibration bands of the protein.[327] Reprinted with permission from ref 327. Copyright 2015 AAAS. (b) Infrared transmission spectra of hBN ribbon arrays with different thicknesses 4,4′-bis(*N*-carbazolyl)-1,1′-biphenyl coating.[104] Reprinted with permission from ref 104, Copyright 2018 Nature Publishing Group. (c) Square array of Au double-dots on a glass substrate covered by a weakly hydrogenated graphene crystal.[464] (d) Graphene-metallic metasurface with small molecules adsorbed on the suspended graphene.[465] Reprinted with permission from ref 465, Copyright 2018 Nature Publishing Group.

future low-energy consumption electronics. To quantitatively compare the state-of-the-art of 2D material-based photodetectors, we list the performance of a few representative cases with plasmonic enhancement, as shown in Table 2.

4.7. Sensors

In biosensing applications, 2D materials that possess rich surface EM modes and high surface-to-volume ratio exhibit significant potential. Many studies have explored biosensors based on 2D material.[457] A few review articles on biosensors, in which 2D materials comprised the sensing media, including graphene, BP, and TMDs, have been published.[458−460] Most of those sensor devices are constructed on pristine 2D nanosheets and operate via a change in their electronic, optical or chemical responses. We highlight the concept of the integration of metamaterial with 2D materials, in particular graphene, for biochemical sensors. The biocompatibility of a 2D material is a prerequisite for biosensing applications. Graphene has been verified to be biologically compatible with biomolecules, cells, and tissues in terms of both its functionalized state and natural condition.[461,462] Considering its surface uniformity and superior optoelectronic properties, graphene is regarded a potential high-sensitivity biosensing platform. Additionally,

https://dx.doi.org/10.1021/acs.chemrev.9b00592
Chem. Rev. 2020, 120, 6197−6246

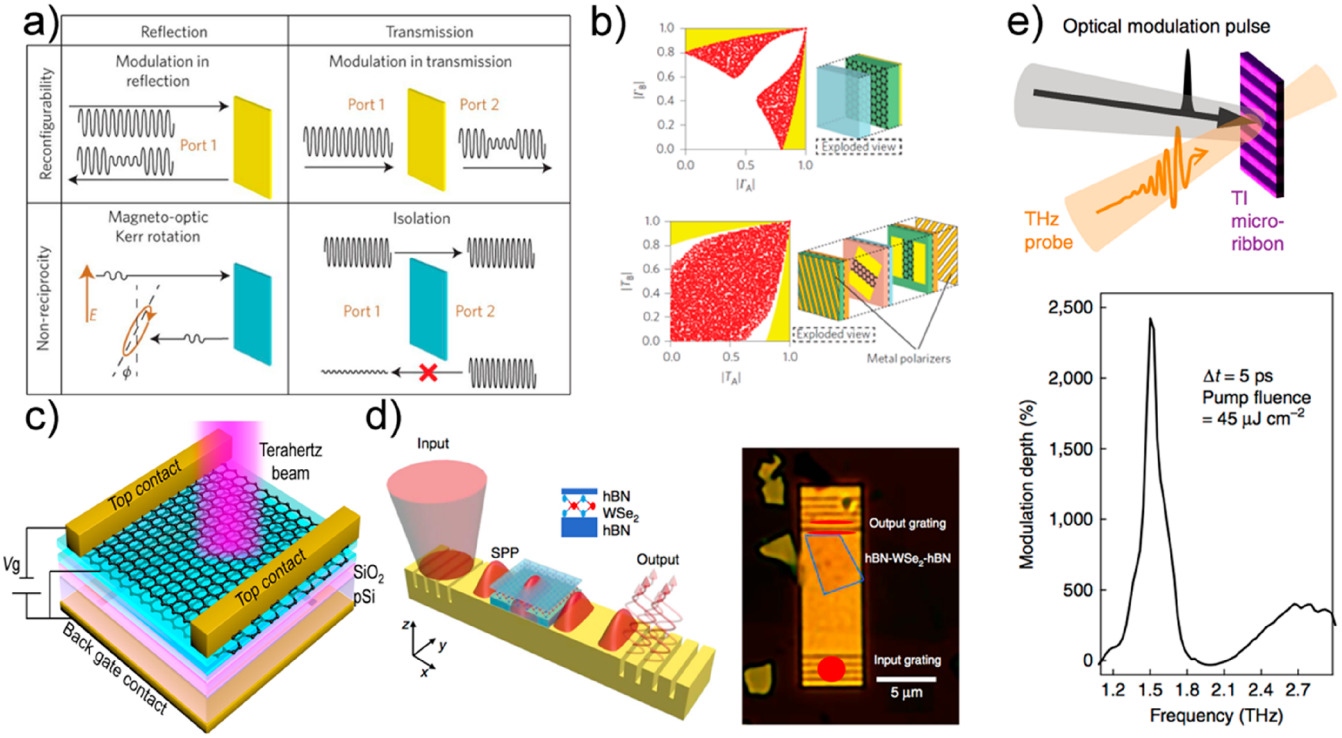

Figure 18. Modulators based on 2D materials and metasurfaces. (a) Graphene-based device capabilities are classified according to the direction (reflection or transmission) and framework (nonreciprocity or reconfigurability).[473] (b) Simulations of randomly generated reflection modulators (top) and simulations of different device topologies for transmission modulation (bottom).[473] (a, b) Reprinted with permission from ref 473. Copyright 2014 Nature Publishing Group. (c) Device structure of a gate-tunable low-loss graphene THz modulator.[183] (d) Plasmonic modulator device based on monolayer WSe_2 (left) and an optical image (right).[475] Reprinted with permission from ref 475, Copyright 2019 Nature Publishing Group. (e) Ultrahigh modulation depth by utilizing topological SPs in Bi_2Se_3 microribbons.[476] Reprinted with permission from ref 476, Copyright 2015 Nature Publishing Group.

research has shown that large-area high-quality graphene film can be directly transferred damage-free onto any target substrate,[463] which is a considerable advancement toward practical sensing applications.

Figure 17a shows a schematic of a mid-IR plasmonic biosensor constructed of nanostructured graphene.[327] As shown in the inset of Figure 17a, graphene nanoribbons with a desired width, length, and separation can be readily produced by the well-developed lithographical method. As discussed in Section 2.3, graphene supports low-loss plasmon polaritons with extremely strong IR light confinement that is two orders of magnitude stronger than metals, which enables ultrasensitive detection of the refractive index and vibrational fingerprints of nanometric biomolecules by monitoring the extinction spectra acquired by Fourier transform infrared spectroscopy. The most attractive point of this graphene biosensor design is that the protein can be selectively probed at different frequencies, which benefits from the dynamically tuned plasmonic resonance of graphene nanostructures by tuning the Fermi level in graphene via external electrical gating. Arrays of graphene nanoribbons that feature highly confined and extensively tunable plasmon resonances have also afforded the capability of simultaneous detection of in-plane and out-of-plane vibrational modes of ultrathin polymer films with high sensitivity.[466] Label-free identification of gas molecules has been realized by detecting their rotational−vibrational modes via graphene plasmons,[467] in which the high physisorption of gas molecules on the graphene nanoribbons combined with the ultraconfined plasmonic near-fields were critical for overcoming the extremely weak dielectric responses of gas molecules and achieving high sensitivity.

A hybrid metasurface composed of Au nanoantennas and graphene was designed to quantitatively detect monolayers of subnanometer-sized molecules or particles.[267,383,464,465] As shown in Figure 17c, by using reversible hydrogenation of graphene and binding of streptavidin−biotin, a level of fgmm^{-2} and detection of individual biomolecules, respectively, are demonstrated with mass sensitivity, which offers a method toward simple and scalable single molecule label-free biosensing technologies. In hybrid metasurface biosensors (refer to Figure 17d), a combination of molecule induced carrier doping and plasmon resonance shift of graphene contributed to the high sensitivity, which enables enhanced fingerprinting of minute quantities of polymer and glucose molecules. Hybrid M&M with 2D materials can be employed for molecular recognition and produces unparalleled sensitivity at the single molecule level, which provides an alternative to existing biological and chemical sensing technologies. The reported hybrid metamaterials sensors are suitable for high throughput multisensing platforms.

In addition to the extensively investigated graphene nanopatterns with various geometry features and designed plasmonic resonance,[84,267,268,330,468−470] hBN nanoresonators that hold lower-loss IR PhPs recently demonstrated strong interaction with molecular vibrations in the strong coupling regime, which were experimentally and numerically confirmed (Figure 17b).[104] We also note that the optical biosensors using hydrogenated MoS_2 nanosheets were demonstrated based on tunable plasmon resonances in the near-IR.[471] The combina-

https://dx.doi.org/10.1021/acs.chemrev.9b00592
Chem. Rev. 2020, 120, 6197−6246

tion of 2D materials (graphene, hBN, and MoO_3) with a metasurface for biosensors affords enhanced sensitivity, dynamic controllability, and tunable spectral selectivity, which may highlight future 2D material biosensors based on low-loss plasmon polaritons, PhPs, and their hybrids.

Additionally, the selectivity of 2D material-based chemical sensors is advantageous compared with conventional metal-based plasmonic sensing. Although similar surface functionalization strategies can be introduced to 2D materials to enable the surface selectivity to specific chemical groups. However, 2D sensors endow several unique optical properties (as discussed in Section 2) to achieve sensing selectivity. First, 2D sensors can be dynamically tuned over a broad spectral range through electrical gating, for instance, when utilizing SPs of graphene. Patterning 2D materials with designed geometric parameters (e.g., size, shape, period, fill factors) also provides a way to control the photonic resonances and thus spectral selectivity to molecules. Furthermore, the combination of 2D materials with conventional metamaterials offers extra merits toward highly sensitive and selective chemical sensors. We note that the surface of 2D materials could be an inherently excellent platform for immobilizing chemical species. For example, it has been demonstrated that layered material α-MoO_3 support low-loss hyperbolic PhPs in the mid-IR; the surface of α-MoO_3 terminated by O atoms can form hydrogen bonding with specific molecules, which offer another approach to tune the polaritonic effect.

4.8. Modulator

2D material modulators can be generally classified into different types according to the principle of operation (all-optical, electro-optic, thermo-optic, magneto-optic, acousto-optic, and mechano-optic), the attribute of light (wavelength, amplitude, phase, polarization, time, and direction), and the optical property of the material (absorptive property correlated with the imaginary part of the refractive index, and refractive property correlated with the real part).[472] To realize high-performance 2D material modulators, several key figures of merits, including modulation speed and depth, operation frequency range, insertion loss, stability, and compatibility, need to be considered. By the design of metamaterial structures, enhanced light modulation in 2D materials can be expected. For example, a high modulation depth to 95% and a modulation time less than 10 ns in the mid-IR spectral range were achieved in a graphene-based metasurface perfect absorber, as discussed in Section 4.5.[432] Particularly, the recently demonstrated hybrid plasmon−phonon polaritons in graphene/hBN heterostructures exhibited enhanced light−matter interactions with loss lower than that exhibited by individual graphene plasmons (refer to Section 2.3 in this review),[197] which implies their potential in the realization of highly efficient modulators in the mid-IR or THz region. Similarly, combining in-plane anisotropic and ultralow-loss polaritons in α-MoO_3,[88] ultrahigh-performance IR light modulation with polarization sensitivity is achievable in graphene/α-MoO_3 heterostructures.

Due to its easy, broad, and dynamic tunability of Fermi energy via electrical gating, graphene is extensively investigated in electro-optic modulation, which requires a highly dynamic reconfiguration of carrier conductivity. The fundamental limit of the performance of graphene modulators is only associated with the conductivity tensor of graphene. Figure 18a shows the device capabilities of graphene amplitude modulators, which are classified by the direction (i.e., transmission and reflection) and framework (i.e., reconfigurability and nonreciprocity).[473] Four types of representative operation mechanisms attract fundamental interest: amplitude modulation in reflection, amplitude modulation in transmission, magneto-optical Kerr rotation, and nonreciprocal isolation based on Faraday rotation. As discussed by Tamagnone et al.,[473] a graphene film that uniformly covers a metal substrate is a very which the single equivalent DoF by changing the permittivity, thickness or number of simple reflection modulator, in layers produces a 1D locus. To obtain a near-optimal modulation performance, graphene nanopatterning or the introduction of additional dielectric layers on graphene has been numerically demonstrated to be an effective alternative (Figure 18b).[473] The frontier of the total random performance is similar to the theoretical upper bound. Graphene modulators that operate in the transmission mode were also calculated, which exhibits a suboptimal performance. This finding is attributed to the high loss in graphene and the mismatch of impedance to the system, which limits the high-transmission modulation rate compared with reflection modulators. For an additional DoF, a polarization twist after transmission can be introduced by an anisotropic metal−graphene hybrid.[474] Therefore, one polarization can be modulated by the designed hybrid metasurface, while the other polarization was sustained to convey feedback in the device system. The discussed theory provides a solid understanding of the operation and basic limits of graphene modulators and may also serve as a model for achieving high-performance modulation by other 2D materials.

Based on the optical modulation effect, highly efficient room-temperature modulation of THz wavelengths was achieved using graphene with both broadband response and low intrinsic signal attenuation (Figure 18c).[183] Experimentally, the THz transmission through graphene was effectively controlled by gate-tuning the density of states available for intraband transitions. The resulting graphene modulator achieved superior modulation performance with a low insertion loss of 5%, a high intensity modulation depth of 15%, and a modulation frequency of 20 kHz. Furthermore, optical frequency combs using graphene and photonic microresonators were demonstrated with gated intracavity tunability.[477] The devices worked well by coupling the gate-tunable optical conductivity to a Si_3N_4 microring resonator, which enabled the effective modulation of the second- and higher-order chromatic dispersions by tuning the Fermi level. Through a dual-layer ion-gel gate, the charge-tunable primary comb lines were produced from 2.3 THz to 7.2 THz with coherent Kerr frequency combs, controllable Cherenkov radiation and soliton states in a single graphene microcavity. Another example is an extensively tunable metasurface that consists of Au antennas on graphene film that was integrated into optical nanocavities, which demonstrates superior mid-IR modulation performance by acting as an electrically tunable MPA (refer to Figure 15b and c).[432] In addition, Gan and coworkers realized an efficient thermo-optic microring graphene modulator, in which the electrical and thermal properties of graphene were utilized by covering a graphene film on a Si microring resonator.[478] Due to the high electrical and thermal conductivity, the graphene thermo-optic modulator showed a large modulation depth of 7 dB with a broad operating wavelength range.

Similar to graphene, various 2D materials, including TMDs,[475] BP,[479] TI,[476] and perovskites,[480] can be employed

https://dx.doi.org/10.1021/acs.chemrev.9b00592
Chem. Rev. 2020, 120, 6197−6246

Table 3. Performance of Representative 2D Material-Based Optical Modulators

2D materials	photonic structures	mechanism	modulation frequency/ wavelength	modulation depth	modulation speed	references
graphene	stacked pairs	electro-optic	570 GHz	15%	20 kHz	183
graphene	microribbon arrays	electro-optic	~3 THz	70%		481
graphene	hexagonal Au meta-atoms	electro-optic	0.6−1.2 THz	47%	100 kHz	81
graphene	Au antenna and optical cavity	electro-optic	5−7 μm	100%	20 GHz	432
graphene	Au grating	electro-optic	1.5 μm	8.3%	>1 GHz	482
graphene	Si PC cavity	electro-optic	1.593 μm	10 dB		483
graphene	Si waveguide	electro-optic	1.35−1.6 μm	4 dB	1.2 GHz	184
graphene	Si microring resonator	electro-optic	1.55 μm	40%	80 GHz	484
graphene	Si_3N_4 microresonator	electro-optic	1.6 μm	~33.3% (extinction change)	600 kHz	477
graphene	Si_3N_4 microresonator	electro-optic	~1.57 μm	15 dB	30 GHz	485
graphene	Si microring resonator	thermo-optic	1.5549 μm	80% (7 dB)	100 GHz	478
graphene	microribbon waveguide	thermo-optic	1.55 μm	30 dB	~15 kHz	486
graphene	Au split-ring array	all-optical	0.9 THz	84.8%		487
WSe_2	Au waveguide	all-optical	~0.713 μm	4.1%	290 PHz	475
Bi_2Se_3	microribbon array	all-optical	1.5 THz	2400%	5 THz	476

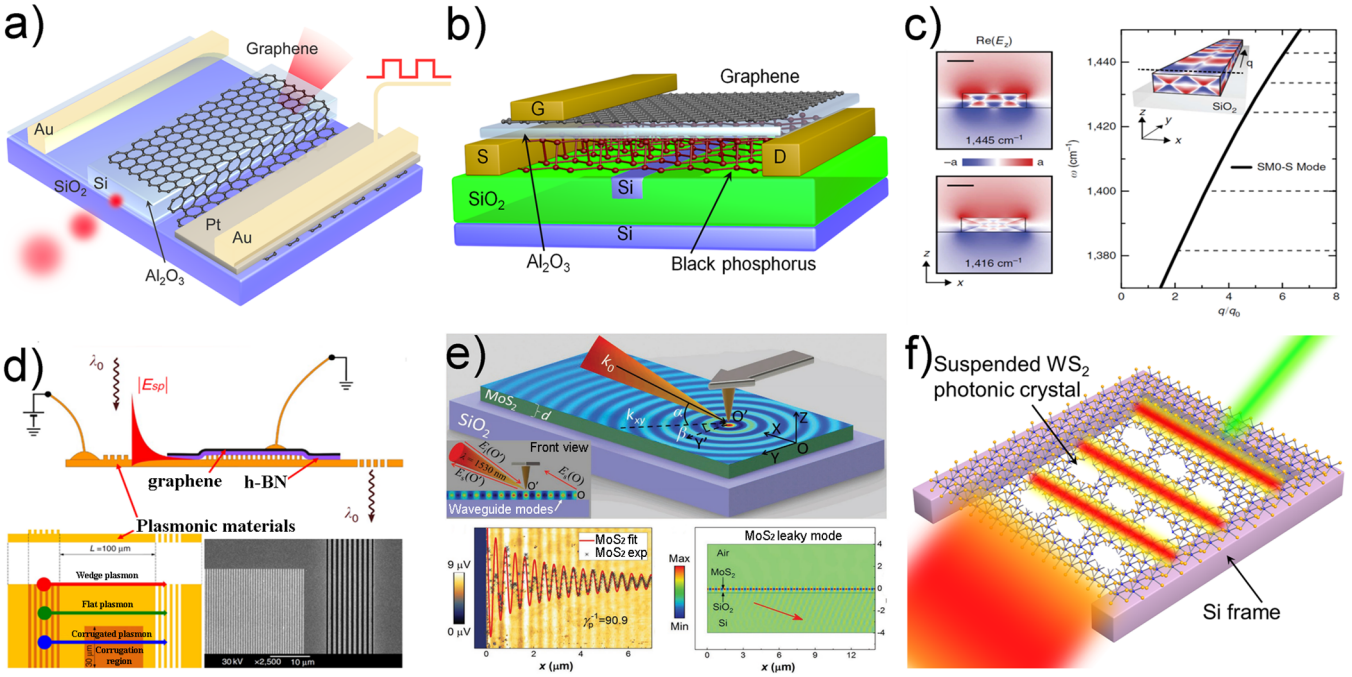

Figure 19. Waveguiding based on 2D materials. (a) The graphene-based integrated waveguide platform for an optical modulator.[184] (b) Illustration of a photodetector. The graphene on top serves as the gate and BP as absorbing photons. The silicon waveguide allowed the measurement of absorption in BP.[490] (c) A rectangular waveguide of hBN with 250 nm width and 65 nm thickness. The left, simulated near-field distribution ($Re(E_z)$) at 1445 cm^{-1} (top) and 1416 cm^{-1} (bottom). The right, calculated dispersion. The inset shows the waveguide and the near-field distribution at 1445 cm^{-1}.[488] Reprinted with permission from ref 488. Copyright 2017 Nature Publishing Group. (d) Nontransparent grating couples light into the flat (green line), corrugated (blue line), or wedge (red line) plasmon mode. The plasmons were decoupled into light through the transparent grating (top and lower left). The SEM images of plasmonic waveguide is shown in the lower right corner.[482] Reprinted with permission from ref 482. Copyright 2015 Nature Publishing Group. (e).The nanoimaging of MoS_2 (thickness: 110 nm) at 1550 nm. k_0 is the free-space wavevector. The lower left is the measured field distribution with the fitting. The lower right is the simulated leaky mode of MoS_2.[496] Reprinted with permission from ref 496. Copyright 2019 John Wiley and Sons. (f) The schematics of PC made of suspended membrane of monolayer WS_2, showing the nature of guiding the visible photons within the atomic thickness.[497]

for effective light modulation. Here, an example of utilizing semiconducting WSe_2 monolayers is shown to realize highly efficient nonlinear plasmonic modulators (Figure 18d).[475] In this design, a monolayer WSe_2 was transferred onto a lithographically defined metallic waveguide, in which the excitons in WSe_2 strongly interacted with SPPs and caused a change in transmission of 73% through the device. An ultrafast response time to 290 fs was achieved by controlling the propagating SPPs via optical and SPP pumps. Benefiting from the intriguing topological SPs, an ultrahigh modulation depth to 2400% in the THz range (approximately 1.5 THz) was achieved in the microribbon arrays of a Bi_2Se_3 topological insulator (Figure 18e).[476] This unprecedented observation was ascribed to two factors. First, the near-zero extinction spectrum from the Fano-like plasmon−phonon-destructive interference contributed a remarkably reduced denominator of the extinction ratio. The second factor is the photoinduced formation of massive 2DEG below the topological surface

https://dx.doi.org/10.1021/acs.chemrev.9b00592
Chem. Rev. 2020, 120, 6197−6246

states, which contributes a substantial increase in the numerator of the extinction ratio. The performance of representative 2D material-based optical modulators are given in Table 3. Therefore, the realization of tunable 2D material modulators based on photonic nanostructures is a promising architecture that crosses atomic layer nanoscience, nanophotonics and ultrafast optoelectronics.

4.9. Waveguide

Their exotic nature renders 2D materials a promising candidate for building an ultrathin and broadband waveguide platform. One approach is to coat the dielectric waveguide with 2D materials, which enables the tunable waveguide response. Alternatively, the polaritons that are generated from the exotic interaction of light with layered 2D materials can also be guided, which forms the polaritonic waveguides.[113,122,488,489] Moreover, the vdW force between layered 2D materials render the large dielectric refractive index and enable the excellent light guiding property, which considers the total internal reflection. Here, we focus on the strategies of the application of the waveguides that rely on 2D materials.

For the application of the modulator[184] (Figure 19a) or the photodetector[490] (Figure 19b), 2D material can be integrated with the waveguide. The benefits are the enhanced and actively tunable interaction of 2D material with light in a broad spectrum of EM frequency, the high speed due to the large carrier mobility, the high responsibility and the low dark current.[491−494] The waveguide can also be designed for the highly confined polaritons, especially the SPPs and PhPs.[482,488] The hyperbolic PhPs comprise the guided mode in a thin hBN slab, which can be quantized (equivalent to the high-order mode) considering the constructive interference condition of the waveguide.[113,123,419] The mode profile and the dispersion of the phonon polariton in hBN are provided in Figure 19c; they manifest the hyperbolic ray nature that bounces back and forth similar to the mode in a conventional waveguide.[488] The propagation nature of SPPs comprise the guide mode at the surface between metallic media (such as graphene and BP) and a dielectric substrate. The structure of these 2D materials can be further engineered to manipulate the waveguiding effects of SPPs.[495] The hybridization of graphene and hBN can also be considered to form a synthetic waveguide on top of corrugated Au (Figure 19d), which supports the flat SPs, corrugated plasmons, and wedge plasmons with a large modulation depth (0.03 dB μm^{-1}) and low propagation loss.[482]

Recent findings have confirmed the high refractive index nature of stacked 2D materials,[496,498] which is particularly interesting considering the guiding effect for all-dielectric M&Ms. For example, the waveguiding effects in subwavelength hBN nanopillars at the visible frequency can be exploited to obtain the 2π phase change by varying its geometry, which can enable the design of ultrathin vdW metalens.[499] Moreover, the waveguide can be simply achieved by the high permittivity of vdW materials (Figure 19e). The anisotropic nature of vdW materials guarantees the different group velocity of the TE and TM modes, which enables the modal birefringence with potential applications of phase retarders.[496] The high refractive index can be observed in the ultimate limit, monolayer or few layer materials.[497,500] The theoretical proposal of visible photon guiding in the monolayer can be experimentally demonstrated with the near unitary effective index (Figure 19f).[497] Photonic crystals can also be achieved by few-layer materials with a leaky wave.

The exotic light matter interactions supported in layered 2D materials can provide an exciting platform for guiding photons in polaritonic form or waveguide mode, which can even be demonstrated in a thickness of a few atoms. This finding is extremely important for ultrathin, on-chip, high-capability, and tunable photonic circuits, optoelectronic devices, and even quantum applications.

4.10. Emitters

Light emission is an important and interesting property of 2D semiconductor materials. We note that an increasing amount of attention has been focused on single-photon sources based on 2D materials (e.g., hBN and WSe_2), with applications in quantum computing circuits beyond conventional LED displays.[33,115,501] The interesting term is the chirality or spin/valley polarization of emitted photons from 2D TMDs, which endows a new DoF to tune the light emission and a novel design of optoelectronic devices.[502−504] Despite the ultimate thin form of 2D semiconductors, they can exhibit strong light emission efficiency, for example, with near-unity PL quantum yield and enhanced minority carrier lifetime in MoS_2 monolayers treated by an organic superacid[505] or electrostatic doping.[506] By utilizing the high emission efficiency of 2D semiconductor monolayers, high-performance ultrathin LEDs with graphene−hBN−TMD quantum well structures showed a high external quantum efficiency to 8.4%,[507] a record of 2D material-based electroluminescent devices and a large advancement from the perspective of fundamental research.

Coupling 2D materials with metamaterials is a straightforward way to improve the light emission efficiency and manipulate the emission behavior (e.g., polarization and directionality) to create an efficient emitter. Wang et al. obtained a giant PL enhancement factor of approximately 20 000 from a suspended WSe_2 monolayer on Au nanostructure-based plasmonic metasurfaces, which was ascribed to the concentration of the excitation EM field in the sub-20 nm Au nanogrooves (refer to Figure 20).[508] Tuning of the lateral gap plasmon resonances by changing the pitch of the structures can effectively match different wavelengths of the pump laser, which provides sufficient room for adjustment to enhance the optical absorption and emission in other 2D crystals and incident laser systems. Designing doubly resonant nanostructures with directional control can achieve further PL enhancements such as the horizontally or vertically cascaded plasmonic nanostructures in Figure 20. Note that the giant emission enhancement in the WSe_2−Au arrays system was only caused by the trapping of the pump laser (633 nm) without careful consideration of the out-coupling of the WSe_2 emission spectrum window (700−820 nm). The light emission efficiency in this coupling regime can be improved. In addition, many approaches for realizing directional/polarized emission from 2D materials have been demonstrated by using subwavelength plasmonic metallic[392,509,510] or photonic dielectric structures.[511−513] The incorporation of metamaterial design in 2D semiconductors provides an effective platform for creating novel high-performance multifunctional 2D emitters. The bandgap (eV), PL quantum yield, EL quantum yield, photonic structures, and PL enhancement factor of light emitters based on a few representative TMDs are summarized in Table 4.

In addition to the enhancement of the exciton emission of 2D materials, coupling with metasurfaces can achieve the steering of nonlinear photon emission. Optical waveguide

https://dx.doi.org/10.1021/acs.chemrev.9b00592
Chem. Rev. 2020, 120, 6197−6246

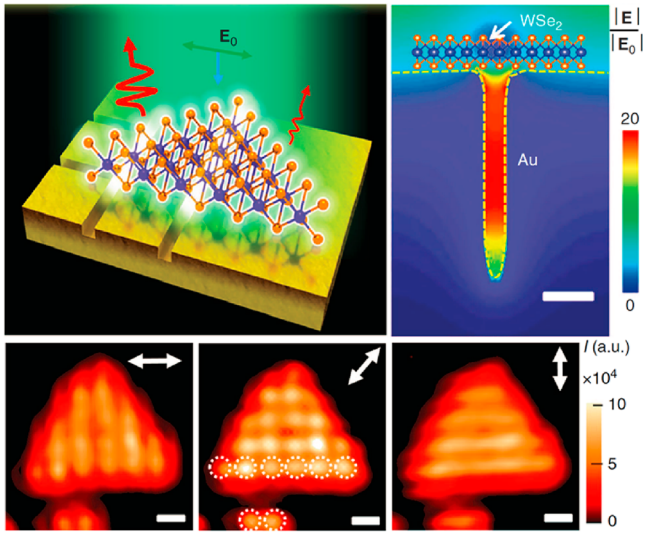

Figure 20. Top right, schematic of PL emission from a single crystal monolayer WSe_2 flake on a patterned Au substrate. Top left presents the simulation of the electric field distribution of the lateral gap plasmons with a WSe_2 monolayer flake suspended over a single trench and the polarization of the incident laser field. The bottom depicts PL intensity mappings with polarization angles of 0°, 45°, and 90°.[508] Reprinted with permission from ref 508, Copyright 2016 Nature Publishing Group.

structures that are based on silicon circular rings have been proposed to enhance SHG from $MoSe_2$ monolayers, which further enables phase matching of the nonlinear process.[250] Electrons have two intrinsic degrees of freedom, namely, charge and spin. Based on these two degrees of freedom, researchers have developed the extensively applied electronic technology and the increasingly mature field of spintronics. In recent years, 2D materials such as single-layer TMDs, have formed an additional DoF due to their special inversion symmetry: valley pseudospin (K and K').[517] Valley freedom as an information carrier enables a variety of new functional devices. Compared with traditional electronic components, the new 2D valley electronic devices have the advantages of information nonvolatility, fast processing speed, low energy consumption, high integration and long transmission distance.[504] However, the lifetime of the energy-excited state is very short at RT, and the thickness of the single-layer 2D material is only of the order of the atomic layer, which causes a weak coherence with the external excitation field, which severely limits the efficiency of the valley degree.[518,519] T Therefore, improving the efficiency and valley coefficient of nonlinear processes in 2D materials is an urgent task to be solved in the field of electronics/spintronics.

A type of nonlinear optical interface that consists of a noble metal nanopore array and a single layer of 2D material was proposed.[393] This interface solves the issue of multidimensional control over the conversion efficiency of the SHG on a nanometer scale. Hu et al. has recently realized a new nonlinear optical interface for the efficient operation of nonlinear energy valley-photons in single-layer WS_2 (Figure 21).[83]

The gradient phase information of the Au nanopore array was successfully designed and collected. When the left (right) circularly polarized light passes through the Au nanopore, a right (left) circularly biased fundamental light with phase information is generated. According to the SHG selection rule, the specific energy valley K (K') is excited and produces a left (right) spin SHG, which is near 100% in the experiment. Due to the local field enhancement effect of the Au nanopore, the interaction between the light field and the energy valley is enhanced, and the SHG conversion efficiency is improved by 3 orders of magnitude. The SHG photons locked by the valley can carry phase information and realize various functions such as controlling the angle of emission. The scheme is applicable to medium superstructure surfaces and other 2D material systems, which provides a very simple and reliable way for 2D materials to control, encode and read information. This type of 2D material-metasurface hybrid system stimulates research on future RT and free-space nonlinear and valleytronic devices.

5. CONCLUDING REMARKS AND OUTLOOK

In this review, we focused on describing research on the overlap between layered 2D materials and metamaterials and metasurfaces. We established the potential of 2D materials that behave as natural born "metamaterials" with exotic properties that were previously believed to be only attainable in artificially engineered structured materials. The outstanding properties of materials with a 2D nature include broadband light−matter interactions, few losses, flexible tunability, strong nonlinearities, and the emergence of various types of polaritons. While the traditional plasmonic or all-dielectric M&Ms can be exploited to manipulate 2D materials, additional functionalities and novel M&Ms can be obtained by increasing the complexity of the subwavelength compositions from structured layered 2D materials. With the disclosure of these optical properties and construction methods, we understand the microscopic origin of the interaction between 2D layered materials and metamaterials. This fundamental knowledge is important in the search for reliable applications. The first steps in this direction have also been described in this review, and the fabrication of several devices, such as planar lenses, cloaks, photodetectors and sensors, has been demonstrated.

5.1. Outlook

Current research in metaphotonics focuses on theoretical designs and calculations. Particularly, many theories have been proposed for traditional metal-based metasurfaces and metamaterials, for example, regarding thin MPA[520] or

Table 4. Performance of Light Emitters Based on TMDs[a]

2D materials	bandgap (eV)	PL quantum yield (%)	EL quantum yield (%)	photonic structures	PL enhancement factor
MoS_2	1.8	95[b,505]	8.4[d,507]	Si_3N_4 PC[513]	1300
WS_2	2.05	90[c,506]	1.32[d,507]	photonic hypercrystal[512]	60
WSe_2	1.7	8[506]	5[514]	Au trenches[508]	20 000
$MoSe_2$	1.5	8[c,506]		Au rectangular nanoantennas[515]	3
$MoTe_2$	1.1		9.5[e,516]		

[a]All of the parameters were obtained for monolayers at RT except those indicated. [b]Chemically treated. [c]Electrostatically doped. [d]At 6 K. [e]At 83 K.

https://dx.doi.org/10.1021/acs.chemrev.9b00592
Chem. Rev. 2020, 120, 6197−6246

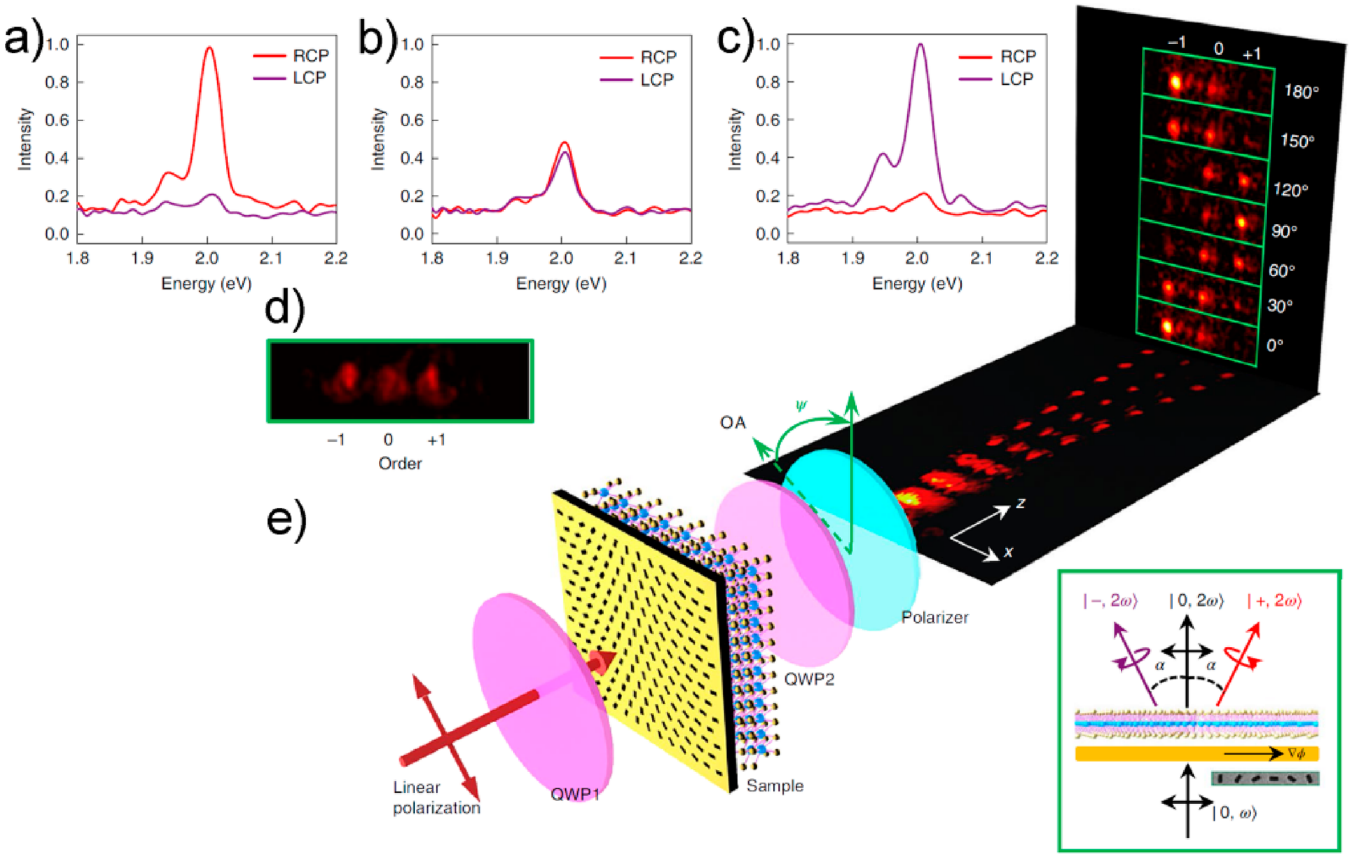

Figure 21. (a–c) Experimentally measured intensity of the two chiral components in the first (a), zeroth (b), and first orders (c). (d) The field distribution at z = 120 μm, with three distinct orders; it is measured without quarter-wave plate (QWP)2 and the polarizer. (e) Schematic of the experimental optical setup. The incident linearly polarized beam has a wavelength of 1240 nm. QWP1 can change the incident polarization to circularly polarized. QWP2 and the linear polarizer are used to test the chirality of the emitted second-harmonic photons. The horizontal image is the experimental result from the evolution of the light splitting into three orders. The vertical images depict the field distributions obtained by rotating the linear polarizer, which changes its optical axis (OA) by ψ. Inset: a schematic of the function of the Au–WS_2 metasurface. The inset SEM image shows one period of the nanohole array.[83] Reprinted with permission from ref 83. Copyright 2019 Nature Publishing Group.

hyperbolic metamaterials.[105] Recently, the concept of metamaterials has been extended to 2D optical materials as the interest in graphene and related 2D materials significantly increases. Some representative 2D metamaterials and their applications have been summarized in this review. However, these multilayered architectures that are based on 2D materials and subwavelength metal nanostructures, require complicated, multistep nanofabrication and nanolithography techniques, which may affect or degrade the intrinsic optoelectronic properties of atomically thin layered 2D materials. In general, theory in metaphotonics of 2D materials is leading, while the nanofabrication and practical realization of metaphotonic structures and devices based on these materials is falling behind.

5.1.1. 2D Materials. Both theoretical design and nanofabrication are expected to extend to an extensive range of 2D materials, in addition to graphene, TMDs, and phosphorene. Numerous 2D layered or nonlayered materials have been recently discovered or synthesized with novel optical and electronic properties.[521] In addition to graphene, some elemental monolayers such as germanene, silicene, and stanene have been recently developed,[522] which demonstrates the topological properties of stanene, as an example.[523] These elemental monolayers generally have high charge mobility and Dirac cones that act as semimetals such as graphene. 2D semimetals include TMDs such as $PtTe_2$ with type-II Dirac Fermions,[524] $PtSe_2$ with layer-dependent semiconductor-to-semimetal transition,[525] and WTe_2 with Weyl semimetal states.[526] 2D atomic crystals have displayed spin and valley selective carrier dynamics, which can realize atomic thin spintronic or valleytronic metaphotonics and devices.[162,504,527] 2D chiral perovskites have been recently reported to exhibit controllable spin polarization via molecular design and magnetic fields.[528,529] Another set of new members in the 2D materials family consists of 2D magnets,[324,530,531] such as CrI_3 and Fe_3GeTe_2, which exhibit magnetic field-dependent optical emission and polarization,[532] which contributes to 2D material-based magneto-metaphotonics. 2D metal–organic frameworks, which are usually utilized for gas separation and storage media,[533] have been developed as a new type of semiconductor with direct bandgap and high carrier mobility.[534,535] Therefore, we can anticipate that these new 2D materials, which possess new optical properties, would facilitate the research progress of atomically thin metaphotonics.

5.1.2. Emerging Polaritons. New mechanisms of light–matter interaction with low loss require further exploration for constructing high-performance metaphotonic devices. As we discussed in Section 2, current low-loss polaritons in vdW materials primarily contain plasmon polaritons in graphene and phosphorene and PhPs in hBN and α-MoO3. Note that phosphorene holds in-plane anisotropic plasmon polaritons,

https://dx.doi.org/10.1021/acs.chemrev.9b00592
Chem. Rev. 2020, 120, 6197–6246

while graphene only has isotropic surface plasmon polaritons. Hyperbolic PhPs are supported in both hBN and α-MoO_3, with in-plane anisotropic polaritons experimentally observed only in α-MoO_3. Phonon polaritons generally show lower loss with a longer lifetime than plasmon polaritons, although the plasmonic resonance can be easily and dynamically tuned by changing the Fermi level (e.g., electrostatic gating), which causes a broadband polaritonic response. Conversely, the responsive band of PhPs is relatively narrow due to the intrinsic limited Reststrahlen bands in the lattice vibrations of polar dielectrics. For example, hBN has a polaritonic response within 6.2−7.3 and 12.2−13.4 μm and α-MoO_3 within 9.9−10.4 and 10.3−12.2 μm. Thus, searching for PhPs outside this wavelength range is needed to encompass a wider band spectrum.

Exciton polaritons in TMDs have also been observed in the near-field yet remain considerably unexplored.[87] In addition, several other kinds of polaritons in 2D materials have been theoretically predicted, including cooper pair polaritons and magnon polaritons.[536] Investigation of the coupling and hybridization between two polaritonic modes, such as plasmon−phonon polaritons, are also important in terms of realizing low-loss dynamically tunable polaritons. An extra advantage of using polaritons based on 2D materials instead of metals is that these 2D materials in any form are unlikely to cause electrical problems when employed in metaphotonic structures-integrated optoelectronic devices. Thus, we can foresee a large number of fundamental studies of polaritons supported by 2D materials and applied research that focuses on their novel metaphotonic applications in the near future.

5.1.3. Moiré Patterns. 2D materials with atomically thin forms show intriguing sensitivity due to the stacking angles between adjacent layers, in which the angle affects the optical and electronic properties of vdW heterostructures (a type of metamaterial). The Moiré patterns at small twist angles are created by the lattice misorientation between the vertical atomic layers, which causes long-range modulation of the stacking order.[191] Recent studies of heterostructures composed of bilayer graphene have demonstrated that a flat electronic band structure near zero Fermi energy due to strong interlayer coupling emerges for certain "magic angles" between the two graphene layers.[191] The correlated insulator behavior at half-filling in the graphene superlattice is promising in many aspects, such as studying other 2D quantum phases without a magnetic field or realizing unconventional superconductors and quantum spin liquids.[192] Stacking angles have exhibited a crucial role in 2D materials for many other conditions, such as creating plasmon PCs for nanolight in Moiré graphene superlattices,[500] modifying the SPs in the graphene/hBN stack,[537] improving the conductivities across MoS_2/graphene heterostructures,[538] and modulating the phonon dispersions in twisted bilayer MoS_2.[539] Moiré excitons have also been observed and investigated in 2D twisted stacks, which manifests as multiple emergent peaks around the original TMD monolayer exciton resonance with gate dependences, for example, in $MoSe_2/WSe_2$ and WSe_2/WS_2 heterojunctions.[193,195,540] A recent report also shows a stacking angle-tunable PL of interlayer exciton states in twisted bilayer graphene,[541] which implies a hybrid metal-exciton behavior with high tunability and potential enhancements. These new observations of stacking angle control provide a new tool to manipulate light−matter interactions for 2D materials metaphotonics.

The development of novel metaphotonic device applications should combine both emerging 2D materials with superior properties and new mechanisms of light−matter interaction. We present a few examples in the following section to envision the future scope of 2D material-based metaphotonic devices.

5.1.4. Photonics. Lensing, as an important optical tool, is traditionally based on metal or dielectric nanostructures but can also be constructed of 2D materials with atomic thin layers. Ultrathin flat lenses have been demonstrated using monolayer and multilayer graphene,[337] thin-film reduced GO,[75] and monolayer WSe_2. Engineering the phase front of optical beams that pass through 2D materials also enables the design of few-layer MoS_2 optical lenses (by controlling the optical path length)[542] and hBN pillar array-based metalenses (by levering the high refractive indices).[499] To achieve superhigh focusing efficiency, new lensing mechanisms should be developed by utilizing low-loss polaritons, as discussed in Section 2 of this review. The hyperbolic PhPs in hBN crystals have been demonstrated to show an out-of-plane superlensing effect with superior subdiffractional focusing and near-field imaging.[123,419] Similarly, in-plane focusing and lensing can also be realized by taking into account the recently discovered in-plane anisotropic hyperbolic PhPs in α-MoO_3 crystals.[88] Therefore, a higher focusing efficiency with multifunctionality is expected due to the extreme confinement and unique orientation of these polaritons in 2D materials.

5.1.5. Optoelectronics. The performance of photodetectors can be enhanced by utilizing low-loss polaritons or polaritonic resonances. SPPs induced by metallic nanostructures have been employed to enhance the light absorption and carrier generation in 2D material-based photodetectors.[450,451,543] A few studies also suggest that the photodetection efficiency can be enhanced by phonons in the mid-IR.[544−546] Since the real-space observation of polaritons propagation in graphene and hBN, several attempts of improving IR detection in graphene have been reported, such as using the resonances of plasmon polaritons in graphene nanograting arrays[456] or introducing hBN thin layers on graphene to confine and guide mid-IR nanolight (PhPs).[547] We anticipate that these low-loss polaritons with high-quality factors supported in natural 2D materials will provide viable access to high-efficiency optoelectronic devices such as photodetectors.

5.1.6. Biosensors. Utilizing low-loss polaritons for metaphotonic biosensing applications is another important and promising topic in the field of medical research and clinical diagnostics. The most crucial figure of merit of an optical biosensor is its sensitivity, which is the capability to detect a small number of molecules in highly diluted solutions that relies on the performance of the underlying optical structures.[548,549] Although conventional label-free plasmonic biosensors, which are based on metallic metamaterials, have shown the possibility of detecting biomolecules, their sensitivities remain hindered due to their relatively lower polarizability.[550−553] Hyperbolic metamaterials that use 2D Au diffraction gratings, for instance, were developed to overcome this issue and demonstrated extreme sensitivity biosensing ability to detect ultralow-molecular-weight biomolecules at picomolar (highly diluted) concentrations.[554] Thus, 2D vdW crystals that support lower-loss (hyperbolic) polaritons will enable the realization of unprecedentedly high-performance metaphotonic biosensing platforms.

https://dx.doi.org/10.1021/acs.chemrev.9b00592
Chem. Rev. 2020, 120, 6197−6246

AUTHOR INFORMATION

Corresponding Authors

Cheng-Wei Qiu − *Department of Electrical and Computer Engineering, National University of Singapore, Singapore 117583 Singapore;* orcid.org/0000-0002-6605-500X; Email: eleqc@nus.edu.sg

Qiaoliang Bao − *Department of Materials Science and Engineering, ARC Centre of Excellence in Future Low-Energy Electronics Technologies (FLEET), Monash University, Clayton, Victoria 3800, Australia;* orcid.org/0000-0002-6971-789X; Email: qiaoliang.bao@gmail.com

Authors

Zhigao Dai − *Engineering Research Center of Nano-Geomaterials of Ministry of Education, Faculty of Materials Science and Chemistry, China University of Geosciences, Wuhan 430074, P.R. China; Department of Materials Science and Engineering, ARC Centre of Excellence in Future Low-Energy Electronics Technologies (FLEET), Monash University, Clayton, Victoria 3800, Australia;* orcid.org/0000-0002-3105-4605

Guangwei Hu − *Department of Electrical and Computer Engineering, National University of Singapore, Singapore 117583 Singapore;* orcid.org/0000-0002-3023-9632

Qingdong Ou − *Department of Materials Science and Engineering, ARC Centre of Excellence in Future Low-Energy Electronics Technologies (FLEET), Monash University, Clayton, Victoria 3800, Australia;* orcid.org/0000-0003-2161-2543

Lei Zhang − *Key Laboratory for Physical Electronics and Devices of the Ministry of Education and Shaanxi Key Lab of Information Photonic Technique, School of Electronic Science and Engineering, Xi'an Jiaotong University, Xi'an 710049, P.R. China;* orcid.org/0000-0002-5113-1786

Fengnian Xia − *Department of Electrical Engineering, Yale University, New Haven, Connecticut 06511, United States;* orcid.org/0000-0001-5176-368X

Francisco J. Garcia-Vidal − *Departamento de Fisica Teorica de la Materia Condensada and Condensed Matter Physics Center (IFIMAC), Universidad Autonoma de Madrid, Madrid 28049, Spain; Donostia International Physics Center (DIPC), Donostia−San Sebastian E-20018, Spain;* orcid.org/0000-0003-4354-0982

Complete contact information is available at: https://pubs.acs.org/10.1021/acs.chemrev.9b00592

Notes

The authors declare no competing financial interest.

Biographies

Dr. Zhigao Dai received his Ph.D. (2015) in condensed matter physics from Wuhan University, China. He was a lecturer and postdoctoral research fellow at the School of Printing and Packaging and School of Physics and Technology, respectively, Wuhan University, China, until the August 2019. During November 2016 to December 2018, he was awarded a scholarship under the International Postdoctoral Exchange Fellowship Program by the Office of China Postdoctoral Council as a postdoctoral research fellow at the Department of Materials Science and Engineering, Monash University, Australia. In September 2019, he joined as a Appointed Professor at the Faculty of Materials Science and Chemistry, China University of Geosciences, China. His research interests include plasmons, polaritons in van der Waals materials, and photonics and optoelectronic devices based on noble materials, 2D materials, and perovskites.

Mr. Guangwei Hu is currently a Ph.D. candidate in Department of Electrical and Computer Engineering, National University of Singapore. He obtained a B.Sc. from the Department of Applied Physics in Harbin Institute of Technology, China, in 2016. His current research interests include fundamental light−matter interactions with promising applications such as the multifunctional electromagnetic metamaterials and metasurfaces, the optical engineering of the 2D materials, polaritonics (plasmon, phonon, and exciton), and topological transitions in photonics, among many others.

Dr. Qingdong Ou received his B.Sc. (2012) and M.Sc. (2015) in chemistry from Soochow University, China. He obtained his Ph.D. (2019) in materials science and engineering from Monash University, Australia. He is currently a postdoctoral research fellow at the Department of Materials Science and Engineering, Monash University. His research interests include polaritons in van der Waals materials and optoelectronic devices based on 2D materials, perovskites, and organic semiconductors.

Dr. Lei Zhang received a Bachelor's in physics from Northwest University, Xi'an, China, a Master's in optics from Xi'an Institute of Precision Mechanics and Optics of Chinese Academy of Science, Xi'an, China, and a Ph.D. in physics from the Chinese University of Hong Kong, Hong Kong, in 2005, 2008, and 2012, respectively. He was a Research Fellow with the Department of Electrical and Computer Engineering at National University of Singapore, Singapore, until the end of 2016. In December 2016, he joined as an Associated Professor at the School of Electronic Science and Engineering, Xi'an Jiaotong University, Xi'an, China. His research interests include metasurfaces, nanophotonics, plasmonics, and light−matter interactions as well as their applications to light emission, nonlinear optics, color display, sensing, and so on.

Fengnian Xia received a B.E. with highest honor in electronics engineering from Tsinghua University, Beijing, China and a Ph.D. in electrical engineering from Princeton University, Princeton, New Jersey, United States. He held postdoc, engineer, and research staff positions in IBM Thomas J. Watson research center in Yorktown Heights, New York, United States from 2005 to 2013. He joined Yale University in 2013 as an assistant professor and is currently the Barton L. Weller Associate Professor in Engineering and Science at Department of Electrical Engineering. He explores light−matter interaction and quantum transport in low-dimensional quantum materials and identifies their potential applications in computing, flexible electronics, imaging, optical communications, and energy harvesting.

Francisco J. Garcia-Vidal is a scientific group leader and full professor at the Condensed Matter theory group of the Universidad Autónoma de Madrid. Garcia-Vidal received his Master's degree in Physics (1988) and his Ph.D. degree in Physics (1992) from the Universidad Autonoma de Madrid. From 1994 to 1996 he was a post-doctoral staff researcher at the Imperial College of London, working in the group of Prof. Sir John Pendry, where he began to work in the field of Plasmonics. Since 1997 he has been associated with the Universidad Autónoma de Madrid, first as an associate professor and since December 2007 as a full professor. He is also the founding and current director of the Condensed Matter Physics Center (IFIMAC). He was also the recipient of an ERC Advanced Grant (2012−2017) devoted to analysing quantum effects in Plasmonics. Since January 2018 he is Divisional Associate Editor of *Physical Review Letters*. Prof. Garcia-Vidal and his group have worked in different areas within Plasmonics and Metamaterials such as: Surface Enhanced Raman

https://dx.doi.org/10.1021/acs.chemrev.9b00592
Chem. Rev. 2020, 120, 6197−6246

Scattering, theoretical explanation of the phenomenon of extraordinary transmission of light through subwavelength apertures, development of the concept of spoof surface plasmons and, more recently, Quantum Plasmonics and 2D materials. He has authored more than 270 peer-reviewed journal articles that have received more than 23,000 total citations. His current H-index is 71.

Cheng-Wei Qiu received the B.Eng. degree from the University of Science and Technology of China, Hefei, China, in 2003 and the Ph.D. degree from the National University of Singapore (NUS), Singapore, in 2007. He was a Postdoctoral Fellow with the Physics Department, Massachusetts Institute of Technology (MIT), Cambridge, MA, USA, until 2009. In 2009, he joined the NUS as an Assistant Professor and was promoted to Associate Professor with tenure in 2017. In 2018, he was promoted to Dean's Chair Professor at the Faculty of Engineering, NUS. His research is known for the structured light for beam manipulation and nanoparticle manipulation. Dr. Qiu was a recipient of the SUMMA Graduate Fellowship in Advanced Electromagnetics in 2005, the IEEE AP-S Graduate Research Award in 2006, the URSI Young Scientist Award in 2008, the NUS Young Investigator Award in 2011, the MIT TR35@ Singapore Award in 2012, the Young Scientist Award by the Singapore National Academy of Science in 2013, the Faculty Young Research Award in NUS 2013, the Young Engineering Research Award 2018 from NUS, and SPIE Rising Researcher Award in 2018. He has published over 300 peer-reviewed papers and was listed as Highly Cited Researcher by Clarivate Analytics in 2019. He is in the Editorial Advisory Board of ACS Photonics and Laser & Photonics Reviews. He is Editor-in-Chief of *eLight*, a joint journal between Springer Nature and CIOMP.

Qiaoliang Bao received his B.A. (2000) and M.E. (2003) in materials science and engineering from Wuhan University of Technology (China). He obtained his Ph.D. (2007) in materials physics and chemistry from Wuhan University (China). He worked as postdoctoral fellow at Nanyang Technological University and National University of Singapore from 2007 to 2012. He was appointed as a tenured associate professor at the Department of Materials Science and Engineering, Monash University in 2016. He was the recipient of Discovery Early Career Researcher Award (2012) and Future Fellowship (2015) given by Australian Research Council, First Runner-up of Scopus Young Researcher of the Year Award (2013, Australia), and Young Tall Poppy Science Awards (2015) given by Australian Institute of Policy and Science. His research interests include waveguide-coupled 2D semiconductors and polariton-coupled 2D materials and devices, focusing on the effect of confined-space light−matter interactions on the transport of electrons or other quasi-particles such as plasmon polaritons, exciton polaritons, and phonon polaritons. He has authored or coauthored more than 200 peer-reviewed journal articles with more than 17,000 total citations and an *h*-index of 58. He was listed as Highly Cited (HiCi) researcher by Clarivate Analytics in 2018 and 2019.

ACKNOWLEDGMENTS

We acknowledge support from the National Natural Science Foundation of China (51601131, 61875139, 51702219, and 11604256), Shenzhen Nanshan District Pilotage Team Program (LHTD20170006), and the Australian Research Council (ARC, FT150100450, IH150100006 and CE170100039). Z.D. acknowledges support from the International Postdoctoral Exchange Fellowship Program and Hubei Provincial Natural Science Foundation (2016CFB166), and the Fundamental Research Funds for the Central Universities, China University of Geosciences (Wuhan). C.W.Q. acknowledges the support from the National Research Foundation, Prime Minister's Office, Singapore under its Competitive Research Program (CRP award NRF CRP22-2019-0006), A*STAR Pharos Programme (Grant 152 70 00014 with Project R-263-000-B91-305) and Ministry of Education, Singapore (R-143-000-A68-112).

REFERENCES

(1) Linden, S.; Enkrich, C.; Wegener, M.; Zhou, J.; Koschny, T.; Soukoulis, C. M. Magnetic Response of Metamaterials at 100 Terahertz. *Science* **2004**, *306*, 1351−1353.
(2) Yen, T. J.; Padilla, W. J.; Fang, N.; Vier, D. C.; Smith, D. R.; Pendry, J. B.; Basov, D. N.; Zhang, X. Terahertz Magnetic Response from Artificial Materials. *Science* **2004**, *303*, 1494−1496.
(3) Tsakmakidis, K. L.; Boardman, A. D.; Hess, O. Trapped Rainbow' Storage of Light in Metamaterials. *Nature* **2007**, *450*, 397−401.
(4) Valentine, J.; Zhang, S.; Zentgraf, T.; Ulin-Avila, E.; Genov, D. A.; Bartal, G.; Zhang, X. Three-Dimensional Optical Metamaterial with a Negative Refractive Index. *Nature* **2008**, *455*, 376−379.
(5) Xiao, S. M.; Drachev, V. P.; Kildishev, A. V.; Ni, X. J.; Chettiar, U. K.; Yuan, H. K.; Shalaev, V. M. Loss-Free and Active Optical Negative-Index Metamaterials. *Nature* **2010**, *466*, 735−738.
(6) Zhu, H.; Yi, F.; Cubukcu, E. Plasmonic Metamaterial Absorber for Broadband Manipulation of Mechanical Resonances. *Nat. Photonics* **2016**, *10*, 709−714.
(7) Kshetrimayum, R. S. A Brief Intro to Metamaterials. *IEEE Potentials* **2005**, *23*, 44−46.
(8) Pendry, J. B.; Holden, A.; Stewart, W.; Youngs, I. Extremely Low Frequency Plasmons in Metallic Mesostructures. *Phys. Rev. Lett.* **1996**, *76*, 4773.
(9) Pendry, J. B.; Holden, A. J.; Robbins, D. J.; Stewart, W. Magnetism from Conductors and Enhanced Nonlinear Phenomena. *IEEE Trans. Microwave Theory Tech.* **1999**, *47*, 2075−2084.
(10) Smith, D. R.; Padilla, W. J.; Vier, D.; Nemat-Nasser, S. C.; Schultz, S. Composite Medium with Simultaneously Negative Permeability and Permittivity. *Phys. Rev. Lett.* **2000**, *84*, 4184.
(11) Shelby, R. A.; Smith, D. R.; Schultz, S. Experimental Verification of a Negative Index of Refraction. *Science* **2001**, *292*, 1058847.
(12) Pendry, J. B.; Schurig, D.; Smith, D. R. Controlling Electromagnetic Fields. *Science* **2006**, *312*, 1780−1782.
(13) Li, P.; Dolado, I.; Alfaro-Mozaz, F. J.; Casanova, F.; Hueso, L. E.; Liu, S.; Edgar, J. H.; Nikitin, A. Y.; Vélez, S.; Hillenbrand, R. Infrared Hyperbolic Metasurface Based on Nanostructured Van Der Waals Materials. *Science* **2018**, *359*, 892−896.
(14) Zhu, S.; Zhang, X. Metamaterials: Artificial Materials Beyond Nature. *Nat. Sci. Rev.* **2018**, *5*, 130−131.
(15) Zheludev, N. I. Obtaining Optical Properties on Demand. *Science* **2015**, *348*, 973−974.
(16) Engheta, N.; Ziolkowski, R. W. *Metamaterials: Physics and Engineering Explorations*; John Wiley & Sons: 2006.
(17) Ashton, M.; Paul, J.; Sinnott, S. B.; Hennig, R. G. Topology-Scaling Identification of Layered Solids and Stable Exfoliated 2D Materials. *Phys. Rev. Lett.* **2017**, *118*, 106101.
(18) Li, L.; Yu, Y.; Ye, G. J.; Ge, Q.; Ou, X.; Wu, H.; Feng, D.; Chen, X. H.; Zhang, Y. Black Phosphorus Field-Effect Transistors. *Nat. Nanotechnol.* **2014**, *9*, 372−377.
(19) Koenig, S. P.; Doganov, R. A.; Schmidt, H.; Castro Neto, A.; Oezyilmaz, B. Electric Field Effect in Ultrathin Black Phosphorus. *Appl. Phys. Lett.* **2014**, *104*, 103106.
(20) Liu, H.; Neal, A. T.; Zhu, Z.; Luo, Z.; Xu, X.; Tománek, D.; Ye, P. D. Phosphorene: An Unexplored 2D Semiconductor with a High Hole Mobility. *ACS Nano* **2014**, *8*, 4033−4041.
(21) Lalmi, B.; Oughaddou, H.; Enriquez, H.; Kara, A.; Vizzini, S.; Ealet, B.; Aufray, B. Epitaxial Growth of a Silicene Sheet. *Appl. Phys. Lett.* **2010**, *97*, 223109.

https://dx.doi.org/10.1021/acs.chemrev.9b00592
Chem. Rev. 2020, 120, 6197−6246

(22) Takeda, K.; Shiraishi, K. Theoretical Possibility of Stage Corrugation in Si and Ge Analogs of Graphite. *Phys. Rev. B: Condens. Matter Mater. Phys.* **1994**, *50*, 14916.
(23) Novoselov, K.; Jiang, D.; Schedin, F.; Booth, T.; Khotkevich, V.; Morozov, S.; Geim, A. Two-Dimensional Atomic Crystals. *Proc. Natl. Acad. Sci. U. S. A.* **2005**, *102*, 10451−10453.
(24) Mak, K. F.; Lee, C.; Hone, J.; Shan, J.; Heinz, T. F. Atomically Thin MoS_2: A New Direct-Gap Semiconductor. *Phys. Rev. Lett.* **2010**, *105*, 136805.
(25) Yun, W. S.; Han, S.; Hong, S. C.; Kim, I. G.; Lee, J. Thickness and Strain Effects on Electronic Structures of Transition Metal Dichalcogenides: 2h-MX_2 Semiconductors (M= Mo, W; X= S, Se, Te). *Phys. Rev. B: Condens. Matter Mater. Phys.* **2012**, *85*, 033305.
(26) Watanabe, K.; Taniguchi, T.; Kanda, H. Direct-Bandgap Properties and Evidence for Ultraviolet Lasing of Hexagonal Boron Nitride Single Crystal. *Nat. Mater.* **2004**, *3*, 404−409.
(27) Park, J.-H.; Park, J. C.; Yun, S. J.; Kim, H.; Luong, D. H.; Kim, S. M.; Choi, S. H.; Yang, W.; Kong, J.; Kim, K. K.; Lee, Y. H. Large-Area Monolayer Hexagonal Boron Nitride on Pt Foil. *ACS Nano* **2014**, *8*, 8520−8528.
(28) Naguib, M.; Kurtoglu, M.; Presser, V.; Lu, J.; Niu, J.; Heon, M.; Hultman, L.; Gogotsi, Y.; Barsoum, M. W. Two-Dimensional Nanocrystals: Two-Dimensional Nanocrystals Produced by Exfoliation of Ti_3AlC_2. *Adv. Mater.* **2011**, *23*, 4206−4207.
(29) Bao, Q.; Loh, K. P. Graphene Photonics, Plasmonics, and Broadband Optoelectronic Devices. *ACS Nano* **2012**, *6*, 3677−3694.
(30) Xia, F.; Wang, H.; Xiao, D.; Dubey, M.; Ramasubramaniam, A. Two-Dimensional Material Nanophotonics. *Nat. Photonics* **2014**, *8*, 899−907.
(31) Low, T.; Chaves, A.; Caldwell, J. D.; Kumar, A.; Fang, N. X.; Avouris, P.; Heinz, T. F.; Guinea, F.; Martin-Moreno, L.; Koppens, F. Polaritons in Layered Two-Dimensional Materials. *Nat. Mater.* **2017**, *16*, 182−194.
(32) Zhang, Y.; Tan, Y.-W.; Stormer, H. L.; Kim, P. Experimental Observation of the Quantum Hall Effect and Berry's Phase in Graphene. *Nature* **2005**, *438*, 201−204.
(33) Tran, T. T.; Bray, K.; Ford, M. J.; Toth, M.; Aharonovich, I. Quantum Emission from Hexagonal Boron Nitride Monolayers. *Nat. Nanotechnol.* **2016**, *11*, 37−41.
(34) Li, T.; Liu, H.; Wang, F.; Dong, Z.; Zhu, S.; Zhang, X. Coupling Effect of Magnetic Polariton in Perforated Metal/Dielectric Layered Metamaterials and Its Influence on Negative Refraction Transmission. *Opt. Express* **2006**, *14*, 11155−11163.
(35) Harutyunyan, H.; Beams, R.; Novotny, L. Controllable Optical Negative Refraction and Phase Conjugation in Graphite Thin Films. *Nat. Phys.* **2013**, *9*, 423−425.
(36) Sayem, A. A.; Rahman, M. M.; Mahdy, M. R. C.; Jahangir, I.; Rahman, M. S. Negative Refraction with Superior Transmission in Graphene-Hexagonal Boron Nitride (Hbn) Multilayer Hyper Crystal. *Sci. Rep.* **2016**, *6*, 25442.
(37) Wei, Z. C.; Li, X. P.; Yin, J. J.; Huang, R.; Liu, Y. B.; Wang, W.; Liu, H. Z.; Meng, H. Y.; Liang, R. S. Active Plasmonic Band-Stop Filters Based on Graphene Metamaterial at Thz Wavelengths. *Opt. Express* **2016**, *24*, 14344−14351.
(38) Shah, S.; Lin, X.; Shen, L.; Renuka, M.; Zhang, B.; Chen, H. Interferenceless Polarization Splitting through Nanoscale Van der Waals Heterostructures. *Phys. Rev. Appl.* **2018**, *10*, 034025.
(39) Zhang, S.; Genov, D. A.; Wang, Y.; Liu, M.; Zhang, X. Plasmon-Induced Transparency in Metamaterials. *Phys. Rev. Lett.* **2008**, *101*, 047401.
(40) Zhu, Z.; Cai, X.; Yi, S.; Chen, J.; Dai, Y.; Niu, C.; Guo, Z.; Xie, M.; Liu, F.; Cho, J. H.; et al. Multivalency-Driven Formation of Te-Based Monolayer Materials: A Combined First-Principles and Experimental Study. *Phys. Rev. Lett.* **2017**, *119*, 106101.
(41) Ginn, J. C.; Brener, I.; Peters, D. W.; Wendt, J. R.; Stevens, J. O.; Hines, P. F.; Basilio, L. I.; Warne, L. K.; Ihlefeld, J. F.; Clem, P. G.; Sinclair, M. B. Realizing Optical Magnetism from Dielectric Metamaterials. *Phys. Rev. Lett.* **2012**, *108*, 097402.
(42) Krasnok, A.; Tymchenko, M.; Alù, A. Nonlinear Metasurfaces: A Paradigm Shift in Nonlinear Optics. *Mater. Today* **2018**, *21*, 8−21.
(43) Minovich, A. E.; Miroshnichenko, A. E.; Bykov, A. Y.; Murzina, T. V.; Neshev, D. N.; Kivshar, Y. S. Functional and Nonlinear Optical Metasurfaces. *Laser Photon. Rev.* **2015**, *9*, 195−213.
(44) Butet, J.; Brevet, P.-F.; Martin, O. J. Optical Second Harmonic Generation in Plasmonic Nanostructures: From Fundamental Principles to Advanced Applications. *ACS Nano* **2015**, *9*, 10545−10562.
(45) Autere, A.; Jussila, H.; Dai, Y.; Wang, Y.; Lipsanen, H.; Sun, Z. Nonlinear Optics with 2d Layered Materials. *Adv. Mater.* **2018**, *30*, 1705963.
(46) Kundys, D.; Van Duppen, B.; Marshall, O. P.; Rodriguez, F.; Torre, I.; Tomadin, A.; Polini, M.; Grigorenko, A. N. Nonlinear Light Mixing by Graphene Plasmons. *Nano Lett.* **2018**, *18*, 282−287.
(47) Jiang, T.; Huang, D.; Cheng, J.; Fan, X.; Zhang, Z.; Shan, Y.; Yi, Y.; Dai, Y.; Shi, L.; Liu, K.; Zeng, C.; Zi, J.; Sipe, J. E.; Shen, Y.-R.; Liu, W.-T.; Wu, S. Gate-Tunable Third-Order Nonlinear Optical Response of Massless Dirac Fermions in Graphene. *Nat. Photonics* **2018**, *12*, 430−436.
(48) Soavi, G.; Wang, G.; Rostami, H.; Purdie, D. G.; De Fazio, D.; Ma, T.; Luo, B.; Wang, J.; Ott, A. K.; Yoon, D.; Bourelle, S. A.; Muench, J. E.; Goykhman, I.; Dal Conte, S.; Celebrano, M.; Tomadin, A.; Polini, M.; Cerullo, G.; Ferrari, A. C. Broadband, Electrically Tunable Third-Harmonic Generation in Graphene. *Nat. Nanotechnol.* **2018**, *13*, 583−588.
(49) Dean, J. J.; van Driel, H. M. Graphene and Few-Layer Graphite Probed by Second-Harmonic Generation: Theory and Experiment. *Phys. Rev. B: Condens. Matter Mater. Phys.* **2010**, *82*, 125411.
(50) An, Y. Q.; Nelson, F.; Lee, J. U.; Diebold, A. C. Enhanced Optical Second-Harmonic Generation from the Current-Biased Graphene/SiO_2/Si (001) Structure. *Nano Lett.* **2013**, *13*, 2104−2109.
(51) Majérus, B.; Butet, J.; Bernasconi, G. D.; Valapu, R. T.; Lobet, M.; Henrard, L.; Martin, O. J. Optical Second Harmonic Generation from Nanostructured Graphene: A Full Wave Approach. *Opt. Express* **2017**, *25*, 27015−27027.
(52) Novoselov, K.; Mishchenko, A.; Carvalho, A.; Neto, A. C. 2D Materials and Van der Waals Heterostructures. *Science* **2016**, *353*, aac9439.
(53) Wood, J. D.; Wells, S. A.; Jariwala, D.; Chen, K.-S.; Cho, E.; Sangwan, V. K.; Liu, X.; Lauhon, L. J.; Marks, T. J.; Hersam, M. C. Effective Passivation of Exfoliated Black Phosphorus Transistors against Ambient Degradation. *Nano Lett.* **2014**, *14*, 6964−6970.
(54) Zheng, J.; Yang, Z.; Si, C.; Liang, Z.; Chen, X.; Cao, R.; Guo, Z.; Wang, K.; Zhang, Y.; Ji, J.; Zhang, M.; Fan, D.; Zhang, H. Black Phosphorus Based All-Optical-Signal-Processing: Toward High Performances and Enhanced Stability. *ACS Photonics* **2017**, *4*, 1466−1476.
(55) Echtermeyer, T. J.; Nene, P. S.; Trushin, M.; Gorbachev, R. V.; Eiden, A. L.; Milana, S.; Sun, Z.; Schliemann, J.; Lidorikis, E.; Novoselov, K. S.; Ferrari, A. C. Photothermoelectric and Photoelectric Contributions to Light Detection in Metal-Graphene-Metal Photodetectors. *Nano Lett.* **2014**, *14*, 3733−3742.
(56) Jariwala, D.; Marks, T. J.; Hersam, M. C. Mixed-Dimensional Van der Waals Heterostructures. *Nat. Mater.* **2017**, *16*, 170−181.
(57) Liu, H.; Li, Y.; You, Y. S.; Ghimire, S.; Heinz, T. F.; Reis, D. A. High-Harmonic Generation from an Atomically Thin Semiconductor. *Nat. Phys.* **2017**, *13*, 262−265.
(58) Saynatjoki, A.; Karvonen, L.; Rostami, H.; Autere, A.; Mehravar, S.; Lombardo, A.; Norwood, R. A.; Hasan, T.; Peyghambarian, N.; Lipsanen, H.; Kieu, K.; Ferrari, A. C.; Polini, M.; Sun, Z. Ultra-Strong Nonlinear Optical Processes and Trigonal Warping in MoS_2 Layers. *Nat. Commun.* **2017**, *8*, 893.
(59) Wang, K.; Wang, J.; Fan, J.; Lotya, M.; O'Neill, A.; Fox, D.; Feng, Y.; Zhang, X.; Jiang, B.; Zhao, Q.; Zhang, H.; Coleman, J. N.; Zhang, L.; Blau, W. J. Ultrafast Saturable Absorption of Two-Dimensional MoS_2 Nanosheets. *ACS Nano* **2013**, *7*, 9260−9267.
(60) Geim, A. K.; Grigorieva, I. V. Van der Waals heterostructures. *Nature* **2013**, *499*, 419−425.

https://dx.doi.org/10.1021/acs.chemrev.9b00592
Chem. Rev. 2020, 120, 6197−6246

(61) Li, Y.; Rao, Y.; Mak, K. F.; You, Y.; Wang, S.; Dean, C. R.; Heinz, T. F. Probing Symmetry Properties of Few-Layer MoS_2 and hBN by Optical Second-Harmonic Generation. *Nano Lett.* **2013**, *13*, 3329−3333.
(62) Berova, N.; Nakanishi, K.; Woody, R. W.; Woody, R. *Circular Dichroism: Principles and Applications*; John Wiley & Sons: 2000.
(63) Gansel, J. K.; Thiel, M.; Rill, M. S.; Decker, M.; Bade, K.; Saile, V.; von Freymann, G.; Linden, S.; Wegener, M. Gold Helix Photonic Metamaterial as Broadband Circular Polarizer. *Science* **2009**, *325*, 1513−1515.
(64) Qiu, M.; Zhang, L.; Tang, Z.; Jin, W.; Qiu, C. W.; Lei, D. Y. 3d Metaphotonic Nanostructures with Intrinsic Chirality. *Adv. Funct. Mater.* **2018**, *28*, 1803147.
(65) Hentschel, M.; Schäferling, M.; Duan, X.; Giessen, H.; Liu, N. Chiral Plasmonics. *Sci. Adv.* **2017**, *3*, No. e1602735.
(66) Stauber, T.; Low, T.; Gómez-Santos, G. Chiral Response of Twisted Bilayer Graphene. *Phys. Rev. Lett.* **2018**, *120*, 046801.
(67) Kim, C.-J.; Sánchez-Castillo, A.; Ziegler, Z.; Ogawa, Y.; Noguez, C.; Park, J. Chiral Atomically Thin Films. *Nat. Nanotechnol.* **2016**, *11*, 520−524.
(68) Wang, Z.; Cheng, F.; Winsor, T.; Liu, Y. Optical Chiral Metamaterials: A Review of the Fundamentals, Fabrication Methods and Applications. *Nanotechnology* **2016**, *27*, 412001.
(69) Poshakinskiy, A. V.; Kazanov, D. R.; Shubina, T. V.; Tarasenko, S. A. Optical Activity in Chiral Stacks of 2d Semiconductors. *Nanophotonics* **2018**, *7*, 753−762.
(70) Appelbaum, I.; Huang, B.; Monsma, D. J. Electronic Measurement and Control of Spin Transport in Silicon. *Nature* **2007**, *447*, 295−298.
(71) Wolf, S.; Awschalom, D.; Buhrman, R.; Daughton, J.; Von Molnar, S.; Roukes, M.; Chtchelkanova, A. Y.; Treger, D. Spintronics: A Spin-Based Electronics Vision for the Future. *Science* **2001**, *294*, 1488−1495.
(72) Mak, K. F.; He, K.; Shan, J.; Heinz, T. F. Control of Valley Polarization in Monolayer Mos2 by Optical Helicity. *Nat. Nanotechnol.* **2012**, *7*, 494−498.
(73) Zeng, H.; Dai, J.; Yao, W.; Xiao, D.; Cui, X. Valley Polarization in MoS_2 Monolayers by Optical Pumping. *Nat. Nanotechnol.* **2012**, *7*, 490−493.
(74) Cao, T.; Wang, G.; Han, W.; Ye, H.; Zhu, C.; Shi, J.; Niu, Q.; Tan, P.; Wang, E.; Liu, B.; Feng, J.; et al. Valley-Selective Circular Dichroism of Monolayer Molybdenum Disulphide. *Nat. Commun.* **2012**, *3*, 887.
(75) Zheng, X.; Jia, B.; Lin, H.; Qiu, L.; Li, D.; Gu, M. Highly Efficient and Ultra-Broadband Graphene Oxide Ultrathin Lenses with Three-Dimensional Subwavelength Focusing. *Nat. Commun.* **2015**, *6*, 8433.
(76) Schurig, D.; Mock, J. J.; Justice, B. J.; Cummer, S. A.; Pendry, J. B.; Starr, A. F.; Smith, D. R. Metamaterial Electromagnetic Cloak at Microwave Frequencies. *Science* **2006**, *314*, 977−980.
(77) Valentine, J.; Li, J. S.; Zentgraf, T.; Bartal, G.; Zhang, X. An Optical Cloak Made of Dielectrics. *Nat. Mater.* **2009**, *8*, 568−571.
(78) Ergin, T.; Stenger, N.; Brenner, P.; Pendry, J. B.; Wegener, M. Three-Dimensional Invisibility Cloak at Optical Wavelengths. *Science* **2010**, *328*, 337−339.
(79) Vakil, A.; Engheta, N. Transformation Optics Using Graphene. *Science* **2011**, *332*, 1291−1294.
(80) Papasimakis, N.; Luo, Z. Q.; Shen, Z. X.; De Angelis, F.; Di Fabrizio, E.; Nikolaenko, A. E.; Zheludev, N. I. Graphene in a Photonic Metamaterial. *Opt. Express* **2010**, *18*, 8353−8359.
(81) Lee, S. H.; Choi, M.; Kim, T. T.; Lee, S.; Liu, M.; Yin, X.; Choi, H. K.; Lee, S. S.; Choi, C. G.; Choi, S. Y.; et al. Switching Terahertz Waves with Gate-Controlled Active Graphene Metamaterials. *Nat. Mater.* **2012**, *11*, 936−941.
(82) Kim, T.-T.; Kim, H.-D.; Zhao, R.; Oh, S. S.; Ha, T.; Chung, D. S.; Lee, Y. H.; Min, B.; Zhang, S. Electrically Tunable Slow Light Using Graphene Metamaterials. *ACS Photonics* **2018**, *5*, 1800−1807.
(83) Hu, G.; Hong, X.; Wang, K.; Wu, J.; Xu, H.-X.; Zhao, W.; Liu, W.; Zhang, S.; Garcia-Vidal, F.; Wang, B.; et al. Coherent Steering of Nonlinear Chiral Valley Photons with a Synthetic Au−WS_2 Metasurface. *Nat. Photonics* **2019**, *13*, 467−472.
(84) Ju, L.; Geng, B.; Horng, J.; Girit, C.; Martin, M.; Hao, Z.; Bechtel, H. A.; Liang, X.; Zettl, A.; Shen, Y. R.; et al. Graphene Plasmonics for Tunable Terahertz Metamaterials. *Nat. Nanotechnol.* **2011**, *6*, 630−634.
(85) Lin, H.; Sturmberg, B. C. P.; Lin, K.-T.; Yang, Y.; Zheng, X.; Chong, T. K.; de Sterke, C. M.; Jia, B. A 90-Nm-Thick Graphene Metamaterial for Strong and Extremely Broadband Absorption of Unpolarized Light. *Nat. Photonics* **2019**, *13*, 270−276.
(86) Dai, S.; Ma, Q.; Liu, M. K.; Andersen, T.; Fei, Z.; Goldflam, M. D.; Wagner, M.; Watanabe, K.; Taniguchi, T.; Thiemens, M.; Keilmann, F.; Janssen, G. C. A. M.; Zhu, S-E.; Jarillo-Herrero, P.; Fogler, M. M.; Basov, D. N. Graphene on Hexagonal Boron Nitride as a Tunable Hyperbolic Metamaterial. *Nat. Nanotechnol.* **2015**, *10*, 682−686.
(87) Hu, F.; Luan, Y.; Scott, M. E.; Yan, J.; Mandrus, D. G.; Xu, X.; Fei, Z. Imaging Exciton−Polariton Transport in $MoSe_2$ Waveguides. *Nat. Photonics* **2017**, *11*, 356−360.
(88) Ma, W.; Alonso-González, P.; Li, S.; Nikitin, A. Y.; Yuan, J.; Martín-Sánchez, J.; Taboada-Gutiérrez, J.; Amenabar, I.; Li, P.; Vélez, S.; et al. In-Plane Anisotropic and Ultra-Low-Loss Polaritons in a Natural Van Der Waals Crystal. *Nature* **2018**, *562*, 557−562.
(89) Narimanov, E. E.; Kildishev, A. V. Metamaterials: Naturally Hyperbolic. *Nat. Photonics* **2015**, *9*, 214−216.
(90) Ferrari, L.; Wu, C.; Lepage, D.; Zhang, X.; Liu, Z. Hyperbolic Metamaterials and Their Applications. *Prog. Quantum Electron.* **2015**, *40*, 1−40.
(91) Smolyaninov, I. I.; Smolyaninova, V. N. Hyperbolic Metamaterials: Novel Physics and Applications. *Solid-State Electron.* **2017**, *136*, 102−112.
(92) Smith, D.; Schurig, D. Electromagnetic Wave Propagation in Media with Indefinite Permittivity and Permeability Tensors. *Phys. Rev. Lett.* **2003**, *90*, 077405.
(93) Lee, H.; Liu, Z.; Xiong, Y.; Sun, C.; Zhang, X. Development of Optical Hyperlens for Imaging Below the Diffraction Limit. *Opt. Express* **2007**, *15*, 15886−15891.
(94) Jacob, Z.; Alekseyev, L. V.; Narimanov, E. Optical Hyperlens: Far-Field Imaging Beyond the Diffraction Limit. *Opt. Express* **2006**, *14*, 8247−8256.
(95) Podolskiy, V. A.; Narimanov, E. E. Strongly Anisotropic Waveguide as a Nonmagnetic Left-Handed System. *Phys. Rev. B: Condens. Matter Mater. Phys.* **2005**, *71*, 201101.
(96) Yao, J.; Liu, Z.; Liu, Y.; Wang, Y.; Sun, C.; Bartal, G.; Stacy, A. M.; Zhang, X. Optical Negative Refraction in Bulk Metamaterials of Nanowires. *Science* **2008**, *321*, 930−930.
(97) Liu, Y.; Bartal, G.; Zhang, X. All-Angle Negative Refraction and Imaging in a Bulk Medium Made of Metallic Nanowires in the Visible Region. *Opt. Express* **2008**, *16*, 15439−15448.
(98) Lu, D.; Kan, J. J.; Fullerton, E. E.; Liu, Z. Enhancing Spontaneous Emission Rates of Molecules Using Nanopatterned Multilayer Hyperbolic Metamaterials. *Nat. Nanotechnol.* **2014**, *9*, 48−53.
(99) Shalaginov, M. Y.; Ishii, S.; Liu, J.; Liu, J.; Irudayaraj, J.; Lagutchev, A.; Kildishev, A.; Shalaev, V. Broadband Enhancement of Spontaneous Emission from Nitrogen-Vacancy Centers in Nanodiamonds by Hyperbolic Metamaterials. *Appl. Phys. Lett.* **2013**, *102*, 173114.
(100) Biehs, S.-A.; Tschikin, M.; Messina, R.; Ben-Abdallah, P. Super-Planckian near-Field Thermal Emission with Phonon-Polaritonic Hyperbolic Metamaterials. *Appl. Phys. Lett.* **2013**, *102*, 131106.
(101) Liu, X.; Zhang, R.; Zhang, Z. Near-Field Thermal Radiation between Hyperbolic Metamaterials: Graphite and Carbon Nanotubes. *Appl. Phys. Lett.* **2013**, *103*, 213102.
(102) Guo, Y.; Jacob, Z. Thermal Hyperbolic Metamaterials. *Opt. Express* **2013**, *21*, 15014−15019.
(103) Biehs, S.-A.; Tschikin, M.; Ben-Abdallah, P. Hyperbolic Metamaterials as an Analog of a Blackbody in the near Field. *Phys. Rev. Lett.* **2012**, *109*, 104301.

https://dx.doi.org/10.1021/acs.chemrev.9b00592
Chem. Rev. 2020, 120, 6197−6246

(104) Autore, M.; Li, P.; Dolado, I.; Alfaro-Mozaz, F. J; Esteban, R.; Atxabal, A.; Casanova, F.; Hueso, L. E; Alonso-Gonzalez, P.; Aizpurua, J.; Nikitin, A. Y; Velez, S.; Hillenbrand, R. Boron Nitride Nanoresonators for Phonon-Enhanced Molecular Vibrational Spectroscopy at the Strong Coupling Limit. *Light: Sci. Appl.* **2018**, *7*, No. 17172.
(105) Poddubny, A.; Iorsh, I.; Belov, P.; Kivshar, Y. Hyperbolic Metamaterials. *Nat. Photonics* **2013**, *7*, 948−957.
(106) Agranovich, V.; Kravtsov, V. Notes on Crystal Optics of Superlattices. *Solid State Commun.* **1985**, *55*, 85−90.
(107) Drachev, V. P.; Podolskiy, V. A.; Kildishev, A. V. Hyperbolic Metamaterials: New Physics Behind a Classical Problem. *Opt. Express* **2013**, *21*, 15048−15064.
(108) Sun, J.; Litchinitser, N. M.; Zhou, J. Indefinite by Nature: From Ultraviolet to Terahertz. *ACS Photonics* **2014**, *1*, 293−303.
(109) Sun, J.; Zhou, J.; Li, B.; Kang, F. Indefinite Permittivity and Negative Refraction in Natural Material: Graphite. *Appl. Phys. Lett.* **2011**, *98*, 101901.
(110) Guritanu, V.; Kuzmenko, A.; Van Der Marel, D.; Kazakov, S.; Zhigadlo, N.; Karpinski, J. Anisotropic Optical Conductivity and Two Colors of MgB_2. *Phys. Rev. B: Condens. Matter Mater. Phys.* **2006**, *73*, 104509.
(111) Mirri, C.; Baldassarre, L.; Lupi, S.; Ortolani, M.; Fittipaldi, R.; Vecchione, A.; Calvani, P. Anisotropic Optical Conductivity of $Sr_3Ru_2O_7$. *Phys. Rev. B: Condens. Matter Mater. Phys.* **2008**, *78*, 155132.
(112) Katsufuji, T.; Kasai, M.; Tokura, Y. In-Plane and Out-of-Plane Optical Spectra of Sr2ruo4. *Phys. Rev. Lett.* **1996**, *76*, 126.
(113) Dai, S.; Fei, Z.; Ma, Q.; Rodin, A. S.; Wagner, M.; McLeod, A. S.; Liu, M. K.; Gannett, W.; Regan, W.; Watanabe, K.; et al. Tunable Phonon Polaritons in Atomically Thin Van der Waals Crystals of Boron Nitride. *Science* **2014**, *343*, 1125−1129.
(114) Caldwell, J. D.; Kretinin, A. V.; Chen, Y.; Giannini, V.; Fogler, M. M.; Francescato, Y.; Ellis, C. T.; Tischler, J. G.; Woods, C. R.; Giles, A. J.; et al. Sub-Diffractional Volume-Confined Polaritons in the Natural Hyperbolic Material Hexagonal Boron Nitride. *Nat. Commun.* **2014**, *5*, 5221.
(115) Xiao, J.; Zhao, M.; Wang, Y.; Zhang, X. Excitons in Atomically Thin 2D Semiconductors and Their Applications. *Nanophotonics* **2017**, *6*, 1309−1328.
(116) Mueller, T.; Malic, E. Exciton Physics and Device Application of Two-Dimensional Transition Metal Dichalcogenide Semiconductors. *NPJ. 2D Mater. Appl.* **2018**, *2*, 29.
(117) Cassabois, G.; Valvin, P.; Gil, B. Hexagonal Boron Nitride Is an Indirect Bandgap Semiconductor. *Nat. Photonics* **2016**, *10*, 262−266.
(118) Watanabe, K.; Taniguchi, T.; Niiyama, T.; Miya, K.; Taniguchi, M. Far-Ultraviolet Plane-Emission Handheld Device Based on Hexagonal Boron Nitride. *Nat. Photonics* **2009**, *3*, 591−594.
(119) Ambrosio, A.; Jauregui, L. A.; Dai, S.; Chaudhary, K.; Tamagnone, M.; Fogler, M. M.; Basov, D. N.; Capasso, F.; Kim, P.; Wilson, W. L. Mechanical Detection and Imaging of Hyperbolic Phonon Polaritons in Hexagonal Boron Nitride. *ACS Nano* **2017**, *11*, 8741−8746.
(120) Dai, S.; Ma, Q.; Yang, Y.; Rosenfeld, J.; Goldflam, M. D.; McLeod, A.; Sun, Z.; Andersen, T. I.; Fei, Z.; Liu, M.; et al. Efficiency of Launching Highly Confined Polaritons by Infrared Light Incident on a Hyperbolic Material. *Nano Lett.* **2017**, *17*, 5285−5290.
(121) Yoxall, E.; Schnell, M.; Nikitin, A. Y.; Txoperena, O.; Woessner, A.; Lundeberg, M. B.; Casanova, F.; Hueso, L. E.; Koppens, F. H. L.; Hillenbrand, R. Direct Observation of Ultraslow Hyperbolic Polariton Propagation with Negative Phase Velocity. *Nat. Photonics* **2015**, *9*, 674−678.
(122) Dai, S.; Tymchenko, M.; Yang, Y.; Ma, Q.; Pita-Vidal, M.; Watanabe, K.; Taniguchi, T.; Jarillo-Herrero, P.; Fogler, M. M.; Alù, A.; et al. Manipulation and Steering of Hyperbolic Surface Polaritons in Hexagonal Boron Nitride. *Adv. Mater.* **2018**, *30*, 1706358.
(123) Dai, S.; Ma, Q.; Andersen, T.; McLeod, A. S.; Fei, Z.; Liu, M. K.; Wagner, M.; Watanabe, K.; Taniguchi, T.; Thiemens, M.; et al. Subdiffractional Focusing and Guiding of Polaritonic Rays in a Natural Hyperbolic Material. *Nat. Commun.* **2015**, *6*, 6963.
(124) Low, T.; Roldán, R.; Wang, H.; Xia, F.; Avouris, P.; Moreno, L. M.; Guinea, F. Plasmons and Screening in Monolayer and Multilayer Black Phosphorus. *Phys. Rev. Lett.* **2014**, *113*, 106802.
(125) Guan, S.; Huang, S. Y.; Yao, Y.; Yang, S. A. Tunable Hyperbolic Dispersion and Negative Refraction in Natural Electride Materials. *Phys. Rev. B: Condens. Matter Mater. Phys.* **2017**, *95*, 165436.
(126) Gjerding, M. N.; Petersen, R.; Pedersen, T. G.; Mortensen, N. A.; Thygesen, K. S. Layered Van der Waals Crystals with Hyperbolic Light Dispersion. *Nat. Commun.* **2017**, *8*, 320.
(127) Giles, A. J.; Dai, S.; Vurgaftman, I.; Hoffman, T.; Liu, S.; Lindsay, L.; Ellis, C. T.; Assefa, N.; Chatzakis, I.; Reinecke, T. L.; Tischler, J. G.; Fogler, M. M.; Edgar, J. H.; Basov, D. N.; Caldwell, J. D. Ultralow-Loss Polaritons in Isotopically Pure Boron Nitride. *Nat. Mater.* **2018**, *17*, 134−139.
(128) Chen, J.; Badioli, M.; Alonso-Gonzalez, P.; Thongrattanasiri, S.; Huth, F.; Osmond, J.; Spasenovic, M.; Centeno, A.; Pesquera, A.; Godignon, P.; Zurutuza Elorza, A.; Camara, N.; de Abajo, F. J. G.; Hillenbrand, R.; Koppens, F. H. L. Optical Nano-Imaging of Gate-Tunable Graphene Plasmons. *Nature* **2012**, *487*, 77−81.
(129) Fei, Z.; Rodin, A. S.; Andreev, G. O.; Bao, W.; McLeod, A. S.; Wagner, M.; Zhang, L. M.; Zhao, Z.; Thiemens, M.; Dominguez, G.; et al. Gate-Tuning of Graphene Plasmons Revealed by Infrared Nano-Imaging. *Nature* **2012**, *487*, 82−85.
(130) Hofmann, J.; Das Sarma, S. Surface Plasmon Polaritons in Topological Weyl Semimetals. *Phys. Rev. B: Condens. Matter Mater. Phys.* **2016**, *93*, 241402.
(131) Tan, C.; Yue, Z.; Dai, Z.; Bao, Q.; Wang, X.; Lu, H.; Wang, L. Nanograting-Assisted Generation of Surface Plasmon Polaritons in Weyl Semimetal WTe_2. *Opt. Mater.* **2018**, *86*, 421−423.
(132) Zhang, W.; Yang, F. Negative Refraction at Various Crystal Interfaces. *Opt. Commun.* **2008**, *281*, 3081−3086.
(133) Hess, O.; Pendry, J. B.; Maier, S. A.; Oulton, R. F.; Hamm, J. M.; Tsakmakidis, K. L. Active Nanoplasmonic Metamaterials. *Nat. Mater.* **2012**, *11*, 573−584.
(134) Kildishev, A. V.; Boltasseva, A.; Shalaev, V. M. Planar Photonics with Metasurfaces. *Science* **2013**, *339*, 1232009.
(135) Simovski, C. R.; Belov, P. A.; Atrashchenko, A. V.; Kivshar, Y. S. Wire Metamaterials: Physics and Applications. *Adv. Mater.* **2012**, *24*, 4229−4248.
(136) Meinzer, N.; Barnes, W. L.; Hooper, I. R. Plasmonic Meta-Atoms and Metasurfaces. *Nat. Photonics* **2014**, *8*, 889−898.
(137) Schuller, J. A.; Barnard, E. S.; Cai, W.; Jun, Y. C.; White, J. S.; Brongersma, M. L. Plasmonics for Extreme Light Concentration and Manipulation. *Nat. Mater.* **2010**, *9*, 193−204.
(138) Lapine, M.; Shadrivov, I. V.; Kivshar, Y. S. Colloquium: Nonlinear Metamaterials. *Rev. Mod. Phys.* **2014**, *86*, 1093−1123.
(139) Li, G.; Zhang, S.; Zentgraf, T. Nonlinear Photonic Metasurfaces. *Nat. Rev. Mater.* **2017**, *2*, 17010.
(140) Kauranen, M.; Zayats, A. V. Nonlinear Plasmonics. *Nat. Photonics* **2012**, *6*, 737−748.
(141) Kuzmenko, A. B.; Van Heumen, E.; Carbone, F.; Van Der Marel, D. Universal Optical Conductance of Graphite. *Phys. Rev. Lett.* **2008**, *100*, 117401.
(142) Stauber, T.; Peres, N. M. R.; Geim, A. K. The Optical Conductivity of Graphene in the Visible Region of the Spectrum. *Phys. Rev. B: Condens. Matter Mater. Phys.* **2008**, *78*, 085432.
(143) Nair, R. R.; Blake, P.; Grigorenko, A. N.; Novoselov, K. S.; Booth, T. J.; Stauber, T.; Peres, N. M.; Geim, A. K. Fine Structure Constant Defines Visual Transparency of Graphene. *Science* **2008**, *320*, 1308−1308.
(144) George, P. a.; Strait, J.; Dawlaty, J.; Shivaraman, S.; Chandrashekhar, M.; Rana, F.; Spencer, M. G. Ultrafast Optical-Pump Terahertz-Probespectroscopy of the Carrier Relaxation Epitaxial Graphene. *Nano Lett.* **2008**, *8*, 4248−4251.
(145) Bao, Q.; Zhang, H.; Wang, Y.; Ni, Z.; Yan, Y.; Shen, Z. X.; Loh, K. P.; Tang, D. Y. Atomic-Layer Graphene as a Saturable

https://dx.doi.org/10.1021/acs.chemrev.9b00592
Chem. Rev. 2020, 120, 6197−6246

Absorber for Ultrafast Pulsed Lasers. *Adv. Funct. Mater.* **2009**, *19*, 3077−3083.
(146) Jin, F.; Roldán, R.; Katsnelson, M. I.; Yuan, S. Screening and Plasmons in Pure and Disordered Single- and Bilayer Black Phosphorus. *Phys. Rev. B: Condens. Matter Mater. Phys.* **2015**, *92*, 115440.
(147) Tran, V.; Soklaski, R.; Liang, Y.; Yang, L. Layer-Controlled Band Gap and Anisotropic Excitons in Few-Layer Black Phosphorus. *Phys. Rev. B: Condens. Matter Mater. Phys.* **2014**, *89*, 235319.
(148) Engel, M.; Steiner, M.; Avouris, P. Black Phosphorus Photodetector for Multispectral, High-Resolution Imaging. *Nano Lett.* **2014**, *14*, 6414−6417.
(149) Castellanos-Gomez, A. Black Phosphorus: Narrow Gap, Wide Applications. *J. Phys. Chem. Lett.* **2015**, *6*, 4280−4291.
(150) Asahina, H.; Morita, A. Band Structure and Optical Properties of Black Phosphorus. *J. Phys. C: Solid State Phys.* **1984**, *17*, 1839.
(151) Ling, X.; Wang, H.; Huang, S.; Xia, F.; Dresselhaus, M. S. The Renaissance of Black Phosphorus. *Proc. Natl. Acad. Sci. U. S. A.* **2015**, *112*, 4523−4530.
(152) Correas-Serrano, D.; Gomez-Diaz, J.; Melcon, A. A.; Alù, A. Black Phosphorus Plasmonics: Anisotropic Elliptical Propagation and Nonlocality-Induced Canalization. *J. Opt.* **2016**, *18*, 104006.
(153) High, A. A.; Devlin, R. C.; Dibos, A.; Polking, M.; Wild, D. S.; Perczel, J.; de Leon, N. P.; Lukin, M. D.; Park, H. Visible-Frequency Hyperbolic Metasurface. *Nature* **2015**, *522*, 192−196.
(154) Gomez-Diaz, J. S.; Tymchenko, M.; Alù, A. Hyperbolic Plasmons and Topological Transitions over Uniaxial Metasurfaces. *Phys. Rev. Lett.* **2015**, *114*, 233901.
(155) Cheiwchanchamnangij, T.; Lambrecht, W. R. L. Quasiparticle Band Structure Calculation of Monolayer, Bilayer, and Bulk MoS_2. *Phys. Rev. B: Condens. Matter Mater. Phys.* **2012**, *85*, 205302.
(156) Jones, A. M.; Yu, H.; Ghimire, N. J.; Wu, S.; Aivazian, G.; Ross, J. S.; Zhao, B.; Yan, J.; Mandrus, D. G.; Xiao, D.; et al. Optical Generation of Excitonic Valley Coherence in Monolayer WSe_2. *Nat. Nanotechnol.* **2013**, *8*, 634−638.
(157) Seyler, K. L.; Schaibley, J. R.; Gong, P.; Rivera, P.; Jones, A. M.; Wu, S.; Yan, J.; Mandrus, D. G.; Yao, W.; Xu, X. Electrical Control of Second-Harmonic Generation in a WSe_2 Monolayer Transistor. *Nat. Nanotechnol.* **2015**, *10*, 407−411.
(158) Malic, E.; Selig, M.; Feierabend, M.; Brem, S.; Christiansen, D.; Wendler, F.; Knorr, A.; Berghäuser, G. Dark Excitons in Transition Metal Dichalcogenides. *Phys. Rev. Mater.* **2018**, *2*, 014002.
(159) Baranowski, M.; Surrente, A.; Maude, D.; Ballottin, M.; Mitioglu, A.; Christianen, P.; Kung, Y.; Dumcenco, D.; Kis, A.; Plochocka, P. Dark Excitons and the Elusive Valley Polarization in Transition Metal Dichalcogenides. *2D Mater.* **2017**, *4*, 025016.
(160) Wang, X.; Tang, Z. Circular Dichroism Studies on Plasmonic Nanostructures. *Small* **2017**, *13*, 1601115.
(161) Zhang, C.; Chen, Y.; Johnson, A.; Li, M. Y.; Li, L. J.; Mende, P. C.; Feenstra, R. M.; Shih, C. K. Probing Critical Point Energies of Transition Metal Dichalcogenides: Surprising Indirect Gap of Single Layer WSe_2. *Nano Lett.* **2015**, *15*, 6494−6500.
(162) Mak, K. F.; Shan, J. Photonics and Optoelectronics of 2D Semiconductor Transition Metal Dichalcogenides. *Nat. Photonics* **2016**, *10*, 216−226.
(163) Schneider, C.; Glazov, M. M.; Korn, T.; Höfling, S.; Urbaszek, B. Two-Dimensional Semiconductors in the Regime of Strong Light-Matter Coupling. *Nat. Commun.* **2018**, *9*, 2695.
(164) Qi, X.; Zhang, Y.; Ou, Q.; Ha, S. T.; Qiu, C. W.; Zhang, H.; Cheng, Y. B.; Xiong, Q.; Bao, Q. Photonics and Optoelectronics of 2D Metal-Halide Perovskites. *Small* **2018**, *14*, 1800682.
(165) Kubota, Y.; Watanabe, K.; Tsuda, O.; Taniguchi, T.; et al. Deep Ultraviolet Light-Emitting Hexagonal Boron Nitride Synthesized at Atmospheric Pressure. *Science* **2007**, *317*, 932−935.
(166) Dean, C. R.; Young, A. F.; Meric, I.; Lee, C.; Wang, L.; Sorgenfrei, S.; Watanabe, K.; Taniguchi, T.; Kim, P.; Shepard, K. L.; et al. Boron Nitride Substrates for High-Quality Graphene Electronics. *Nat. Nanotechnol.* **2010**, *5*, 722−726.
(167) Naik, G. V.; Shalaev, V. M.; Boltasseva, A. Alternative Plasmonic Materials: Beyond Gold and Silver. *Adv. Mater.* **2013**, *25*, 3264−3294.
(168) Wang, Q.; Rogers, E. T. F.; Gholipour, B.; Wang, C. M.; Yuan, G.; Teng, J.; Zheludev, N. I. Optically Reconfigurable Metasurfaces and Photonic Devices Based on Phase Change Materials. *Nat. Photonics* **2016**, *10*, 60−65.
(169) Duan, X.; Kamin, S.; Liu, N. Dynamic Plasmonic Colour Display. *Nat. Commun.* **2017**, *8*, 14606.
(170) Yu, P.; Li, J.; Zhang, S.; Jin, Z.; Schütz, G.; Qiu, C. W.; Hirscher, M.; Liu, N. Dynamic Janus Metasurfaces in the Visible Spectral Region. *Nano Lett.* **2018**, *18*, 4584−4589.
(171) Huang, Y. W.; Lee, H. W. H.; Sokhoyan, R.; Pala, R. A.; Thyagarajan, K.; Han, S.; Tsai, D. P.; Atwater, H. A. Gate-Tunable Conducting Oxide Metasurfaces. *Nano Lett.* **2016**, *16*, 5319−5325.
(172) Kuzyk, A.; Schreiber, R.; Zhang, H.; Govorov, A. O.; Liedl, T.; Liu, N. Reconfigurable 3D Plasmonic Metamolecules. *Nat. Mater.* **2014**, *13*, 862−866.
(173) Gao, Y.; Huang, C.; Hao, C.; Sun, S.; Zhang, L.; Zhang, C.; Duan, Z.; Wang, K.; Jin, Z.; Zhang, N.; Kildishev, A. V.; Qiu, C.-W.; Song, Q.; Xiao, S. Lead Halide Perovskite Nanostructures for Dynamic Color Display. *ACS Nano* **2018**, *12*, 8847−8854.
(174) Zhang, C.; Xiao, S.; Wang, Y.; Gao, Y.; Fan, Y.; Huang, C.; Zhang, N.; Yang, W.; Song, Q. Lead Halide Perovskite-Based Dynamic Metasurfaces. *Laser Photonics Rev.* **2019**, *13*, 1900079.
(175) Wunsch, B.; Stauber, T.; Sols, F.; Guinea, F. Dynamical Polarization of Graphene at Finite Doping. *New J. Phys.* **2006**, *8*, 318.
(176) Hwang, E. H.; Das Sarma, S. Quasiparticle Spectral Function in Doped Graphene: Electron-Electron Interaction Effects in Arpes. *Phys. Rev. B: Condens. Matter Mater. Phys.* **2008**, *77*, 081412.
(177) Wang, F.; Zhang, Y.; Tian, C.; Girit, C.; Zettl, A.; Crommie, M.; Shen, Y. R. Gate Variable Optical Transitions in Graphene. *Science* **2008**, *320*, 206−209.
(178) Li, Z. Q.; Henriksen, E. A.; Jiang, Z.; Hao, Z.; Martin, M. C.; Kim, P.; Stormer, H. L.; Basov, D. N. Dirac Charge Dynamics in Graphene by Infrared Spectroscopy. *Nat. Phys.* **2008**, *4*, 532−535.
(179) Wu, J.; Xie, L.; Li, Y.; Wang, H.; Ouyang, Y.; Guo, J.; Dai, H. Controlled Chlorine Plasma Reaction for Noninvasive Graphene Doping. *J. Am. Chem. Soc.* **2011**, *133*, 19668−19671.
(180) Chen, W.; Chen, S.; Qi, D. C.; Gao, X. Y.; Wee, A. T. S. Surface Transfer p-Type Doping of Epitaxial Graphene. *J. Am. Chem. Soc.* **2007**, *129*, 10418−10422.
(181) Zhao, L.; He, R.; Rim, K. T.; Schiros, T.; Kim, K. S.; Zhou, H.; Gutiérrez, C.; Chockalingam, S. P.; Arguello, C. J.; Pálová, L.; et al. Visualizing Individual Nitrogen Dopants in Monolayer Graphene. *Science* **2011**, *333*, 999−1003.
(182) Martins, T. B.; Miwa, R. H.; Da Silva, A. J. R.; Fazzio, A. Electronic and Transport Properties of Boron-Doped Graphene Nanoribbons. *Phys. Rev. Lett.* **2007**, *98*, 196803.
(183) Sensale-Rodriguez, B.; Yan, R.; Kelly, M. M.; Fang, T.; Tahy, K.; Hwang, W. S.; Jena, D.; Liu, L.; Xing, H. G. Broadband Graphene Terahertz Modulators Enabled by Intraband Transitions. *Nat. Commun.* **2012**, *3*, 780.
(184) Liu, M.; Yin, X. B.; Ulin-Avila, E.; Geng, B. S.; Zentgraf, T.; Ju, L.; Wang, F.; Zhang, X. A Graphene-Based Broadband Optical Modulator. *Nature* **2011**, *474*, 64−67.
(185) Han, L.; Wang, L.; Xing, H.; Chen, X. Active Tuning of Mid-Infrared Surface Plasmon Resonance and Its Hybridization in Black Phosphorus Sheet Array. *ACS Photonics* **2018**, *5*, 3828−3837.
(186) Wang, Y.; Ou, J. Z.; Chrimes, A. F.; Carey, B. J.; Daeneke, T.; Alsaif, M. M. Y. A.; Mortazavi, M.; Zhuiykov, S.; Medhekar, N.; Bhaskaran, M.; et al. Plasmon Resonances of Highly Doped Two-Dimensional MoS_2. *Nano Lett.* **2015**, *15*, 883−890.
(187) Ye, Y.; Xiao, J.; Wang, H.; Ye, Z.; Zhu, H.; Zhao, M.; Wang, Y.; Zhao, J.; Yin, X.; Zhang, X. Electrical Generation and Control of the Valley Carriers in a Monolayer Transition Metal Dichalcogenide. *Nat. Nanotechnol.* **2016**, *11*, 598−602.
(188) Wang, T.; Zhang, Y.; Liu, Y.; Li, J.; Liu, D.; Luo, J.; Ge, K. Layer-Number-Dependent Exciton Recombination Behaviors of

https://dx.doi.org/10.1021/acs.chemrev.9b00592
Chem. Rev. 2020, 120, 6197−6246

MoS_2 Determined by Fluorescence-Lifetime Imaging Microscopy. *J. Phys. Chem. C* **2018**, *122*, 18651−18658.
(189) Zhang, N.; Surrente, A.; Baranowski, M.; Maude, D. K.; Gant, P.; Castellanos-Gomez, A.; Plochocka, P. Moiré Intralayer Excitons in a $MoSe_2/MoS_2$ Heterostructure. *Nano Lett.* **2018**, *18*, 7651−7657.
(190) Lin, X.; Yang, Y.; Rivera, N.; López, J. J.; Shen, Y.; Kaminer, I.; Chen, H.; Zhang, B.; Joannopoulos, J. D.; Soljačić, M. All-Angle Negative Refraction of Highly Squeezed Plasmon and Phonon Polaritons in Graphene−Boron Nitride Heterostructures. *Proc. Natl. Acad. Sci. U. S. A.* **2017**, *114*, 6717−6721.
(191) Cao, Y.; Fatemi, V.; Demir, A.; Fang, S.; Tomarken, S. L.; Luo, J. Y.; Sanchez-Yamagishi, J. D.; Watanabe, K.; Taniguchi, T.; Kaxiras, E.; et al. Correlated Insulator Behaviour at Half-Filling in Magic-Angle Graphene Superlattices. *Nature* **2018**, *556*, 80−84.
(192) Cao, Y.; Fatemi, V.; Fang, S.; Watanabe, K.; Taniguchi, T.; Kaxiras, E.; Jarillo-Herrero, P. Unconventional Superconductivity in Magic-Angle Graphene Superlattices. *Nature* **2018**, *556*, 43−50.
(193) Seyler, K. L.; Rivera, P.; Yu, H.; Wilson, N. P.; Ray, E. L.; Mandrus, D. G.; Yan, J.; Yao, W.; Xu, X. Signatures of Moiré-Trapped Valley Excitons in $MoSe_2/WSe_2$ Heterobilayers. *Nature* **2019**, *567*, 66−70.
(194) Tran, K.; Moody, G.; Wu, F.; Lu, X.; Choi, J.; Kim, K.; Rai, A.; Sanchez, D. A.; Quan, J.; Singh, A.; et al. Evidence for Moiré Excitons in Van der Waals Heterostructures. *Nature* **2019**, *567*, 71−75.
(195) Jin, C.; Regan, E. C.; Yan, A.; Iqbal Bakti Utama, M.; Wang, D.; Zhao, S.; Qin, Y.; Yang, S.; Zheng, Z.; Shi, S.; et al. Observation of Moiré Excitons in WSe_2/WS_2 Heterostructure Superlattices. *Nature* **2019**, *567*, 76−80.
(196) Alexeev, E. M.; Ruiz-Tijerina, D. A.; Danovich, M.; Hamer, M. J.; Terry, D. J.; Nayak, P. K.; Ahn, S.; Pak, S.; Lee, J.; Sohn, J. I.; et al. Resonantly Hybridized Excitons in Moiré Superlattices in Van der Waals Heterostructures. *Nature* **2019**, *567*, 81−86.
(197) Woessner, A.; Lundeberg, M. B.; Gao, Y.; Principi, A.; Alonso-Gonzalez, P.; Carrega, M.; Watanabe, K.; Taniguchi, T.; Vignale, G.; Polini, M.; et al. Highly Confined Low-Loss Plasmons in Graphene-Boron Nitride Heterostructures. *Nat. Mater.* **2015**, *14*, 421−425.
(198) Lin, Y.; Ling, X.; Yu, L.; Huang, S.; Hsu, A. L.; Lee, Y. H.; Kong, J.; Dresselhaus, M. S.; Palacios, T. Dielectric Screening of Excitons and Trions in Single-Layer MoS_2. *Nano Lett.* **2014**, *14*, 5569−5576.
(199) Scholz, A.; Stauber, T.; Schliemann, J. Plasmons and Screening in a Monolayer of Mos2. *Phys. Rev. B: Condens. Matter Mater. Phys.* **2013**, *88*, 035135.
(200) Fei, Z.; Andreev, G. O.; Bao, W.; Zhang, L. M.; McLeod, A. S.; Wang, C.; Stewart, M. K.; Zhao, Z.; Dominguez, G.; Thiemens, M.; Fogler, M. M.; Tauber, M. J.; Castro-Neto, A. H.; Lau, C. N.; Keilmann, F.; Basov, D. N.; et al. Infrared Nanoscopy of Dirac Plasmons at the Graphene-SiO_2 Interface. *Nano Lett.* **2011**, *11*, 4701−4705.
(201) Eberlein, T.; Bangert, U.; Nair, R. R.; Jones, R.; Gass, M.; Bleloch, A. L.; Novoselov, K. S.; Geim, A.; Briddon, P. R. Plasmon Spectroscopy of Free-Standing Graphene Films. *Phys. Rev. B: Condens. Matter Mater. Phys.* **2008**, *77*, 233406.
(202) Ni, G. X.; McLeod, A. S.; Sun, Z.; Wang, L.; Xiong, L.; Post, K. W.; Sunku, S. S.; Jiang, B. Y.; Hone, J.; Dean, C. R.; et al. Fundamental Limits to Graphene Plasmonics. *Nature* **2018**, *557*, 530−533.
(203) Caldwell, J. D.; Lindsay, L.; Giannini, V.; Vurgaftman, I.; Reinecke, T. L.; Maier, S. A.; Glembocki, O. J. Low-Loss, Infrared and Terahertz Nanophotonics Using Surface Phonon Polaritons. *Nanophotonics* **2015**, *4*, 44−68.
(204) Si, C.; Sun, Z.; Liu, F. Strain Engineering of Graphene: A Review. *Nanoscale* **2016**, *8*, 3207−3217.
(205) Quereda, J.; San-Jose, P.; Parente, V.; Vaquero-Garzon, L.; Molina-Mendoza, A. J.; Agraït, N.; Rubio-Bollinger, G.; Guinea, F.; Roldán, R.; Castellanos-Gomez, A. Strong Modulation of Optical Properties in Black Phosphorus through Strain-Engineered Rippling. *Nano Lett.* **2016**, *16*, 2931−2937.
(206) Lee, C.; Wei, X.; Kysar, J. W.; Hone, J. Measurement of the Elastic Properties and Intrinsic Strength of Monolayer Graphene. *Science* **2008**, *321*, 385−388.
(207) An, X.; Sun, J.; Lu, Z.; Ma, F.; Zhang, G. Pressure-Induced Insulator-Semiconductor Transition in Bilayer Hexagonal Boron Nitride. *Ceram. Int.* **2017**, *43*, 6626−6630.
(208) Dou, X.; Ding, K.; Jiang, D.; Sun, B. Tuning and Identification of Interband Transitions in Monolayer and Bilayer Molybdenum Disulfide Using Hydrostatic Pressure. *ACS Nano* **2014**, *8*, 7458−7464.
(209) Johari, P.; Shenoy, V. B. Tuning the Electronic Properties of Semiconducting Transition Metal Dichalcogenides by Applying Mechanical Strains. *ACS Nano* **2012**, *6*, 5449−5456.
(210) Hsu, W.-T.; Lu, L.-S.; Wang, D.; Huang, J.-K.; Li, M.-Y.; Chang, T.-R.; Chou, Y.-C.; Juang, Z.-Y.; Jeng, H.-T.; Li, L.-J.; Chang, W.-H.; et al. Evidence of Indirect Gap in Monolayer WSe_2. *Nat. Commun.* **2017**, *8*, 929.
(211) Gan, X.; Mak, K. F.; Gao, Y.; You, Y.; Hatami, F.; Hone, J.; Heinz, T. F.; Englund, D. Strong Enhancement of Light−Matter Interaction in Graphene Coupled to a Photonic Crystal Nanocavity. *Nano Lett.* **2012**, *12*, 5626−5631.
(212) Youngblood, N.; Peng, R.; Nemilentsau, A.; Low, T.; Li, M. Layer-Tunable Third-Harmonic Generation in Multilayer Black Phosphorus. *ACS Photonics* **2017**, *4*, 8−14.
(213) Psilodimitrakopoulos, S.; Mouchliadis, L.; Paradisanos, I.; Lemonis, A.; Kioseoglou, G.; Stratakis, E. Ultrahigh-Resolution Nonlinear Optical Imaging of the Armchair Orientation in 2D Transition Metal Dichalcogenides. *Light: Sci. Appl.* **2018**, *7*, No. 18005.
(214) Cheng, J. L.; Vermeulen, N.; Sipe, J. E. Second Order Optical Nonlinearity of Graphene Due to Electric Quadrupole and Magnetic Dipole Effects. *Sci. Rep.* **2017**, *7*, 43843.
(215) Cadelano, E.; Palla, P. L.; Giordano, S.; Colombo, L. Nonlinear Elasticity of Monolayer Graphene. *Phys. Rev. Lett.* **2009**, *102*, 235502.
(216) Lin, K. H.; Weng, S. W.; Lyu, P. W.; Tsai, T. R.; Su, W. B. Observation of Optical Second Harmonic Generation from Suspended Single-Layer and Bi-Layer Graphene. *Appl. Phys. Lett.* **2014**, *105*, 151605.
(217) An, Y. Q.; Rowe, J. E.; Dougherty, D. B.; Lee, J. U.; Diebold, A. C. Optical Second-Harmonic Generation Induced by Electric Current in Graphene on Si and Sic Substrates. *Phys. Rev. B: Condens. Matter Mater. Phys.* **2014**, *89*, 115310.
(218) Liu, Z.; Wang, Y.; Zhang, X.; Xu, Y.; Chen, Y.; Tian, J. Nonlinear Optical Properties of Graphene Oxide in Nanosecond and Picosecond Regimes. *Appl. Phys. Lett.* **2009**, *94*, 92.
(219) Rapoport, Y.; Grimalsky, V.; Lavrinenko, A. V.; Boardman, A. Double Resonant Excitation of the Second Harmonic of Terahertz Raditation in Dielectric-Graphene Layered Metamaterials. *J. Opt.* **2017**, *19*, 095104.
(220) Wu, S.; Mao, L.; Jones, A. M.; Yao, W.; Zhang, C.; Xu, X. Quantum-Enhanced Tunable Second-Order Optical Nonlinearity in Bilayer Graphene. *Nano Lett.* **2012**, *12*, 2032−2036.
(221) Gu, T.; Petrone, N.; McMillan, J. F.; van der Zande, A.; Yu, M.; Lo, G. Q.; Kwong, D. L.; Hone, J.; Wong, C. W. Regenerative Oscillation and Four-Wave Mixing in Graphene Optoelectronics. *Nat. Photonics* **2012**, *6*, 554−559.
(222) Cheng, J. L.; Vermeulen, N.; Sipe, J. Third-Order Nonlinearity of Graphene: Effects of Phenomenological Relaxation and Finite Temperature. *Phys. Rev. B: Condens. Matter Mater. Phys.* **2015**, *91*, 235320.
(223) Hong, S. Y.; Dadap, J. I.; Petrone, N.; Yeh, P. C.; Hone, J.; Osgood, R. M. Optical Third-Harmonic Generation in Graphene. *Phys. Rev. X* **2013**, *3*, 021014.
(224) Kumar, N.; Kumar, J.; Gerstenkorn, C.; Wang, R.; Chiu, H. Y.; Smirl, A. L.; Zhao, H. Third Harmonic Generation in Graphene and Few-Layer Graphite Films. *Phys. Rev. B: Condens. Matter Mater. Phys.* **2013**, *87*, 121406.

https://dx.doi.org/10.1021/acs.chemrev.9b00592
Chem. Rev. 2020, 120, 6197−6246

(225) Zhang, H.; Virally, S.; Bao, Q.; Kian Ping, L.; Massar, S.; Godbout, N.; Kockaert, P. Z-Scan Measurement of the Nonlinear Refractive Index of Graphene. *Opt. Lett.* **2012**, *37*, 1855−1856.
(226) Yang, H.; Feng, X.; Wang, Q.; Huang, H.; Chen, W.; Wee, A. T. S.; Ji, W. Giant Two-Photon Absorption in Bilayer Graphene. *Nano Lett.* **2011**, *11*, 2622−2627.
(227) Hendry, E.; Hale, P. J.; Moger, J.; Savchenko, A.; Mikhailov, S. Coherent Nonlinear Optical Response of Graphene. *Phys. Rev. Lett.* **2010**, *105*, 097401.
(228) Zhang, F.; Hu, X. Y.; Yang, H.; Gong, Q. H. Low-Power All-Optical Tunable Plasmonic-Mode Coupling in Nonlinear Metamaterials. *Appl. Phys. Lett.* **2014**, *104*, 131110.
(229) Lu, C. C.; Hu, X. Y.; Zhang, F.; Yang, H.; Gong, Q. H. Multilayer Graphene: Polycrystalline Ito for Ultralow-Power Active Control of Polarization-Insensitive, Metamaterial-Induced Transparency. *Adv. Opt. Mater.* **2014**, *2*, 1141−1148.
(230) Yang, X. Y.; Yang, J. H.; Hu, X. Y.; Zhu, Y.; Yang, H.; Gong, Q. H. Multilayer-WS_2:Ferroelectric Composite for Ultrafast Tunable Metamaterial-Induced Transparency Applications. *Appl. Phys. Lett.* **2015**, *107*, 081110.
(231) Zhou, Y.; Yang, X. Y.; Hu, X. Y.; Yang, H.; Gong, Q. H. Multilayer-MoS_2-Microsheet/(Nano-Au: $LiNbO_3$) for All-Optical Tunable Metamaterial-Induced Transparency. *J. Opt.* **2015**, *17*, 105102.
(232) Shi, S. F.; Zeng, B.; Han, H. L.; Hong, X.; Tsai, H. Z.; Jung, H. S.; Zettl, A.; Crommie, M. F.; Wang, F. Optimizing Broadband Terahertz Modulation with Hybrid Graphene/Metasurface Structures. *Nano Lett.* **2015**, *15*, 372−377.
(233) Rapoport, Y.; Grimalsky, V.; Iorsh, I.; Kalinich, N.; Koshevaya, S.; Castrejon-Martinez, C.; Kivshar, Y. S. Nonlinear Reshaping of Terahertz Pulses with Graphene Metamaterials. *JETP Lett.* **2013**, *98*, 503−506.
(234) Chen, X.; Fan, W. H. Polarization-Insensitive Tunable Multiple Electromagnetically Induced Transparencies Analogue in Terahertz Graphene Metamaterial. *Opt. Mater. Express* **2016**, *6*, 2607−2615.
(235) Hamedi, H. R.; Asadpour, S. H. Realization of Optical Bistability and Multistability in Landau-Quantized Graphene. *J. Appl. Phys.* **2015**, *117*, 183101.
(236) Shoaei, M.; Moravvej-Farshi, M. K.; Yousefi, L. All-Optical Switching of Nonlinear Hyperbolic Metamaterials in Visible and near-Infrared Regions. *J. Opt. Soc. Am. B* **2015**, *32*, 2358−2365.
(237) Nikolaenko, A. E.; Papasimakis, N.; Atmatzakis, E.; Luo, Z. Q.; Shen, Z. X.; De Angelis, F.; Boden, S. A.; Di Fabrizio, E.; Zheludev, N. I. Nonlinear Graphene Metamaterial. *Appl. Phys. Lett.* **2012**, *100*, 181109.
(238) Shen, M.; Ruan, L. X.; Chen, X.; Shi, J. L.; Ding, H. X.; Xi, N.; Wang, Q. Nonlinear Surface Waves near the Dirac Point in Negative-Zero-Positive Index Metamaterial. *J. Opt.* **2010**, *12*, 085201.
(239) Shen, M.; Ruan, L. X.; Wang, X. L.; Shi, J. L.; Wang, Q. Tunable Band Gap near the Dirac Point in Nonlinear Negative-Zero-Positive Index Metamaterial Waveguide. *Phys. Rev. A: At., Mol., Opt. Phys.* **2011**, *83*, 045804.
(240) Wang, X.; Jiang, A.; Zheng, F. Large and Bistable Goos-Hänchen Shifts from the Kretschmann Configuration with a Nonlinear Negative-Zero-Positive Index Metamaterial. *J. Opt.* **2014**, *16*, 045101.
(241) Malard, L. M.; Alencar, T. V.; Barboza, A. P. M.; Mak, K. F.; De Paula, A. M. Observation of Intense Second Harmonic Generation from MoS_2 Atomic Crystals. *Phys. Rev. B: Condens. Matter Mater. Phys.* **2013**, *87*, 201401.
(242) Yin, X.; Ye, Z.; Chenet, D. A.; Ye, Y.; O'Brien, K.; Hone, J. C.; Zhang, X. Edge Nonlinear Optics on a MoS_2 Monolayer. *Science* **2014**, *344*, 488−490.
(243) Kim, D. H.; Lim, D. Optical Second-Harmonic Generation in Few-Layer $MoSe_2$. *J. Korean Phys. Soc.* **2015**, *66*, 816−820.
(244) Wang, Z.; Dong, Z.; Zhu, H.; Jin, L.; Chiu, M.-H.; Li, L.-J.; Xu, Q.-H.; Eda, G.; Maier, S. A.; Wee, A. T. S.; Qiu, C.-W.; Yang, J. K. W. Selectively Plasmon-Enhanced Second-Harmonic Generation from Monolayer Tungsten Diselenide on Flexible Substrates. *ACS Nano* **2018**, *12*, 1859−1867.
(245) Janisch, C.; Wang, Y.; Ma, D.; Mehta, N.; Elias, A. L.; Perea-Lopez, N.; Terrones, M.; Crespi, V.; Liu, Z. Extraordinary Second Harmonic Generation in Tungsten Disulfide Monolayers. *Sci. Rep.* **2015**, *4*, 5530.
(246) Xiao, J.; Ye, Z.; Wang, Y.; Zhu, H.; Wang, Y.; Zhang, X. Nonlinear Optical Selection Rule Based on Valley-Exciton Locking in Monolayer WS_2. *Light: Sci. Appl.* **2015**, *4*, No. e366.
(247) Lin, K.-Q.; Bange, S.; Lupton, J. M. Quantum Interference in Second-Harmonic Generation from Monolayer WSe_2. *Nat. Phys.* **2019**, *15*, 242−246.
(248) Lee, J.; Tymchenko, M.; Argyropoulos, C.; Chen, P. Y.; Lu, F.; Demmerle, F.; Boehm, G.; Amann, M. C.; Alù, A.; Belkin, M. A. Giant Nonlinear Response from Plasmonic Metasurfaces Coupled to Intersubband Transitions. *Nature* **2014**, *511*, 65−69.
(249) Kuznetsov, A. I.; Miroshnichenko, A. E.; Brongersma, M. L.; Kivshar, Y. S.; Luk'yanchuk, B. Optically Resonant Dielectric Nanostructures. *Science* **2016**, *354*, aag2472.
(250) Chen, H.; Corboliou, V.; Solntsev, A. S.; Choi, D.-Y.; Vincenti, M. A.; de Ceglia, D.; de Angelis, C.; Lu, Y.; Neshev, D. N. Enhanced Second-Harmonic Generation from Two-Dimensional $MoSe_2$ on a Silicon Waveguide. *Light: Sci. Appl.* **2017**, *6*, No. e17060.
(251) Boltasseva, A.; Atwater, H. A. Low-Loss Plasmonic Metamaterials. *Science* **2011**, *331*, 290−291.
(252) Khurgin, J. B. How to Deal with the Loss in Plasmonics and Metamaterials. *Nat. Nanotechnol.* **2015**, *10*, 2−6.
(253) Atwater, H. A.; Polman, A. Plasmonics for Improved Photovoltaic Devices. *Nat. Mater.* **2010**, *9*, 205−213.
(254) Davies, P. M. Z.; Hamm, J. M.; Sonnefraud, Y.; Maier, S. A.; Hess, O. Plasmonic Nanogap Tilings: Light-Concentrating Surfaces for Low-Loss Photonic Integration. *ACS Nano* **2013**, *7*, 7093−7100.
(255) Khurgin, J. B.; Sun, G. In Search of the Elusive Lossless Metal. *Appl. Phys. Lett.* **2010**, *96*, 181102.
(256) Ginn, J. C.; Jarecki, R. L., Jr; Shaner, E. A.; Davids, P. S. Infrared Plasmons on Heavily-Doped Silicon. *J. Appl. Phys.* **2011**, *110*, 043110.
(257) Fang, Z.; Wang, Y.; Liu, Z.; Schlather, A.; Ajayan, P. M.; Koppens, F. H. L.; Nordlander, P.; Halas, N. J. Plasmon-Induced Doping of Graphene. *ACS Nano* **2012**, *6*, 10222−10228.
(258) Liu, X.; Swihart, M. T. Heavily-Doped Colloidal Semiconductor and Metal Oxide Nanocrystals: An Emerging New Class of Plasmonic Nanomaterials. *Chem. Soc. Rev.* **2014**, *43*, 3908−3920.
(259) Soref, R.; Hendrickson, J.; Cleary, J. W. Mid-to Long-Wavelength Infrared Plasmonic-Photonics Using Heavily Doped n-Ge/Ge and n-GeSn/GeSn Heterostructures. *Opt. Express* **2012**, *20*, 3814−3824.
(260) Garcia, G.; Buonsanti, R.; Runnerstrom, E. L.; Mendelsberg, R. J.; Llordes, A.; Anders, A.; Richardson, T. J.; Milliron, D. J. Dynamically Modulating the Surface Plasmon Resonance of Doped Semiconductor Nanocrystals. *Nano Lett.* **2011**, *11*, 4415−4420.
(261) Naik, G. V.; Kim, J.; Boltasseva, A. Oxides and Nitrides as Alternative Plasmonic Materials in the Optical Range. *Opt. Mater. Express* **2011**, *1*, 1090−1099.
(262) Low, T.; Avouris, P. Graphene Plasmonics for Terahertz to Mid-Infrared Applications. *ACS Nano* **2014**, *8*, 1086−1101.
(263) Koppens, F. H. L.; Chang, D. E.; García De Abajo, F. J. Graphene Plasmonics: A Platform for Strong Light-Matter Interactions. *Nano Lett.* **2011**, *11*, 3370−3377.
(264) Fallahi, A.; Perruisseau-Carrier, J. Design of Tunable Biperiodic Graphene Metasurfaces. *Phys. Rev. B: Condens. Matter Mater. Phys.* **2012**, *86*, 195408.
(265) Huang, X.; Zhao, L.; Long, Y.; Wang, P.; Chen, D.; Yang, Z.; Liang, H.; Xue, M.; Weng, H.; Fang, Z.; Dai, X.; Chen, G. Observation of the Chiral-Anomaly-Induced Negative Magnetoresistance in 3D Weyl Semimetal Taas. *Phys. Rev. X* **2015**, *5*, 031023.
(266) Willets, K. A.; Wilson, A. J.; Sundaresan, V.; Joshi, P. B. Super-Resolution Imaging and Plasmonics. *Chem. Rev.* **2017**, *117*, 7538−7582.

https://dx.doi.org/10.1021/acs.chemrev.9b00592
Chem. Rev. 2020, 120, 6197−6246

(267) Dai, Z.-g.; Xiao, X.-h.; Wu, W.; Zhang, Y.-p.; Liao, L.; Guo, S.-s.; Ying, J.-j.; Shan, C.-x.; Sun, M.-t.; Jiang, C.-z. Plasmon-Driven Reaction Controlled by the Number of Graphene Layers and Localized Surface Plasmon Distribution During Optical Excitation. *Light: Sci. Appl.* **2015**, *4*, No. e342.
(268) Zhang, X.; Dai, Z.; Si, S.; Zhang, X.; Wu, W.; Deng, H.; Wang, F.; Xiao, X.; Jiang, C. Ultrasensitive Sers Substrate Integrated with Uniform Subnanometer Scale "Hot Spots" Created by a Graphene Spacer for the Detection of Mercury Ions. *Small* **2017**, *13*, 1603347.
(269) Zhang, X.; Xiao, X.; Dai, Z.; Wu, W.; Zhang, X.; Fu, L.; Jiang, C. Ultrasensitive Sers Performance in 3D "Sunflower-Like" Nano-arrays Decorated with Ag Nanoparticles. *Nanoscale* **2017**, *9*, 3114−3120.
(270) Xue, T.; Liang, W.; Li, Y.; Sun, Y.; Xiang, Y.; Zhang, Y.; Dai, Z.; Duo, Y.; Wu, L.; Qi, K.; Shivananju, B. N.; Zhang, L.; Cui, X.; Zhang, H.; Bao, Q. Ultrasensitive Detection of Mirna with an Antimonene-Based Surface Plasmon Resonance Sensor. *Nat. Commun.* **2019**, *10*, 28.
(271) Ni, X.; Ishii, S.; Kildishev, A. V.; Shalaev, V. M. Ultra-Thin, Planar, Babinet-Inverted Plasmonic Metalenses. *Light: Sci. Appl.* **2013**, *2*, No. e72.
(272) Alù, A.; Engheta, N. Achieving Transparency with Plasmonic and Metamaterial Coatings. *Phys. Rev. E* **2005**, *72*, 016623.
(273) Ni, X.; Emani, N. K.; Kildishev, A. V.; Boltasseva, A.; Shalaev, V. M. Broadband Light Bending with Plasmonic Nanoantennas. *Science* **2012**, *335*, 427−427.
(274) Papadakis, G. T.; Fleischman, D.; Davoyan, A.; Yeh, P.; Atwater, H. A. Optical Magnetism in Planar Metamaterial Heterostructures. *Nat. Commun.* **2018**, *9*, 296.
(275) Boriskina, S. V.; Cooper, T. A.; Zeng, L.; Ni, G.; Tong, J. K.; Tsurimaki, Y.; Huang, Y.; Meroueh, L.; Mahan, G.; Chen, G. Losses in Plasmonics: From Mitigating Energy Dissipation to Embracing Loss-Enabled Functionalities. *Adv. Opt. Photonics* **2017**, *9*, 775−827.
(276) Mikhailov, S. A.; Ziegler, K. New Electromagnetic Mode in Graphene. *Phys. Rev. Lett.* **2007**, *99*, 016803.
(277) Jablan, M.; Buljan, H.; Soljačić, M. Plasmonics in Graphene at Infrared Frequencies. *Phys. Rev. B: Condens. Matter Mater. Phys.* **2009**, *80*, 245435.
(278) Huidobro, P. A.; Kraft, M.; Maier, S. A.; Pendry, J. B. Graphene as a Tunable Anisotropic or Isotropic Plasmonic Metasurface. *ACS Nano* **2016**, *10*, 5499−5506.
(279) Wang, X.; Jones, A. M.; Seyler, K. L.; Tran, V.; Jia, Y.; Zhao, H.; Wang, H.; Yang, L.; Xu, X.; Xia, F. Highly Anisotropic and Robust Excitons in Monolayer Black Phosphorus. *Nat. Nanotechnol.* **2015**, *10*, 517−521.
(280) Zhang, Q.; Li, X.; Hossain, M. M.; Xue, Y.; Zhang, J.; Song, J.; Liu, J.; Turner, M. D.; Fan, S.; Bao, Q.; Gu, M.; et al. Graphene Surface Plasmons at the near-Infrared Optical Regime. *Sci. Rep.* **2015**, *4*, 6559.
(281) Manjavacas, A.; Garcia de Abajo, F. J. Tunable Plasmons in Atomically Thin Gold Nanodisks. *Nat. Commun.* **2014**, *5*, 3548.
(282) Li, X.; Zhu, J.; Wei, B. Hybrid Nanostructures of Metal/Two-Dimensional Nanomaterials for Plasmon-Enhanced Applications. *Chem. Soc. Rev.* **2016**, *45*, 3145−3187.
(283) Zhang, G.; Huang, S.; Chaves, A.; Song, C.; Ozcelik, V. O.; Low, T.; Yan, H. Infrared Fingerprints of Few-Layer Black Phosphorus. *Nat. Commun.* **2017**, *8*, 14071.
(284) Xia, F.; Wang, H.; Jia, Y. Rediscovering Black Phosphorus as an Anisotropic Layered Material for Optoelectronics and Electronics. *Nat. Commun.* **2014**, *5*, 4458.
(285) Qiao, J.; Kong, X.; Hu, Z. X.; Yang, F.; Ji, W. High-Mobility Transport Anisotropy and Linear Dichroism in Few-Layer Black Phosphorus. *Nat. Commun.* **2014**, *5*, 4475.
(286) Nemilentsau, A.; Low, T.; Hanson, G. Anisotropic 2D Materials for Tunable Hyperbolic Plasmonics. *Phys. Rev. Lett.* **2016**, *116*, 066804.
(287) Xu, Y.; Yuan, J.; Fei, L.; Wang, X.; Bao, Q.; Wang, Y.; Zhang, K.; Zhang, Y. Selenium-Doped Black Phosphorus for High-Responsivity 2D Photodetectors. *Small* **2016**, *12*, 5000−5007.
(288) Wang, J.; Jiang, Y. Infrared Absorber Based on Sandwiched Two-Dimensional Black Phosphorus Metamaterials. *Opt. Express* **2017**, *25*, 5206−5216.
(289) Liu, Z.; Aydin, K. Localized Surface Plasmons in Nanostructured Monolayer Black Phosphorus. *Nano Lett.* **2016**, *16*, 3457−3462.
(290) Wang, X.; Lan, S. Optical Properties of Black Phosphorus. *Adv. Opt. Photonics* **2016**, *8*, 618−655.
(291) Song, X.; Liu, Z.; Xiang, Y.; Aydin, K. Biaxial Hyperbolic Metamaterials Using Anisotropic Few-Layer Black Phosphorus. *Opt. Express* **2018**, *26*, 5469−5469.
(292) Slobozhanyuk, A. P.; Ginzburg, P.; Powell, D. A.; Iorsh, I.; Shalin, A. S.; Segovia, P.; Krasavin, A. V.; Wurtz, G. A.; Podolskiy, V. A.; Belov, P. A.; Zayats, A. V. Purcell Effect in Hyperbolic Metamaterial Resonators. *Phys. Rev. B: Condens. Matter Mater. Phys.* **2015**, *92*, 195127.
(293) Krasnok, A. E.; Slobozhanyuk, A. P.; Simovski, C. R.; Tretyakov, S. A.; Poddubny, A. N.; Miroshnichenko, A. E.; Kivshar, Y. S.; Belov, P. A. An Antenna Model for the Purcell Effect. *Sci. Rep.* **2015**, *5*, 12956.
(294) Purcell, E. M. Spontaneous Emission Probabilities at Radio Frequencies. *NATO ASI Ser., Ser. B* **1946**, *69*, 1946.
(295) Caldwell, J. D.; Glembocki, O. J.; Francescato, Y.; Sharac, N.; Giannini, V.; Bezares, F. J.; Long, J. P.; Owrutsky, J. C.; Vurgaftman, I.; Tischler, J. G.; et al. Low-Loss, Extreme Subdiffraction Photon Confinement Via Silicon Carbide Localized Surface Phonon Polariton Resonators. *Nano Lett.* **2013**, *13*, 3690−3697.
(296) Wang, T.; Li, P.; Hauer, B.; Chigrin, D. N.; Taubner, T. Optical Properties of Single Infrared Resonant Circular Microcavities for Surface Phonon Polaritons. *Nano Lett.* **2013**, *13*, 5051−5055.
(297) Huber, A.; Ocelic, N.; Kazantsev, D.; Hillenbrand, R. Near-Field Imaging of Mid-Infrared Surface Phonon Polariton Propagation. *Appl. Phys. Lett.* **2005**, *87*, 081103.
(298) Giles, A. J.; Dai, S.; Glembocki, O. J.; Kretinin, A. V.; Sun, Z.; Ellis, C. T.; Tischler, J. G.; Taniguchi, T.; Watanabe, K.; Fogler, M. M.; et al. Imaging of Anomalous Internal Reflections of Hyperbolic Phonon-Polaritons in Hexagonal Boron Nitride. *Nano Lett.* **2016**, *16*, 3858−3865.
(299) Xu, X. G.; Ghamsari, B. G.; Jiang, J. H.; Gilburd, L.; Andreev, G. O.; Zhi, C.; Bando, Y.; Golberg, D.; Berini, P.; Walker, G. C. One-Dimensional Surface Phonon Polaritons in Boron Nitride Nanotubes. *Nat. Commun.* **2014**, *5*, 5782.
(300) Brown, L. V.; Davanco, M.; Sun, Z.; Kretinin, A.; Chen, Y.; Matson, J. R.; Vurgaftman, I.; Sharac, N.; Giles, A. J.; Fogler, M. M.; et al. Nanoscale Mapping and Spectroscopy of Nonradiative Hyperbolic Modes in Hexagonal Boron Nitride Nanostructures. *Nano Lett.* **2018**, *18*, 1628−1636.
(301) Wang, T.; Li, P.; Chigrin, D. N.; Giles, A. J.; Bezares, F. J.; Glembocki, O. J.; Caldwell, J. D.; Taubner, T. Phonon-Polaritonic Bowtie Nanoantennas: Controlling Infrared Thermal Radiation at the Nanoscale. *ACS Photonics* **2017**, *4*, 1753−1760.
(302) Ocelic, N.; Hillenbrand, R. Subwavelength-Scale Tailoring of Surface Phonon Polaritons by Focused Ion-Beam Implantation. *Nat. Mater.* **2004**, *3*, 606−609.
(303) Principi, A.; Carrega, M.; Lundeberg, M. B.; Woessner, A.; Koppens, F. H. L.; Vignale, G.; Polini, M. Plasmon Losses Due to Electron-Phonon Scattering: The Case of Graphene Encapsulated in Hexagonal Boron Nitride. *Phys. Rev. B: Condens. Matter Mater. Phys.* **2014**, *90*, 165408.
(304) Xue, J.; Sanchez-Yamagishi, J.; Bulmash, D.; Jacquod, P.; Deshpande, A.; Watanabe, K.; Taniguchi, T.; Jarillo-Herrero, P.; Leroy, B. J. Scanning Tunnelling Microscopy and Spectroscopy of Ultra-Flat Graphene on Hexagonal Boron Nitride. *Nat. Mater.* **2011**, *10*, 282−285.
(305) Wang, L. One-Dimensional Electrical Contact to a Two-Dimensional Material. *Science* **2013**, *342*, 614−617.
(306) Liu, Y.; Willis, R. F. Plasmon-Phonon Strongly-Coupled Mode in Epitaxial Graphene. *Phys. Rev. B: Condens. Matter Mater. Phys.* **2010**, *81*, 081406.

https://dx.doi.org/10.1021/acs.chemrev.9b00592
Chem. Rev. 2020, 120, 6197−6246

(307) Joshi, T.; Kang, J. H.; Jiang, L.; Wang, S.; Tarigo, T.; Lyu, T.; Kahn, S.; Shi, Z.; Shen, Y. R.; Crommie, M. F.; et al. Coupled One-Dimensional Plasmons and Two-Dimensional Phonon Polaritons in Hybrid Silver Nanowire/Silicon Carbide Structures. *Nano Lett.* **2017**, *17*, 3662−3667.
(308) Brar, V. W.; Jang, M. S.; Sherrott, M.; Kim, S.; Lopez, J. J.; Kim, L. B.; Choi, M.; Atwater, H. Hybrid Surface-Phonon-Plasmon Polariton Modes in Graphene/Monolayer H-Bn Heterostructures. *Nano Lett.* **2014**, *14*, 3876−3880.
(309) Kumar, A.; Low, T.; Fung, K. H.; Avouris, P.; Fang, N. X. Tunable Light-Matter Interaction and the Role of Hyperbolicity in Graphene-Hbn System. *Nano Lett.* **2015**, *15*, 3172−3180.
(310) Qu, S.; Liu, H.; Dong, L.; Wu, L.; Ma, C.; Wang, S. Graphene-Hexagonal Boron Nitride Heterostructure as a Tunable Phonon−Plasmon Coupling System. *Crystals* **2017**, *7*, 49−49.
(311) Li, Y.; Yan, H.; Farmer, D. B.; Meng, X.; Zhu, W.; Osgood, R. M.; Heinz, T. F.; Avouris, P. Graphene Plasmon Enhanced Vibrational Sensing of Surface-Adsorbed Layers. *Nano Lett.* **2014**, *14*, 1573−1577.
(312) Guo, Q.; Guinea, F.; Deng, B.; Sarpkaya, I.; Li, C.; Chen, C.; Ling, X.; Kong, J.; Xia, F. Electrothermal Control of Graphene Plasmon−Phonon Polaritons. *Adv. Mater.* **2017**, *29*, 1700566.
(313) Barcelos, I. D.; Cadore, A. R.; Alencar, A. B.; Maia, F. C. B.; Mania, E.; Oliveira, R. F.; Bufon, C. C. B.; Malachias, Â.; Freitas, R. O.; Moreira, R. L.; et al. Infrared Fingerprints of Natural 2D Talc and Plasmon-Phonon Coupling in Graphene-Talc Heterostructures. *ACS Photonics* **2018**, *5*, 1912−1918.
(314) Bezares, F. J.; Sanctis, A. D.; Saavedra, J. R. M.; Woessner, A.; Alonso-González, P.; Amenabar, I.; Chen, J.; Bointon, T. H.; Dai, S.; Fogler, M. M.; et al. Intrinsic Plasmon-Phonon Interactions in Highly Doped Graphene: A near-Field Imaging Study. *Nano Lett.* **2017**, *17*, 5908−5913.
(315) Hwang, E. H.; Sensarma, R.; Sarma, S. D. Plasmon-Phonon Coupling in Graphene. *Phys. Rev. B: Condens. Matter Mater. Phys.* **2010**, *82*, 195406.
(316) Yan, H.; Low, T.; Zhu, W.; Wu, Y.; Freitag, M.; Li, X.; Guinea, F.; Avouris, P.; Xia, F. Damping Pathways of Mid-Infrared Plasmons in Graphene Nanostructures. *Nat. Photonics* **2013**, *7*, 394−399.
(317) Falk, A. L.; Chiu, K.-C.; Farmer, D. B.; Cao, Q.; Tersoff, J.; Lee, Y.-H.; Avouris, P.; Han, S.-J. Coherent Plasmon and Phonon-Plasmon Resonances in Carbon Nanotubes. *Phys. Rev. Lett.* **2017**, *118*, 257401.
(318) Yan, H.; Low, T.; Guinea, F.; Xia, F.; Avouris, P. Tunable Phonon-Induced Transparency in Bilayer Graphene Nanoribbons. *Nano Lett.* **2014**, *14*, 4581−4586.
(319) Hajian, H.; Ghobadi, A.; Dereshgi, S. A.; Butun, B.; Ozbay, E. Hybrid Plasmon−Phonon Polariton Bands in Graphene−Hexagonal Boron Nitride Metamaterials. *J. Opt. Soc. Am. B* **2017**, *34*, D29−D35.
(320) Yu, L.; Huang, Y.; Liu, C.; Hu, F.; Jin, Y.; Yan, Y.; Xu, X. Giant Plasmonic Mode Splitting in Thz Metamaterials Mediated by Coupling with Lorentz Phonon Mode. *Appl. Phys. Lett.* **2018**, *112*, 151101.
(321) Johnson, P. B.; Christy, R.-W. Optical Constants of the Noble Metals. *Phys. Rev. B* **1972**, *6*, 4370.
(322) Shen, J. T.; Catrysse, P. B.; Fan, S. Mechanism for Designing Metallic Metamaterials with a High Index of Refraction. *Phys. Rev. Lett.* **2005**, *94*, 197401.
(323) Garcia-Vidal, F. J.; Martin-Moreno, L.; Ebbesen, T. W.; Kuipers, L. Light Passing through Subwavelength Apertures. *Rev. Mod. Phys.* **2010**, *82*, 729−787.
(324) Huang, B.; Clark, G.; Navarro-Moratalla, E.; Klein, D. R.; Cheng, R.; Seyler, K. L.; Zhong, D.; Schmidgall, E.; McGuire, M. A.; Cobden, D. H.; et al. Layer-Dependent Ferromagnetism in a Van Der Waals Crystal Down to the Monolayer Limit. *Nature* **2017**, *546*, 270−273.
(325) Fei, Z.; Goldflam, M. D.; Wu, J. S.; Dai, S.; Wagner, M.; McLeod, A. S.; Liu, M. K.; Post, K. W.; Zhu, S.; Janssen, G. C. A. M.; et al. Edge and Surface Plasmons in Graphene Nanoribbons. *Nano Lett.* **2015**, *15*, 8271−8276.
(326) Hu, F.; Luan, Y.; Fei, Z.; Palubski, I. Z.; Goldflam, M. D.; Dai, S.; Wu, J. S.; Post, K. W.; Janssen, G.; Fogler, M. M.; et al. Imaging the Localized Plasmon Resonance Modes in Graphene Nanoribbons. *Nano Lett.* **2017**, *17*, 5423−5428.
(327) Rodrigo, D.; Limaj, O.; Janner, D.; Etezadi, D.; de Abajo, F. J. G.; Pruneri, V.; Altug, H. Mid-Infrared Plasmonic Biosensing with Graphene. *Science* **2015**, *349*, 165−168.
(328) Di Pietro, P.; Ortolani, M.; Limaj, O.; Di Gaspare, A.; Giliberti, V.; Giorgianni, F.; Brahlek, M.; Bansal, N.; Koirala, N.; Oh, S.; Calvani, P.; Lupi, S.; et al. Observation of Dirac Plasmons in a Topological Insulator. *Nat. Nanotechnol.* **2013**, *8*, 556−560.
(329) Jia, Y.; Zhao, H.; Guo, Q.; Wang, X.; Wang, H.; Xia, F. Tunable Plasmon−Phonon Polaritons in Layered Graphene−Hexagonal Boron Nitride Heterostructures. *ACS Photonics* **2015**, *2*, 907−912.
(330) Yan, H.; Li, X.; Chandra, B.; Tulevski, G.; Wu, Y.; Freitag, M.; Zhu, W.; Avouris, P.; Xia, F. Tunable Infrared Plasmonic Devices Using Graphene/Insulator Stacks. *Nat. Nanotechnol.* **2012**, *7*, 330−334.
(331) Caldwell, J. D.; Novoselov, K. S. Van der Waals Heterostructures: Mid-Infrared Nanophotonics. *Nat. Mater.* **2015**, *14*, 364−366.
(332) Thongrattanasiri, S.; Koppens, F. H.; De Abajo, F. J. G. Complete Optical Absorption in Periodically Patterned Graphene. *Phys. Rev. Lett.* **2012**, *108*, 047401.
(333) Yan, H.; Xia, F.; Li, Z.; Avouris, P. Plasmonics of Coupled Graphene Micro-Structures. *New J. Phys.* **2012**, *14*, 125001.
(334) Fang, Z.; Wang, Y.; Schlather, A. E.; Liu, Z.; Ajayan, P. M.; García de Abajo, F. J.; Nordlander, P.; Zhu, X.; Halas, N. J. Active Tunable Absorption Enhancement with Graphene Nanodisk Arrays. *Nano Lett.* **2014**, *14*, 299−304.
(335) Fang, Z.; Thongrattanasiri, S.; Schlather, A.; Liu, Z.; Ma, L.; Wang, Y.; Ajayan, P. M.; Nordlander, P.; Halas, N. J.; García de Abajo, F. J. Gated Tunability and Hybridization of Localized Plasmons in Nanostructured Graphene. *ACS Nano* **2013**, *7*, 2388−2395.
(336) Zhang, K.; Yap, F. L.; Li, K.; Ng, C. T.; Li, L. J.; Loh, K. P. Large Scale Graphene/Hexagonal Boron Nitride Heterostructure for Tunable Plasmonics. *Adv. Funct. Mater.* **2014**, *24*, 731−738.
(337) Kong, X.-T.; Khan, A. A.; Kidambi, P. R.; Deng, S.; Yetisen, A. K.; Dlubak, B.; Hiralal, P.; Montelongo, Y.; Bowen, J.; Xavier, S.; Jiang, K.; Amaratunga, G. A. J.; Hofmann, S.; Wilkinson, T. D.; Dai, Q.; Butt, H. Graphene-Based Ultrathin Flat Lenses. *ACS Photonics* **2015**, *2*, 200−207.
(338) Fan, S.; Joannopoulos, J. D. Analysis of Guided Resonances in Photonic Crystal Slabs. *Phys. Rev. B: Condens. Matter Mater. Phys.* **2002**, *65*, 235112.
(339) Pan, D.; Yu, R.; Xu, H.; Garcia de Abajo, F. J. Topologically Protected Dirac Plasmons in a Graphene Superlattice. *Nat. Commun.* **2017**, *8*, 1243.
(340) Jin, D.; Christensen, T.; Soljacic, M.; Fang, N. X.; Lu, L.; Zhang, X. Infrared Topological Plasmons in Graphene. *Phys. Rev. Lett.* **2017**, *118*, 245301.
(341) Alfaro-Mozaz, F. J.; Rodrigo, S. G.; Alonso-Gonzalez, P.; Velez, S.; Dolado, I.; Casanova, F.; Hueso, L. E.; Martin-Moreno, L.; Hillenbrand, R.; Nikitin, A. Y. Deeply Subwavelength Phonon-Polaritonic Crystal Made of a Van der Waals Material. *Nat. Commun.* **2019**, *10*, 42.
(342) Soukoulis, C. M.; Wegener, M. Past Achievements and Future Challenges in the Development of Three-Dimensional Photonic Metamaterials. *Nat. Photonics* **2011**, *5*, 523−530.
(343) Klein, M. W.; Enkrich, C.; Wegener, M.; Linden, S. Second-Harmonic Generation from Magnetic Metamaterials. *Science* **2006**, *313*, 502−504.
(344) Shen, N. H.; Tassin, P.; Koschny, T.; Soukoulis, C. M. Comparison of Gold- and Graphene-Based Resonant Nanostructures for Terahertz Metamaterials and an Ultrathin Graphene-Based Modulator. *Phys. Rev. B: Condens. Matter Mater. Phys.* **2014**, *90*, 115437.

https://dx.doi.org/10.1021/acs.chemrev.9b00592
Chem. Rev. 2020, 120, 6197−6246

(345) Wang, J.; Lu, W. B.; Li, X. B.; Gu, X. F.; Dong, Z. G. Plasmonic Metamaterial Based on the Complementary Split Ring Resonators Using Graphene. *J. Phys. D: Appl. Phys.* **2014**, *47*, 325102.
(346) He, X. Y. Tunable Terahertz Graphene Metamaterials. *Carbon* **2015**, *82*, 229−237.
(347) Zouaghi, W.; Voss, D.; Gorath, M.; Nicoloso, N.; Roskos, H. G. How Good Would the Conductivity of Graphene Have to Be to Make Single-Layer-Graphene Metamaterials for Terahertz Frequencies Feasible? *Carbon* **2015**, *94*, 301−308.
(348) Fan, Y.; Wei, Z.; Zhang, Z.; Li, H. Enhancing Infrared Extinction and Absorption in a Monolayer Graphene Sheet by Harvesting the Electric Dipolar Mode of Split Ring Resonators. *Opt. Lett.* **2013**, *38*, 5410−5413.
(349) Zhang, Q. F.; Ma, Q. X.; Yan, S. T.; Wu, F. M.; He, X. J.; Jiang, J. X. Tunable Terahertz Absorption in Graphene-Based Metamaterial. *Opt. Commun.* **2015**, *353*, 70−75.
(350) Wu, P. C.; Papasimakis, N.; Tsai, D. P. Self-Affine Graphene Metasurfaces for Tunable Broadband Absorption. *Phys. Rev. Appl.* **2016**, *6*, 044019.
(351) Liu, L.; Chen, J.; Zhou, Z.; Yi, Z.; Ye, X. Tunable Absorption Enhancement in Electric Split-Ring Resonators-Shaped Graphene Arrays. *Mater. Res. Express* **2018**, *5*, 045802.
(352) Papasimakis, N.; Thongrattanasiri, S.; Zheludev, N. I.; García de Abajo, F. J. The Magnetic Response of Graphene Split-Ring Metamaterials. *Light: Sci. Appl.* **2013**, *2*, No. e78.
(353) Shi, X.; Han, D.; Dai, Y.; Yu, Z.; Sun, Y.; Chen, H.; Liu, X.; Zi, J. Plasmonic Analog of Electromagnetically Induced Transparency in Nanostructure Graphene. *Opt. Express* **2013**, *21*, 28438−28443.
(354) Lu, W. B.; Liu, J. L.; Zhang, J.; Wang, J.; Liu, Z. G. Polarization-Independent Transparency Window Induced by Complementary Graphene Metasurfaces. *J. Phys. D: Appl. Phys.* **2017**, *50*, 015106.
(355) Gao, Y.; Ren, G.; Zhu, B.; Huang, L.; Li, H.; Yin, B.; Jian, S. Tunable Plasmonic Filter Based on Graphene Split-Ring. *Plasmonics* **2016**, *11*, 291−296.
(356) Hu, X.; Wang, J. High-Speed Gate-Tunable Terahertz Coherent Perfect Absorption Using a Split-Ring Graphene. *Opt. Lett.* **2015**, *40*, 5538−5541.
(357) He, X. J.; Zhang, Q. F.; Lu, G. J.; Ying, G. B.; Wu, F. M.; Jiang, J. X. Tunable Ultrasensitive Terahertz Sensor Based on Complementary Graphene Metamaterials. *RSC Adv.* **2016**, *6*, 52212−52218.
(358) Tang, W. W.; Wang, L.; Chen, X. S.; Liu, C. L.; Yu, A. Q.; Lu, W. Dynamic Metamaterial Based on the Graphene Split Ring High-Q Fano-Resonnator for Sensing Applications. *Nanoscale* **2016**, *8*, 15196−15204.
(359) Liu, Y.; Huang, Y.; Duan, X. Van Der Waals Integration before and Beyond Two-Dimensional Materials. *Nature* **2019**, *567*, 323−333.
(360) Liu, Y.; Weiss, N. O.; Duan, X.; Cheng, H.-C.; Huang, Y.; Duan, X. Van Der Waals Heterostructures and Devices. *Nat. Rev. Mater.* **2016**, *1*, 16042.
(361) Caldwell, J. D.; Vurgaftman, I.; Tischler, J. G.; Glembocki, O. J.; Owrutsky, J. C.; Reinecke, T. L. Atomic-Scale Photonic Hybrids for Mid-Infrared and Terahertz Nanophotonics. *Nat. Nanotechnol.* **2016**, *11*, 9−15.
(362) Chaudhary, K.; Tamagnone, M.; Rezaee, M.; Bediako, D. K.; Ambrosio, A.; Kim, P.; Capasso, F. Engineering Phonon Polaritons in Van Der Waals Heterostructures to Enhance in-Plane Optical Anisotropy. *Sci. Adv.* **2019**, *5*, No. eaau7171.
(363) Chenet, D. A.; Aslan, O. B.; Huang, P. Y.; Fan, C.; van der Zande, A. M.; Heinz, T. F.; Hone, J. C. In-Plane Anisotropy in Mono- and Few-Layer Res2 Probed by Raman Spectroscopy and Scanning Transmission Electron Microscopy. *Nano Lett.* **2015**, *15*, 5667−5672.
(364) Ni, G. X.; Wang, H.; Wu, J. S.; Fei, Z.; Goldflam, M. D.; Keilmann, F.; Ozyilmaz, B.; Castro Neto, A. H.; Xie, X. M.; Fogler, M. M.; Basov, D. N. Plasmons in Graphene Moire Superlattices. *Nat. Mater.* **2015**, *14*, 1217−1222.
(365) Li, Z.; Liu, C.; Rong, X.; Luo, Y.; Cheng, H.; Zheng, L.; Lin, F.; Shen, B.; Gong, Y.; Zhang, S.; et al. Tailoring Mos2 Valley-Polarized Photoluminescence with Super Chiral near-Field. *Adv. Mater.* **2018**, *30*, 1801908.
(366) Marqués, R.; Medina, F.; Rafii-El-Idrissi, R. Role of Bianisotropy in Negative Permeability and Left-Handed Metamaterials. *Phys. Rev. B: Condens. Matter Mater. Phys.* **2002**, *65*, 144440.
(367) Ziolkowski, R. W. Design, Fabrication, and Testing of Double Negative Metamaterials. *IEEE Trans. Antennas Propag.* **2003**, *51*, 1516−1529.
(368) Lim, S.; Caloz, C.; Itoh, T. Electronically Scanned Composite Right/Left Handed Microstrip Leaky-Wave Antenna. *IEEE Micro. Wirel. Co.* **2004**, *14*, 277−279.
(369) Arnedo, I.; Illescas, J.; Flores, M.; Lopetegi, T.; Laso, M.A.G.; Falcone, F.; Bonache, J.; Garcia-Garcia, J.; Martin, F.; Marcotegui, J.A.; Marques, R.; Sorolla, M. Forward and Backward Leaky Wave Radiation in Split-Ring-Resonator-Based Metamaterials. *IET Microw. Antenna P.* **2007**, *1*, 65−68.
(370) Antoniades, M. A.; Eleftheriades, G. V. A Broadband Series Power Divider Using Zero-Degree Metamaterial Phase-Shifting Lines. *IEEE Micro. Wirel. Co.* **2005**, *15*, 808−810.
(371) Martın, F.; Bonache, J.; Falcone, F. a.; Sorolla, M.; Marqués, R. Split Ring Resonator-Based Left-Handed Coplanar Waveguide. *Appl. Phys. Lett.* **2003**, *83*, 4652.
(372) Falcone, F.; Martin, F.; Bonache, J.; Marqués, R.; Sorolla, M. Coplanar Waveguide Structures Loaded with Split-Ring Resonators. *Microw. Opt. Techn. Lett.* **2004**, *40*, 3−6.
(373) Chen, H. T.; Padilla, W. J.; Zide, J. M. O.; Gossard, A. C.; Taylor, A. J.; Averitt, R. D. Active Terahertz Metamaterial Devices. *Nature* **2006**, *444*, 597−600.
(374) Chen, H.-T.; Padilla, W. J.; Cich, M. J.; Azad, A. K.; Averitt, R. D.; Taylor, A. J. A Metamaterial Solid-State Terahertz Phase Modulator. *Nat. Photonics* **2009**, *3*, 148−151.
(375) Yan, R.; Sensale-Rodriguez, B.; Liu, L.; Jena, D.; Xing, H. G. A New Class of Electrically Tunable Metamaterial Terahertz Modulators. *Opt. Express* **2012**, *20*, 28664−28671.
(376) Vasić, B.; Jakovljević, M. M.; Isić, G.; Gajić, R. Tunable Metamaterials Based on Split Ring Resonators and Doped Graphene. *Appl. Phys. Lett.* **2013**, *103*, 011102.
(377) Valmorra, F.; Scalari, G.; Maissen, C.; Fu, W. Y.; Schonenberger, C.; Choi, J. W.; Park, H. G.; Beck, M.; Faist, J. Low-Bias Active Control of Terahertz Waves by Coupling Large-Area Cvd Graphene to a Terahertz Metamaterial. *Nano Lett.* **2013**, *13*, 3193−3198.
(378) Degl'Innocenti, R.; Jessop, D. S.; Shah, Y. D.; Sibik, J.; Zeitler, J. A.; Kidambi, P. R.; Hofmann, S.; Beere, H. E.; Ritchie, D. A. Low-Bias Terahertz Amplitude Modulator Based on Split-Ring Resonators and Graphene. *ACS Nano* **2014**, *8*, 2548−2554.
(379) Smirnova, D. A.; Miroshnichenko, A. E.; Kivshar, Y. S.; Khanikaev, A. B. Tunable Nonlinear Graphene Metasurfaces. *Phys. Rev. B: Condens. Matter Mater. Phys.* **2015**, *92*, 161406.
(380) Li, Q.; Cong, L. Q.; Singh, R. J.; Xu, N. N.; Cao, W.; Zhang, X. Q.; Tian, Z.; Du, L. L.; Han, J. G.; Zhang, W. L. Monolayer Graphene Sensing Enabled by the Strong Fano-Resonant Metasurface. *Nanoscale* **2016**, *8*, 17278−17284.
(381) Xiao, S.; Wang, T.; Jiang, X.; Yan, X.; Cheng, L.; Wang, B.; Xu, C. Strong Interaction between Graphene Layer and Fano Resonance in Terahertz Metamaterials. *J. Phys. D: Appl. Phys.* **2017**, *50*, 195101.
(382) Sarau, G.; Lahiri, B.; Banzer, P.; Gupta, P.; Bhattacharya, A.; Vollmer, F.; Christiansen, S. Enhanced Raman Scattering of Graphene Using Arrays of Split Ring Resonators. *Adv. Opt. Mater.* **2013**, *1*, 151−157.
(383) Dai, Z.; Mei, F.; Xiao, X.; Liao, L.; Wu, W.; Zhang, Y.; Ying, J.; Wang, L.; Ren, F.; Jiang, C. Monolayer Graphene on Nanostructured Ag for Enhancement of Surface-Enhanced Raman Scattering Stable Platform. *Nanotechnology* **2015**, *26*, 125603.
(384) Li, Q.; Tian, Z.; Zhang, X. Q.; Xu, N. N.; Singh, R. J.; Gu, J. Q.; Lv, P.; Luo, L. B.; Zhang, S.; Han, J. G.; et al. Dual Control of Active Graphene-Silicon Hybrid Metamaterial Devices. *Carbon* **2015**, *90*, 146−153.

https://dx.doi.org/10.1021/acs.chemrev.9b00592
Chem. Rev. 2020, 120, 6197−6246

(385) Liu, P. Q.; Luxmoore, I. J.; Mikhailov, S. A.; Savostianova, N. A.; Valmorra, F.; Faist, J.; Nash, G. R. Highly Tunable Hybrid Metamaterials Employing Split-Ring Resonators Strongly Coupled to Graphene Surface Plasmons. *Nat. Commun.* **2015**, *6*, 8969.
(386) Hosseinbeig, A.; Pirooj, A.; Zarrabi, F. B. A Reconfigurable Subwavelength Plasmonic Fano Nano-Antenna Based on Split Ring Resonator. *J. Magn. Magn. Mater.* **2017**, *423*, 203−207.
(387) Zhao, X. L.; Yuan, C.; Lv, W. H.; Xu, S. L.; Yao, J. Q. Plasmon-Induced Transparency in Metamaterial Based on Graphene and Split-Ring Resonators. *IEEE Photonics Technol. Lett.* **2015**, *27*, 1321−1324.
(388) He, X. J.; Yang, X. Y.; Li, S. P.; Shi, S.; Wu, F. M.; Jiang, J. X. Electrically Active Manipulation of Electromagnetic Induced Transparency in Hybrid Terahertz Metamaterial. *Opt. Mater. Express* **2016**, *6*, 3075−3085.
(389) Jadidi, M. M.; Sushkov, A. B.; Myers-Ward, R. L.; Boyd, A. K.; Daniels, K. M.; Gaskill, D. K.; Fuhrer, M. S.; Drew, H. D.; Murphy, T. E. Tunable Terahertz Hybrid Metal-Graphene Plasmons. *Nano Lett.* **2015**, *15*, 7099−7104.
(390) Miao, Z. Q.; Wu, Q.; Li, X.; He, Q.; Ding, K.; An, Z. H.; Zhang, Y. B.; Zhou, L. Widely Tunable Terahertz Phase Modulation with Gate-Controlled Graphene Metasurfaces. *Phys. Rev. X* **2015**, *5*, 041027.
(391) Mousavi, S. H.; Kholmanov, I.; Alici, K. B.; Purtseladze, D.; Arju, N.; Tatar, K.; Fozdar, D. Y.; Suk, J. W.; Hao, Y. F.; Khanikaev, A. B.; et al. Inductive Tuning of Fano-Resonant Metasurfaces Using Plasmonic Response of Graphene in the Mid-Infrared. *Nano Lett.* **2013**, *13*, 1111−1117.
(392) Li, Z.; Li, Y.; Han, T.; Wang, X.; Yu, Y.; Tay, B.; Liu, Z.; Fang, Z. Tailoring MoS_2 Exciton-Plasmon Interaction by Optical Spin-Orbit Coupling. *ACS Nano* **2017**, *11*, 1165−1171.
(393) Chen, J. W.; Wang, K.; Long, H.; Han, X. B.; Hu, H. B.; Liu, W. W.; Wang, B.; Lu, P. X. Tungsten Disulfide-Gold Nanohole Hybrid Metasurfaces for Nonlinear Metalenses in the Visible Region. *Nano Lett.* **2018**, *18*, 1344−1350.
(394) Liu, J.-T.; Liu, N.-H.; Li, J.; Jing Li, X.; Huang, J.-H. Enhanced Absorption of Graphene with One-Dimensional Photonic Crystal. *Appl. Phys. Lett.* **2012**, *101*, 052104.
(395) Zhao, B.; Zhang, Z. M. M. Strong Plasmonic Coupling between Graphene Ribbon Array and Metal Gratings. *ACS Photonics* **2015**, *2*, 1611−1618.
(396) Gao, W.; Shi, G.; Jin, Z.; Shu, J.; Zhang, Q.; Vajtai, R.; Ajayan, P. M.; Kono, J.; Xu, Q. Excitation and Active Control of Propagating Surface Plasmon Polaritons in Graphene. *Nano Lett.* **2013**, *13*, 3698−3702.
(397) Gao, W.; Shu, J.; Qiu, C.; Xu, Q. Excitation of Plasmonic Waves in Graphene by Guided-Mode Resonances. *ACS Nano* **2012**, *6*, 7806−7813.
(398) Tang, L.; Shi, H.; Yang, J.; Du, C.; Gao, F.; Zhu, J.; Du, J. Complete Optical Absorption in Graphene by Using Nano-Gratings to Excite Graphene Surface Plasmons. *Microelectron. Eng.* **2015**, *145*, 58−61.
(399) Kumar, M.; Tervo, J.; Kaplas, T.; Svirko, Y. Graphene-Enhanced Waveguide-Resonance Gratings. *J. Nanophotonics* **2016**, *10*, 012518.
(400) Chen, C.; Youngblood, N.; Peng, R.; Yoo, D.; Mohr, D. A.; Johnson, T. W.; Oh, S. H.; Li, M. Three-Dimensional Integration of Black Phosphorus Photodetector with Silicon Photonics and Nanoplasmonics. *Nano Lett.* **2017**, *17*, 985−991.
(401) Wu, S.; Buckley, S.; Schaibley, J. R.; Feng, L.; Yan, J.; Mandrus, D. G.; Hatami, F.; Yao, W.; Vuckovic, J.; Majumdar, A.; et al. Monolayer Semiconductor Nanocavity Lasers with Ultralow Thresholds. *Nature* **2015**, *520*, 69−72.
(402) Chang, Y. C.; Liu, C. H.; Liu, C. H.; Zhang, S. Y.; Marder, S. R.; Narimanov, E. E.; Zhong, Z. H.; Norris, T. B. Realization of Mid-Infrared Graphene Hyperbolic Metamaterials. *Nat. Commun.* **2016**, *7*, 10568.
(403) Wu, S.; Buckley, S.; Jones, A. M.; Ross, J. S.; Ghimire, N. J.; Yan, J.; Mandrus, D. G.; Yao, W.; Hatami, F.; Vučković, J.; et al. Control of Two-Dimensional Excitonic Light Emission Via Photonic Crystal. *2D Mater.* **2014**, *1*, 011001.
(404) Gan, X.; Gao, Y.; Fai Mak, K.; Yao, X.; Shiue, R.-J.; van der Zande, A.; Trusheim, M. E.; Hatami, F.; Heinz, T. F.; Hone, J.; Englund, D. Controlling the Spontaneous Emission Rate of Monolayer MoS_2 in a Photonic Crystal Nanocavity. *Appl. Phys. Lett.* **2013**, *103*, 181119.
(405) Song, J.; Zhang, L.; Xue, Y.; Wu, Q. Y. S.; Xia, F.; Zhang, C.; Zhong, Y.-L.; Zhang, Y.; Teng, J.; Premaratne, M.; et al. Efficient Excitation of Multiple Plasmonic Modes on Three-Dimensional Graphene: An Unexplored Dimension. *ACS Photonics* **2016**, *3*, 1986−1992.
(406) Wu, C. H.; Arju, N.; Kelp, G.; Fan, J. A.; Dominguez, J.; Gonzales, E.; Tutuc, E.; Brener, I.; Shvets, G. Spectrally Selective Chiral Silicon Metasurfaces Based on Infrared Fano Resonances. *Nat. Commun.* **2014**, *5*, 3892.
(407) Limonov, M. F.; Rybin, M. V.; Poddubny, A. N.; Kivshar, Y. S. Fano Resonances in Photonics. *Nat. Photonics* **2017**, *11*, 543−554.
(408) Argyropoulos, C. Enhanced Transmission Modulation Based on Dielectric Metasurfaces Loaded with Graphene. *Opt. Express* **2015**, *23*, 23787−23797.
(409) Liu, C.; Bai, Y.; Zhou, J.; Zhao, Q.; Qiao, L. Large-Scale Modulation of Left-Handed Passband in Hybrid Graphene/Dielectric Metasurface. *Ann. Phys. (Berlin, Ger.)* **2017**, *529*, 1700125.
(410) Liu, C.; Bai, Y.; Zhou, J.; Zhao, Q.; Qiao, L. A Review of Graphene Plasmons and Its Combination with Metasurface. *Han'guk Seramik Hakhoechi* **2017**, *54*, 349−365.
(411) Liu, Z. W.; Lee, H.; Xiong, Y.; Sun, C.; Zhang, X. Far-Field Optical Hyperlens Magnifying Sub-Diffraction-Limited Objects. *Science* **2007**, *315*, 1686−1686.
(412) Tumkur, T.; Zhu, G.; Black, P.; Barnakov, Y. A.; Bonner, C.; Noginov, M. Control of Spontaneous Emission in a Volume of Functionalized Hyperbolic Metamaterial. *Appl. Phys. Lett.* **2011**, *99*, 151115.
(413) Rho, J.; Ye, Z. L.; Xiong, Y.; Yin, X. B.; Liu, Z. W.; Choi, H.; Bartal, G.; Zhang, X. A. Spherical Hyperlens for Two-Dimensional Sub-Diffractional Imaging at Visible Frequencies. *Nat. Commun.* **2010**, *1*, 143.
(414) Fan, Y.; Wei, Z.; Li, H.; Chen, H.; Soukoulis, C. M. Photonic Band Gap of a Graphene-Embedded Quarter-Wave Stack. *Phys. Rev. B: Condens. Matter Mater. Phys.* **2013**, *88*, 241403.
(415) Yu, N.; Capasso, F. Flat Optics with Designer Metasurfaces. *Nat. Mater.* **2014**, *13*, 139−150.
(416) Zhang, L.; Mei, S. T.; Huang, K.; Qiu, C. W. Advances in Full Control of Electromagnetic Waves with Metasurfaces. *Adv. Opt. Mater.* **2016**, *4*, 818−833.
(417) Li, P.; Taubner, T. Broadband Subwavelength Imaging Using a Tunable Graphene-Lens. *ACS Nano* **2012**, *6*, 10107−10114.
(418) Zheng, Z.; Chen, J.; Wang, Y.; Wang, X.; Chen, X.; Liu, P.; Xu, J.; Xie, W.; Chen, H.; Deng, S.; et al. Highly Confined and Tunable Hyperbolic Phonon Polaritons in Van der Waals Semiconducting Transition Metal Oxides. *Adv. Mater.* **2018**, *30*, 1705318.
(419) Li, P.; Lewin, M.; Kretinin, A. V.; Caldwell, J. D.; Novoselov, K. S.; Taniguchi, T.; Watanabe, K.; Gaussmann, F.; Taubner, T. Hyperbolic Phonon-Polaritons in Boron Nitride for near-Field Optical Imaging and Focusing. *Nat. Commun.* **2015**, *6*, 7507.
(420) Ni, X.; Wong, Z. J.; Mrejen, M.; Wang, Y.; Zhang, X. An Ultrathin Invisibility Skin Cloak for Visible Light. *Science* **2015**, *349*, 1310−1314.
(421) Chen, P.-Y.; Alù, A. Atomically Thin Surface Cloak Using Graphene Monolayers. *ACS Nano* **2011**, *5*, 5855−5863.
(422) Chen, P. Y.; Soric, J.; Padooru, Y. R.; Bernety, H. M.; Yakovlev, A. B.; Alu, A. Nanostructured Graphene Metasurface for Tunable Terahertz Cloaking. *New J. Phys.* **2013**, *15*, 123029.
(423) Alù, A. Mantle Cloak: Invisibility Induced by a Surface. *Phys. Rev. B: Condens. Matter Mater. Phys.* **2009**, *80*, 245115.
(424) Da, H.; Bao, Q.; Sanaei, R.; Teng, J.; Loh, K. P.; Garcia-Vidal, F. J.; Qiu, C.-W. Monolayer Graphene Photonic Metastructures:

https://dx.doi.org/10.1021/acs.chemrev.9b00592
Chem. Rev. 2020, 120, 6197−6246

Giant Faraday Rotation and Nearly Perfect Transmission. *Phys. Rev. B: Condens. Matter Mater. Phys.* **2013**, *88*, 205405.
(425) Alzetta, G. Induced Transparency. *Phys. Today* **1997**, *50*, 36−42.
(426) Boller, K.-J.; Imamoğlu, A.; Harris, S. E. Observation of Electromagnetically Induced Transparency. *Phys. Rev. Lett.* **1991**, *66*, 2593.
(427) Zhao, X. L.; Yuan, C.; Zhu, L.; Yao, J. Q. Graphene-Based Tunable Terahertz Plasmon-Induced Transparency Metamaterial. *Nanoscale* **2016**, *8*, 15273−15280.
(428) Liu, J. Q.; Zhou, Y. X.; Li, L.; Wang, P.; Zayats, A. V. Controlling Plasmon-Induced Transparency of Graphene Metamolecules with External Magnetic Field. *Opt. Express* **2015**, *23*, 12524−12532.
(429) Lu, C. C.; Hu, X. Y.; Shi, K. B.; Hu, Q.; Zhu, R.; Yang, H.; Gong, Q. H. An Actively Ultrafast Tunable Giant Slow-Light Effect in Ultrathin Nonlinear Metasurfaces. *Light: Sci. Appl.* **2015**, *4*, No. e302.
(430) Crassee, I.; Levallois, J.; Walter, A. L.; Ostler, M.; Bostwick, A.; Rotenberg, E.; Seyller, T.; van der Marel, D.; Kuzmenko, A. B. Giant Faraday Rotation in Single- and Multilayer Graphene. *Nat. Phys.* **2011**, *7*, 48−51.
(431) Standley, B.; Bao, W.; Zhang, H.; Bruck, J.; Lau, C. N.; Bockrath, M. Graphene-Based Atomic-Scale Switches. *Nano Lett.* **2008**, *8*, 3345−3349.
(432) Yao, Y.; Shankar, R.; Kats, M. A.; Song, Y.; Kong, J.; Loncar, M.; Capasso, F. Electrically Tunable Metasurface Perfect Absorbers for Ultrathin Mid-Infrared Optical Modulators. *Nano Lett.* **2014**, *14*, 6526−6532.
(433) Chang, Y. C.; Kildishev, A. V.; Narimanov, E. E.; Norris, T. B. Metasurface Perfect Absorber Based on Guided Resonance of a Photonic Hypercrystal. *Phys. Rev. B: Condens. Matter Mater. Phys.* **2016**, *94*, 155430.
(434) Song, S. C.; Chen, Q.; Jin, L.; Sun, F. H. Great Light Absorption Enhancement in a Graphene Photodetector Integrated with a Metamaterial Perfect Absorber. *Nanoscale* **2013**, *5*, 9615−9619.
(435) Jia, X. L.; Wang, X. O.; Yuan, C. X.; Meng, Q. X.; Zhou, Z. X. Novel Dynamic Tuning of Broadband Visible Metamaterial Perfect Absorber Using Graphene. *J. Appl. Phys.* **2016**, *120*, 033101.
(436) Cai, Y. J.; Zhu, J. F.; Liu, Q. H. Tunable Enhanced Optical Absorption of Graphene Using Plasmonic Perfect Absorbers. *Appl. Phys. Lett.* **2015**, *106*, 043105.
(437) Alaee, R.; Farhat, M.; Rockstuhl, C.; Lederer, F. A Perfect Absorber Made of a Graphene Micro-Ribbon Metamaterial. *Opt. Express* **2012**, *20*, 28017−28024.
(438) Salisbury, W. W. Absorbent Body for Electromagnetic Waves. U.S. Patent 2,599,944, Jun 10, 1952.
(439) Yao, G.; Ling, F. R.; Yue, J.; Luo, C. Y.; Ji, J.; Yao, J. Q. Dual-Band Tunable Perfect Metamaterial Absorber in the Thz Range. *Opt. Express* **2016**, *24*, 1518−1527.
(440) Xia, S.-X.; Zhai, X.; Huang, Y.; Liu, J.-Q.; Wang, L.-L.; Wen, S.-C. Multi-Band Perfect Plasmonic Absorptions Using Rectangular Graphene Gratings. *Opt. Lett.* **2017**, *42*, 3052−3055.
(441) Zhang, L.; Dong, Z.; Wang, Y. M.; Liu, Y. J.; Zhang, S.; Yang, J. K. W.; Qiu, C.-W. Dynamically Configurable Hybridization of Plasmon Modes in Nanoring Dimer Arrays. *Nanoscale* **2015**, *7*, 12018−12022.
(442) Grigorenko, A. N.; Polini, M.; Novoselov, K. S. Graphene Plasmonics. *Nat. Photonics* **2012**, *6*, 749−758.
(443) Wu, J. P.; Jiang, L. Y.; Guo, J.; Dai, X. Y.; Xiang, Y. J.; Wen, S. C. Tunable Perfect Absorption at Infrared Frequencies by a Graphene-Hbn Hyper Crystal. *Opt. Express* **2016**, *24*, 17103−17114.
(444) Nefedov, I. S; Valagiannopoulos, C. A; Melnikov, L. A Perfect Absorption in Graphene Multilayers. *J. Opt.* **2013**, *15*, 114003.
(445) Baranov, D. G.; Edgar, J. H.; Hoffman, T.; Bassim, N.; Caldwell, J. D. Perfect Interferenceless Absorption at Infrared Frequencies by a Van Der Waals Crystal. *Phys. Rev. B: Condens. Matter Mater. Phys.* **2015**, *92*, 201405.
(446) Vicarelli, L.; Vitiello, M. S.; Coquillat, D.; Lombardo, A.; Ferrari, A. C.; Knap, W.; Polini, M.; Pellegrini, V.; Tredicucci, A. Graphene Field-Effect Transistors as Room-Temperature Terahertz Detectors. *Nat. Mater.* **2012**, *11*, 865−871.
(447) Wang, J.; Han, J.; Chen, X.; Wang, X. Design Strategies for Two-Dimensional Material Photodetectors to Enhance Device Performance. *InfoMat* **2019**, *1*, 33−53.
(448) Cai, X.; Sushkov, A. B.; Suess, R. J.; Jadidi, M. M.; Jenkins, G. S.; Nyakiti, L. O.; Myers-Ward, R. L.; Li, S.; Yan, J.; Gaskill, D. K.; et al. Sensitive Room-Temperature Terahertz Detection Via the Photothermoelectric Effect in Graphene. *Nat. Nanotechnol.* **2014**, *9*, 814−819.
(449) Echtermeyer, T. J.; Britnell, L.; Jasnos, P. K.; Lombardo, A.; Gorbachev, R. V.; Grigorenko, A. N.; Geim, A. K.; Ferrari, A. C.; Novoselov, K. S. Strong Plasmonic Enhancement of Photovoltage in Graphene. *Nat. Commun.* **2011**, *2*, 458.
(450) Liu, Y.; Cheng, R.; Liao, L.; Zhou, H.; Bai, J.; Liu, G.; Liu, L.; Huang, Y.; Duan, X. Plasmon Resonance Enhanced Multicolour Photodetection by Graphene. *Nat. Commun.* **2011**, *2*, 579.
(451) Fang, J. R.; Wang, D.; DeVault, C. T.; Chung, T. F.; Chen, Y. P.; Boltasseva, A.; Shalaev, V. M.; Kildishev, A. V. Enhanced Graphene Photodetector with Fractal Metasurface. *Nano Lett.* **2017**, *17*, 57−62.
(452) Wang, W.; Klots, A.; Prasai, D.; Yang, Y.; Bolotin, K. I.; Valentine, J. Hot Electron-Based near-Infrared Photodetection Using Bilayer MoS_2. *Nano Lett.* **2015**, *15*, 7440−7444.
(453) Dai, M.; Chen, H.; Feng, R.; Feng, W.; Hu, Y.; Yang, H.; Liu, G.; Chen, X.; Zhang, J.; Xu, C. Y.; et al. A Dual-Band Multilayer Inse Self-Powered Photodetector with High Performance Induced by Surface Plasmon Resonance and Asymmetric Schottky Junction. *ACS Nano* **2018**, *12*, 8739−8747.
(454) Venuthurumilli, P. K.; Ye, P. D.; Xu, X. Plasmonic Resonance Enhanced Polarization-Sensitive Photodetection by Black Phosphorus in near Infrared. *ACS Nano* **2018**, *12*, 4861−4867.
(455) Miao, J.; Hu, W.; Jing, Y.; Luo, W.; Liao, L.; Pan, A.; Wu, S.; Cheng, J.; Chen, X.; Lu, W. Surface Plasmon-Enhanced Photodetection in Few Layer MoS_2 Phototransistors with Au Nanostructure Arrays. *Small* **2015**, *11*, 2392−2398.
(456) Freitag, M.; Low, T.; Zhu, W.; Yan, H.; Xia, F.; Avouris, P. Photocurrent in Graphene Harnessed by Tunable Intrinsic Plasmons. *Nat. Commun.* **2013**, *4*, 1951.
(457) Shivananju, B. N.; Yu, W.; Liu, Y.; Zhang, Y.; Lin, B.; Li, S.; Bao, Q. The Roadmap of Graphene-Based Optical Biochemical Sensors. *Adv. Funct. Mater.* **2017**, *27*, 1603918.
(458) Anichini, C.; Czepa, W.; Pakulski, D.; Aliprandi, A.; Ciesielski, A.; Samori, P. Chemical Sensing with 2D Materials. *Chem. Soc. Rev.* **2018**, *47*, 4860−4908.
(459) Wen, W.; Song, Y.; Yan, X.; Zhu, C.; Du, D.; Wang, S.; Asiri, A. M.; Lin, Y. Recent Advances in Emerging 2d Nanomaterials for Biosensing and Bioimaging Applications. *Mater. Today* **2018**, *21*, 164−177.
(460) Luo, M.; Fan, T.; Zhou, Y.; Zhang, H.; Mei, L. 2d Black Phosphorus-Based Biomedical Applications. *Adv. Funct. Mater.* **2019**, *29*, 1808306.
(461) Orecchioni, M.; Bedognetti, D.; Newman, L.; Fuoco, C.; Spada, F.; Hendrickx, W.; Marincola, F. M.; Sgarrella, F.; Rodrigues, A. F.; Menard-Moyon, C.; Cesareni, G.; Kostarelos, K.; Bianco, A.; Delogu, L. G Single-Cell Mass Cytometry and Transcriptome Profiling Reveal the Impact of Graphene on Human Immune Cells. *Nat. Commun.* **2017**, *8*, 1109.
(462) Kurapati, R.; Mukherjee, S. P.; Martin, C.; Bepete, G.; Vazquez, E.; Penicaud, A.; Fadeel, B.; Bianco, A. Degradation of Single-Layer and Few-Layer Graphene by Neutrophil Myeloperoxidase. *Angew. Chem., Int. Ed.* **2018**, *57*, 11722−11727.
(463) Sun, J.; Chen, Y.; Priydarshi, M. K.; Gao, T.; Song, X.; Zhang, Y.; Liu, Z. Graphene Glass from Direct Cvd Routes: Production and Applications. *Adv. Mater.* **2016**, *28*, 10333−10339.
(464) Kravets, V. G.; Schedin, F.; Jalil, R.; Britnell, L.; Gorbachev, R. V.; Ansell, D.; Thackray, B.; Novoselov, K. S.; Geim, A. K.; Kabashin, A. V.; Grigorenko, A. N. Singular Phase Nano-Optics in Plasmonic

https://dx.doi.org/10.1021/acs.chemrev.9b00592
Chem. Rev. 2020, 120, 6197−6246

Metamaterials for Label-Free Single-Molecule Detection. *Nat. Mater.* **2013**, *12*, 304−309.
(465) Zhu, Y.; Li, Z.; Hao, Z.; DiMarco, C.; Maturavongsadit, P.; Hao, Y.; Lu, M.; Stein, A.; Wang, Q.; Hone, J.; Yu, N.; Lin, Q.; et al. Optical Conductivity-Based Ultrasensitive Mid-Infrared Biosensing on a Hybrid Metasurface. *Light: Sci. Appl.* **2018**, *7*, No. e67.
(466) Hu, H.; Yang, X.; Zhai, F.; Hu, D.; Liu, R.; Liu, K.; Sun, Z.; Dai, Q. Far-Field Nanoscale Infrared Spectroscopy of Vibrational Fingerprints of Molecules with Graphene Plasmons. *Nat. Commun.* **2016**, *7*, 12334.
(467) Hu, H.; Yang, X.; Guo, X.; Khaliji, K.; Biswas, S. R.; Garcia de Abajo, F. J.; Low, T.; Sun, Z.; Dai, Q. Gas Identification with Graphene Plasmons. *Nat. Commun.* **2019**, *10*, 1131.
(468) Fang, Z.; Wang, Y.; Schlather, A. E.; Liu, Z.; Ajayan, P. M.; de Abajo, F. J.; Nordlander, P.; Zhu, X.; Halas, N. J. Active Tunable Absorption Enhancement with Graphene Nanodisk Arrays. *Nano Lett.* **2014**, *14*, 299−304.
(469) Yeung, K. Y.; Chee, J.; Yoon, H.; Song, Y.; Kong, J.; Ham, D. Far-Infrared Graphene Plasmonic Crystals for Plasmonic Band Engineering. *Nano Lett.* **2014**, *14*, 2479−2484.
(470) Brar, V. W.; Jang, M. S.; Sherrott, M.; Lopez, J. J.; Atwater, H. A. Highly Confined Tunable Mid-Infrared Plasmonics in Graphene Nanoresonators. *Nano Lett.* **2013**, *13*, 2541−2547.
(471) Kalantar-zadeh, K.; Ou, J. Z. Biosensors Based on Two-Dimensional MoS_2. *ACS Sensors* **2016**, *1*, 5−16.
(472) Sun, Z.; Martinez, A.; Wang, F. Optical Modulators with 2D Layered Materials. *Nat. Photonics* **2016**, *10*, 227−238.
(473) Tamagnone, M.; Fallahi, A.; Mosig, J. R.; Perruisseau-Carrier, J. Fundamental Limits and near-Optimal Design of Graphene Modulators and Non-Reciprocal Devices. *Nat. Photonics* **2014**, *8*, 556−563.
(474) Tamagnone, M.; Moldovan, C.; Poumirol, J. M.; Kuzmenko, A. B.; Ionescu, A. M.; Mosig, J. R.; Perruisseau-Carrier, J. Near Optimal Graphene Terahertz Non-Reciprocal Isolator. *Nat. Commun.* **2016**, *7*, 11216.
(475) Klein, M.; Badada, B. H.; Binder, R.; Alfrey, A.; McKie, M.; Koehler, M. R.; Mandrus, D. G.; Taniguchi, T.; Watanabe, K.; LeRoy, B. J.; Schaibley, J. R.; et al. 2D Semiconductor Nonlinear Plasmonic Modulators. *Nat. Commun.* **2019**, *10*, 3264.
(476) Sim, S.; Jang, H.; Koirala, N.; Brahlek, M.; Moon, J.; Sung, J. H.; Park, J.; Cha, S.; Oh, S.; Jo, M. H.; et al. Ultra-High Modulation Depth Exceeding 2,400% in Optically Controlled Topological Surface Plasmons. *Nat. Commun.* **2015**, *6*, 8814.
(477) Yao, B.; Huang, S.-W.; Liu, Y.; Vinod, A. K.; Choi, C.; Hoff, M.; Li, Y.; Yu, M.; Feng, Z.; Kwong, D.-L.; et al. Gate-Tunable Frequency Combs in Graphene-Nitride Microresonators. *Nature* **2018**, *558*, 410−414.
(478) Gan, S.; Cheng, C.; Zhan, Y.; Huang, B.; Gan, X.; Li, S.; Lin, S.; Li, X.; Zhao, J.; Chen, H.; et al. A Highly Efficient Thermo-Optic Microring Modulator Assisted by Graphene. *Nanoscale* **2015**, *7*, 20249−20255.
(479) Peng, R.; Khaliji, K.; Youngblood, N.; Grassi, R.; Low, T.; Li, M. Midinfrared Electro-Optic Modulation in Few-Layer Black Phosphorus. *Nano Lett.* **2017**, *17*, 6315−6320.
(480) Grinblat, G.; Abdelwahab, I.; Nielsen, M. P.; Dichtl, P.; Leng, K.; Oulton, R. F.; Loh, K. P.; Maier, S. A. Ultrafast All-Optical Modulation in 2D Hybrid Perovskites. *ACS Nano* **2019**, *13*, 9504−9510.
(481) Sensale-Rodriguez, B.; Yan, R.; Zhu, M.; Jena, D.; Liu, L.; Grace Xing, H. Efficient Terahertz Electro-Absorption Modulation Employing Graphene Plasmonic Structures. *Appl. Phys. Lett.* **2012**, *101*, 261115.
(482) Ansell, D.; Radko, I. P.; Han, Z.; Rodriguez, F. J.; Bozhevolnyi, S. I.; Grigorenko, A. N. Hybrid Graphene Plasmonic Waveguide Modulators. *Nat. Commun.* **2015**, *6*, 8846.
(483) Gan, X.; Shiue, R. J.; Gao, Y.; Mak, K. F.; Yao, X.; Li, L.; Szep, A.; Walker, D., Jr.; Hone, J.; Heinz, T. F.; et al. High-Contrast Electrooptic Modulation of a Photonic Crystal Nanocavity by Electrical Gating of Graphene. *Nano Lett.* **2013**, *13*, 691−696.
(484) Qiu, C.; Gao, W.; Vajtai, R.; Ajayan, P. M.; Kono, J.; Xu, Q. Efficient Modulation of 1.55 Mum Radiation with Gated Graphene on a Silicon Microring Resonator. *Nano Lett.* **2014**, *14*, 6811−6815.
(485) Phare, C. T.; Daniel Lee, Y.-H.; Cardenas, J.; Lipson, M. Graphene Electro-Optic Modulator with 30 GHz Bandwidth. *Nat. Photonics* **2015**, *9*, 511−514.
(486) Kim, J. T.; Chung, K. H.; Choi, C.-G. Thermo-Optic Mode Extinction Modulator Based on Graphene Plasmonic Waveguide. *Opt. Express* **2013**, *21*, 15280−15286.
(487) Cao, Y. P.; Gan, S.; Geng, Z. X.; Liu, J.; Yang, Y. P.; Bao, Q. L.; Chen, H. D. Optically Tuned Terahertz Modulator Based on Annealed Multilayer MoS_2. *Sci. Rep.* **2016**, *6*, 22899.
(488) Alfaro-Mozaz, F. J.; Alonso-Gonzalez, P.; Velez, S.; Dolado, I.; Autore, M.; Mastel, S.; Casanova, F.; Hueso, L. E.; Li, P.; Nikitin, A. Y.; Hillenbrand, R.; et al. Nanoimaging of Resonating Hyperbolic Polaritons in Linear Boron Nitride Antennas. *Nat. Commun.* **2017**, *8*, 15624.
(489) Nikitin, A. Y.; Alonso-Gonzalez, P.; Velez, S.; Mastel, S.; Centeno, A.; Pesquera, A.; Zurutuza, A.; Casanova, F.; Hueso, L. E.; Koppens, F. H. L.; Hillenbrand, R. Real-Space Mapping of Tailored Sheet and Edge Plasmons in Graphene Nanoresonators. *Nat. Photonics* **2016**, *10*, 239−243.
(490) Youngblood, N.; Chen, C.; Koester, S. J.; Li, M. Waveguide-Integrated Black Phosphorus Photodetector with High Responsivity and Low Dark Current. *Nat. Photonics* **2015**, *9*, 247−252.
(491) Wang, X.; Cheng, Z.; Xu, K.; Tsang, H. K.; Xu, J.-B. High-Responsivity Graphene/Silicon-Heterostructure Waveguide Photodetectors. *Nat. Photonics* **2013**, *7*, 888−891.
(492) Gan, X.; Shiue, R.-J.; Gao, Y.; Meric, I.; Heinz, T. F.; Shepard, K.; Hone, J.; Assefa, S.; Englund, D. Chip-Integrated Ultrafast Graphene Photodetector with High Responsivity. *Nat. Photonics* **2013**, *7*, 883−887.
(493) Pospischil, A.; Humer, M.; Furchi, M. M.; Bachmann, D.; Guider, R.; Fromherz, T.; Mueller, T. Cmos-Compatible Graphene Photodetector Covering All Optical Communication Bands. *Nat. Photonics* **2013**, *7*, 892−896.
(494) Liu, M.; Zhang, X. Graphene Benefits. *Nat. Photonics* **2013**, *7*, 850−851.
(495) Tao, J.; Yu, X. C.; Hu, B.; Dubrovkin, A.; Wang, Q. J. Graphene-Based Tunable Plasmonic Bragg Reflector with a Broad Bandwidth. *Opt. Lett.* **2014**, *39*, 271−274.
(496) Hu, D.; Chen, K.; Chen, X.; Guo, X.; Liu, M.; Dai, Q. Tunable Modal Birefringence in a Low-Loss Van Der Waals Waveguide. *Adv. Mater.* **2019**, *31*, 1807788.
(497) Zhang, X.; De-Eknamkul, C.; Gu, J.; Boehmke, A. L.; Menon, V. M.; Khurgin, J.; Cubukcu, E. Guiding of Visible Photons at the ngström Thickness Limit. *Nat. Nanotechnol.* **2019**, *14*, 844−850.
(498) Verre, R.; Baranov, D. G.; Munkhbat, B.; Cuadra, J.; Käll, M.; Shegai, T. Transition Metal Dichalcogenide Nanodisks as High-Index Dielectric Mie Nanoresonators. *Nat. Nanotechnol.* **2019**, *14*, 679−683.
(499) Liu, C. H.; Zheng, J.; Colburn, S.; Fryett, T. K.; Chen, Y.; Xu, X.; Majumdar, A. Ultrathin Van der Waals Metalenses. *Nano Lett.* **2018**, *18*, 6961−6966.
(500) Sunku, S. S.; Ni, G. X.; Jiang, B. Y.; Yoo, H.; Sternbach, A.; McLeod, A. S.; Stauber, T.; Xiong, L.; Taniguchi, T.; Watanabe, K.; Kim, P.; Fogler, M. M.; Basov, D. N. Photonic Crystals for Nano-Light in Moiré Graphene Superlattices. *Science* **2018**, *362*, 1153−1156.
(501) He, Y. M.; Clark, G.; Schaibley, J. R.; He, Y.; Chen, M. C.; Wei, Y. J.; Ding, X.; Zhang, Q.; Yao, W.; Xu, X.; et al. Single Quantum Emitters in Monolayer Semiconductors. *Nat. Nanotechnol.* **2015**, *10*, 497−502.
(502) Zhang, Y.; Oka, T.; Suzuki, R.; Ye, J.; Iwasa, Y. Electrically Switchable Chiral Light-Emitting Transistor. *Science* **2014**, *344*, 725−728.
(503) Grosso, G. 2d Materials: Valley Polaritons. *Nat. Photonics* **2017**, *11*, 455−456.

https://dx.doi.org/10.1021/acs.chemrev.9b00592
Chem. Rev. 2020, 120, 6197−6246

(504) Schaibley, J. R.; Yu, H.; Clark, G.; Rivera, P.; Ross, J. S.; Seyler, K. L.; Yao, W.; Xu, X. Valleytronics in 2D Materials. *Nat. Rev. Mater.* **2016**, *1*, 16055.
(505) Amani, M.; Lien, D.-H.; Kiriya, D.; Xiao, J.; Azcatl, A.; Noh, J.; Madhvapathy, S. R.; Addou, R.; KC, S.; Dubey, M.; Cho, K.; Wallace, R. M.; Lee, S.-C.; He, J.-H.; Ager, J. W.; Zhang, X.; Yablonovitch, E.; Javey, A. Near-Unity Photoluminescence Quantum Yield in MoS_2. *Science* **2015**, *350*, 1065−1068.
(506) Lien, D.-H.; Uddin, S. Z.; Yeh, M.; Amani, M.; Kim, H.; Ager, J. W.; Yablonovitch, E.; Javey, A. Electrical Suppression of All Nonradiative Recombination Pathways in Monolayer Semiconductors. *Science* **2019**, *364*, 468−471.
(507) Withers, F.; Del Pozo-Zamudio, O.; Mishchenko, A.; Rooney, A. P.; Gholinia, A.; Watanabe, K.; Taniguchi, T.; Haigh, S. J.; Geim, A. K.; Tartakovskii, A. I.; et al. Light-Emitting Diodes by Band-Structure Engineering in Van der Waals Heterostructures. *Nat. Mater.* **2015**, *14*, 301−306.
(508) Wang, Z.; Dong, Z.; Gu, Y.; Chang, Y.-H.; Zhang, L.; Li, L.-J.; Zhao, W.; Eda, G.; Zhang, W.; Grinblat, G.; Maier, S. A.; Yang, J. K. W.; Qiu, C.-W.; Wee, A. T. S.; et al. Giant Photoluminescence Enhancement in Tungsten-Diselenide-Gold Plasmonic Hybrid Structures. *Nat. Commun.* **2016**, *7*, 11283.
(509) Lee, B.; Park, J.; Han, G. H.; Ee, H. S.; Naylor, C. H.; Liu, W.; Johnson, A. T.; Agarwal, R. Fano Resonance and Spectrally Modified Photoluminescence Enhancement in Monolayer Mos2 Integrated with Plasmonic Nanoantenna Array. *Nano Lett.* **2015**, *15*, 3646−3653.
(510) Kern, J.; Trügler, A.; Niehues, I.; Ewering, J.; Schmidt, R.; Schneider, R.; Najmaei, S.; George, A.; Zhang, J.; Lou, J.; et al. Nanoantenna-Enhanced Light-Matter Interaction in Atomically Thin WS_2. *ACS Photonics* **2015**, *2*, 1260−1265.
(511) Chen, H.; Nanz, S.; Abass, A.; Yan, J.; Gao, T.; Choi, D.-Y.; Kivshar, Y. S.; Rockstuhl, C.; Neshev, D. N. Enhanced Directional Emission from Monolayer WSe_2 Integrated onto a Multiresonant Silicon-Based Photonic Structure. *ACS Photonics* **2017**, *4*, 3031−3038.
(512) Galfsky, T.; Sun, Z.; Considine, C. R.; Chou, C. T.; Ko, W. C.; Lee, Y. H.; Narimanov, E. E.; Menon, V. M. Broadband Enhancement of Spontaneous Emission in Two-Dimensional Semiconductors Using Photonic Hypercrystals. *Nano Lett.* **2016**, *16*, 4940−4945.
(513) Zhang, X.; Choi, S.; Wang, D.; Naylor, C. H.; Johnson, A. T. C.; Cubukcu, E. Unidirectional Doubly Enhanced MoS_2 Emission Via Photonic Fano Resonances. *Nano Lett.* **2017**, *17*, 6715−6720.
(514) Withers, F.; Del Pozo-Zamudio, O.; Schwarz, S.; Dufferwiel, S.; Walker, P. M.; Godde, T.; Rooney, A. P.; Gholinia, A.; Woods, C. R.; Blake, P.; et al. WSe_2 Light-Emitting Tunneling Transistors with Enhanced Brightness at Room Temperature. *Nano Lett.* **2015**, *15*, 8223−8228.
(515) Chen, H.; Yang, J.; Rusak, E.; Straubel, J.; Guo, R.; Myint, Y. W.; Pei, J.; Decker, M.; Staude, I.; Rockstuhl, C.; Lu, Y.; Kivshar, Y. S.; Neshev, D.; et al. Manipulation of Photoluminescence of Two-Dimensional $MoSe_2$ by Gold Nanoantennas. *Sci. Rep.* **2016**, *6*, 22296.
(516) Zhu, Y.; Li, Z.; Zhang, L.; Wang, B.; Luo, Z.; Long, J.; Yang, J.; Fu, L.; Lu, Y. High-Efficiency Monolayer Molybdenum Ditelluride Light-Emitting Diode and Photodetector. *ACS Appl. Mater. Interfaces* **2018**, *10*, 43291−43298.
(517) Pesin, D.; MacDonald, A. H. Spintronics and Pseudospintronics in Graphene and Topological Insulators. *Nat. Mater.* **2012**, *11*, 409−416.
(518) Selig, M.; Berghauser, G.; Raja, A.; Nagler, P.; Schuller, C.; Heinz, T. F.; Korn, T.; Chernikov, A.; Malic, E.; Knorr, A. Excitonic Linewidth and Coherence Lifetime in Monolayer Transition Metal Dichalcogenides. *Nat. Commun.* **2016**, *7*, 13279.
(519) Chervy, T.; Azzini, S.; Lorchat, E.; Wang, S.; Gorodetski, Y.; Hutchison, J. A.; Berciaud, S.; Ebbesen, T. W.; Genet, C. Room Temperature Chiral Coupling of Valley Excitons with Spin-Momentum Locked Surface Plasmons. *ACS Photonics* **2018**, *5*, 1281−1287.
(520) Ra'di, Y.; Simovski, C. R.; Tretyakov, S. A. Thin Perfect Absorbers for Electromagnetic Waves: Theory, Design, and Realizations. *Phys. Rev. Appl.* **2015**, *3*, 037001.
(521) Tan, C.; Cao, X.; Wu, X.-J.; He, Q.; Yang, J.; Zhang, X.; Chen, J.; Zhao, W.; Han, S.; Nam, G.-H.; Sindoro, M.; Zhang, H. Recent Advances in Ultrathin Two-Dimensional Nanomaterials. *Chem. Rev.* **2017**, *117*, 6225−6331.
(522) Kong, X.; Liu, Q.; Zhang, C.; Peng, Z.; Chen, Q. Elemental Two-Dimensional Nanosheets Beyond Graphene. *Chem. Soc. Rev.* **2017**, *46*, 2127−2157.
(523) Deng, J.; Xia, B.; Ma, X.; Chen, H.; Shan, H.; Zhai, X.; Li, B.; Zhao, A.; Xu, Y.; Duan, W.; et al. Epitaxial Growth of Ultraflat Stanene with Topological Band Inversion. *Nat. Mater.* **2018**, *17*, 1081−1086.
(524) Yan, M.; Huang, H.; Zhang, K.; Wang, E.; Yao, W.; Deng, K.; Wan, G.; Zhang, H.; Arita, M.; Yang, H.; Sun, Z.; Yao, H.; Wu, Y.; Fan, S.; Duan, W.; Zhou, S.; et al. Lorentz-Violating Type-Ii Dirac Fermions in Transition Metal Dichalcogenide PtTe2. *Nat. Commun.* **2017**, *8*, 257.
(525) Yu, X.; Yu, P.; Wu, D.; Singh, B.; Zeng, Q.; Lin, H.; Zhou, W.; Lin, J.; Suenaga, K.; Liu, Z.; Wang, Q. J.; et al. Atomically Thin Noble Metal Dichalcogenide: A Broadband Mid-Infrared Semiconductor. *Nat. Commun.* **2018**, *9*, 1545.
(526) Ali, M. N.; Xiong, J.; Flynn, S.; Tao, J.; Gibson, Q. D.; Schoop, L. M.; Liang, T.; Haldolaarachchige, N.; Hirschberger, M.; Ong, N. P.; et al. Large, Non-Saturating Magnetoresistance in WTe_2. *Nature* **2014**, *514*, 205−208.
(527) Han, W.; Kawakami, R. K.; Gmitra, M.; Fabian, J. Graphene Spintronics. *Nat. Nanotechnol.* **2014**, *9*, 794−807.
(528) Long, G.; Jiang, C.; Sabatini, R.; Yang, Z.; Wei, M.; Quan, L. N.; Liang, Q.; Rasmita, A.; Askerka, M.; Walters, G.; et al. Spin Control in Reduced-Dimensional Chiral Perovskites. *Nat. Photonics* **2018**, *12*, 528−533.
(529) Giovanni, D.; Chong, W. K.; Liu, Y. Y. F.; Dewi, H. A.; Yin, T.; Lekina, Y.; Shen, Z. X.; Mathews, N.; Gan, C. K.; Sum, T. C. Coherent Spin and Quasiparticle Dynamics in Solution-Processed Layered 2D Lead Halide Perovskites. *Adv. Sci.* **2018**, *5*, 1800664.
(530) Gibertini, M.; Koperski, M.; Morpurgo, A. F.; Novoselov, K. S. Magnetic 2D Materials and Heterostructures. *Nat. Nanotechnol.* **2019**, *14*, 408−419.
(531) Deng, Y.; Yu, Y.; Song, Y.; Zhang, J.; Wang, N. Z.; Sun, Z.; Yi, Y.; Wu, Y. Z.; Wu, S.; Zhu, J.; et al. Gate-Tunable Room-Temperature Ferromagnetism in Two-Dimensional Fe_3GeTe_2. *Nature* **2018**, *563*, 94−99.
(532) Seyler, K. L.; Zhong, D.; Klein, D. R.; Gao, S.; Zhang, X.; Huang, B.; Navarro-Moratalla, E.; Yang, L.; Cobden, D. H.; McGuire, M. A.; et al. Ligand-Field Helical Luminescence in a 2D Ferromagnetic Insulator. *Nat. Phys.* **2018**, *14*, 277−281.
(533) Zhao, M.; Huang, Y.; Peng, Y.; Huang, Z.; Ma, Q.; Zhang, H. Two-Dimensional Metal-Organic Framework Nanosheets: Synthesis and Applications. *Chem. Soc. Rev.* **2018**, *47*, 6267−6295.
(534) Dong, R.; Han, P.; Arora, H.; Ballabio, M.; Karakus, M.; Zhang, Z.; Shekhar, C.; Adler, P.; Petkov, P. S..; Erbe, A.; Mannsfeld, S. C. B.; Felser, C.; Heine, T.; Bonn, M.; Feng, X.; Canovas, E. High-Mobility Band-Like Charge Transport in a Semiconducting Two-Dimensional Metal−Organic Framework. *Nat. Mater.* **2018**, *17*, 1027.
(535) Liao, W.-M.; Zhang, J.-H.; Yin, S.-Y.; Lin, H.; Zhang, X.; Wang, J.; Wang, H.-P.; Wu, K.; Wang, Z.; Fan, Y.-N.; Pan, M.; Su, C.-Y. Tailoring Exciton and Excimer Emission in an Exfoliated Ultrathin 2D Metal-Organic Framework. *Nat. Commun.* **2018**, *9*, 2401.
(536) Basov, D. N.; Fogler, M. M.; Garcia de Abajo, F. J. Polaritons in Van der Waals Materials. *Science* **2016**, *354*, aag1992.
(537) Ni, G. X.; Wang, H.; Wu, J. S.; Fei, Z.; Goldflam, M. D.; Keilmann, F.; Ozyilmaz, B.; Castro Neto, A. H.; Xie, X. M.; Fogler, M. M.; et al. Plasmons in Graphene Moire Superlattices. *Nat. Mater.* **2015**, *14*, 1217−1222.
(538) Liao, M.; Wu, Z.-W.; Du, L.; Zhang, T.; Wei, Z.; Zhu, J.; Yu, H.; Tang, J.; Gu, L.; Xing, Y.; Yang, R.; Shi, D.; Yao, Y.; Zhang, G.; et al. Twist Angle-Dependent Conductivities across MoS_2/Graphene Heterojunctions. *Nat. Commun.* **2018**, *9*, 4068.

https://dx.doi.org/10.1021/acs.chemrev.9b00592
Chem. Rev. 2020, 120, 6197−6246

(539) Lin, M. L.; Tan, Q. H.; Wu, J. B.; Chen, X. S.; Wang, J. H.; Pan, Y. H.; Zhang, X.; Cong, X.; Zhang, J.; Ji, W.; et al. Moire Phonons in Twisted Bilayer MoS_2. *ACS Nano* **2018**, *12*, 8770−8780.
(540) Tran, K.; Moody, G.; Wu, F.; Lu, X.; Choi, J.; Kim, K.; Rai, A.; Sanchez, D. A.; Quan, J.; Singh, A.; et al. Evidence for Moiré Excitons in Van der Waals Heterostructures. *Nature* **2019**, *567*, 71−75.
(541) Patel, H.; Huang, L.; Kim, C. J.; Park, J.; Graham, M. W. Stacking Angle-Tunable Photoluminescence from Interlayer Exciton States in Twisted Bilayer Graphene. *Nat. Commun.* **2019**, *10*, 1445.
(542) Yang, J.; Wang, Z.; Wang, F.; Xu, R.; Tao, J.; Zhang, S.; Qin, Q.; Luther-Davies, B.; Jagadish, C.; Yu, Z.; et al. Atomically Thin Optical Lenses and Gratings. *Light: Sci. Appl.* **2016**, *5*, No. e16046.
(543) Fang, Z.; Liu, Z.; Wang, Y.; Ajayan, P. M.; Nordlander, P.; Halas, N. J. Graphene-Antenna Sandwich Photodetector. *Nano Lett.* **2012**, *12*, 3808−3813.
(544) Badioli, M.; Woessner, A.; Tielrooij, K. J.; Nanot, S.; Navickaite, G.; Stauber, T.; Garcia de Abajo, F. J.; Koppens, F. H. Phonon-Mediated Mid-Infrared Photoresponse of Graphene. *Nano Lett.* **2014**, *14*, 6374−6381.
(545) Freitag, M.; Low, T.; Martin-Moreno, L.; Zhu, W.; Guinea, F.; Avouris, P. Substrate-Sensitive Mid-Infrared Photoresponse in Graphene. *ACS Nano* **2014**, *8*, 8350−8356.
(546) Lu, X.; Jiang, P.; Bao, X. Phonon-Enhanced Photothermoelectric Effect in $SrTiO_3$ Ultra-Broadband Photodetector. *Nat. Commun.* **2019**, *10*, 138.
(547) Woessner, A.; Parret, R.; Davydovskaya, D.; Gao, Y.; Wu, J.-S.; Lundeberg, M. B.; Nanot, S.; Alonso-Gonzalez, P.; Watanabe, K.; Taniguchi, T.; Hillenbrand, R.; Fogler, M. M.; Hone, J.; Koppens, F. H. L.; et al. Electrical Detection of Hyperbolic Phonon-Polaritons in Heterostructures of Graphene and Boron Nitride. *npj 2D Mater. Appl.* **2017**, *1*, 25.
(548) Mejia-Salazar, J. R.; Oliveira, O. N., Jr. Plasmonic Biosensing. *Chem. Rev.* **2018**, *118*, 10617−10625.
(549) Jin, Y. Engineering Plasmonic Gold Nanostructures and Metamaterials for Biosensing and Nanomedicine. *Adv. Mater.* **2012**, *24*, 5153−5165.
(550) Kabashin, A. V.; Evans, P.; Pastkovsky, S.; Hendren, W.; Wurtz, G. A.; Atkinson, R.; Pollard, R.; Podolskiy, V. A.; Zayats, A. V. Plasmonic Nanorod Metamaterials for Biosensing. *Nat. Mater.* **2009**, *8*, 867−871.
(551) Wu, C.; Khanikaev, A. B.; Adato, R.; Arju, N.; Yanik, A. A.; Altug, H.; Shvets, G. Fano-Resonant Asymmetric Metamaterials for Ultrasensitive Spectroscopy and Identification of Molecular Monolayers. *Nat. Mater.* **2012**, *11*, 69−75.
(552) Shen, Y.; Zhou, J.; Liu, T.; Tao, Y.; Jiang, R.; Liu, M.; Xiao, G.; Zhu, J.; Zhou, Z. K.; Wang, X.; et al. Plasmonic Gold Mushroom Arrays with Refractive Index Sensing Figures of Merit Approaching the Theoretical Limit. *Nat. Commun.* **2013**, *4*, 2381.
(553) Cao, C.; Zhang, J.; Wen, X.; Dodson, S. L.; Dao, N. T.; Wong, L. M.; Wang, S.; Li, S.; Phan, A. T.; Xiong, Q. Metamaterials-Based Label-Free Nanosensor for Conformation and Affinity Biosensing. *ACS Nano* **2013**, *7*, 7583−7591.
(554) Sreekanth, K. V.; Alapan, Y.; ElKabbash, M.; Ilker, E.; Hinczewski, M.; Gurkan, U. A.; De Luca, A.; Strangi, G. Extreme Sensitivity Biosensing Platform Based on Hyperbolic Metamaterials. *Nat. Mater.* **2016**, *15*, 621−627.

https://dx.doi.org/10.1021/acs.chemrev.9b00592
Chem. Rev. 2020, 120, 6197−6246